Soil moisture retrieval using high spatial resolution Polarimetric L-Band Multi-beam Radiometer (PLMR) data at the field scale

Dissertation der Fakultät für Geowissenschaften der

Ludwig Maximilians Universität München

vorgelegt von:

Marion Pause

Eingereicht:

München, den 12.10.2010

Not everything that can be counted counts and not everything that counts can be counted.

Albert Einstein

Table of Content

List of Figures

List of Tables

List of abbreviations

AISA	airborne imaging spectro-radiometer for application
DN	digital number
DOY	day of the year
EnMAP	Environmental Mapping and Analyses Program
FDR	Frequency Domain Reflectometry
GI	Gitelson Green Index
L-MEB	L-band Microwave Emission of the Biosphere Model
LPRM	Land Parameter Retrieval Model
MSAVI	Modified Soil Adjusted Vegetation Index
MTVI	Modified Triangular Vegetation Index
NDVI	Normalized Difference Vegetation Index
PLMR	Polarimetric L-band Multibeam Radiometer
PSRI	Plant Senescence Reflectance Index
SMAP	Soil Moisture Active and Passive Mission
SMOS	Soil Moisture and Ocean Salinity Mission
TERENO	Terrestrial Environmental Observatories
VI	vegetation indices
vwc	vegetation water content

List of general notations

CT	correction term
e_h, e_v	emissivity, horizontal and vertical
ε	dielectric constant
f	frequency
Γ	vegetation transmissivity
h	horizontal polarization
h_r	roughness parameter
K	Kelvin
L	antenna size
LAI	Leaf area index
MPDI	microwave polarization difference index
Q	polarization mixing fraction
r	correlation coefficient
r_h, r_v	reflectivity, horizontal and vertical
R^2	coefficient of determination
RMSE	root mean square error
sm	soil moisture
TB	brightness temperature
T_{TIR}	thermal infrared temperature
TIR	thermal infrared
T_s	soil temperature
T	optical depth
u	incidence angel
un	no viewing angle normalization applied
v	vertical polarization
ω	single scattering albedo

Zusammenfassung

Eine ganz wesentliche Rolle bei der Beschreibung der Vegetationsentwicklung sowie Wasser-, Stoff- und Energieflüssen auf allen räumlichen Skalen spielt die Kenntnis des Wassergehaltes in den oberen Zentimetern der Landoberfläche. Die oberflächennahe Bodenfeuchte steuert maßgeblich die Aufteilung des Niederschlages in die Komponenten Oberflächenabfluss, Verdunstung und Infiltration und reguliert die mikrobakterielle Aktivität, sowie biogeo-chemische Umsetzungsprozesse. Die Verfügbarkeit von Wasser ist entscheidend für das Pflanzenwachstum, hat einen Einfluss auf die Artenzusammensetzung und bestimmt über Wechselwirkungen mit dem Strahlungs- und Energiehaushalt das (lokale) Klima. Zudem spielt die räumliche Verteilung der Bodenfeuchte und Ausbildung von Mustern und Strukturen eine wichtige Rolle für die Entwicklung oberflächiger und unterirdischer Wasser- und Stofftransporte. Ziel dieser Arbeit war es oberflächennahe Bodenfeuchte aus räumlich hochauflösenden (50 m) L-Band Radiometerdaten über landwirtschaftlich genutzten Flächen abzuleiten.

Passive L-Band (~ 1.4 GHz) Mikrowellenfernerkundung mittels Radiometern hat sich als eine der meist versprechensten Fernerkundungsmethoden zur Ableitung von Oberflächenbodenfeuchte (ca. 0-10 cm) erwiesen. Die Operationalität dieser Fernerkundungsmethodik zum Bodenfeuchte-Monitoring ist jedoch noch nicht gegeben. Grund dafür ist im Wesentlichen die Signalüberlagerung unterschiedlicher system- und objektspezifischer Faktoren und deren limitierender Einfluss auf die Interpretierbarkeit der vom Radiometer registrierten Strahlungstemperatur hinsichtlich Bodenfeuchte. Bei der Verwendung von Mikrowellenradiometern über vegetationsbedeckten Böden kommt es zu Signalüberlagerungen bis zu endgültigem Verlust der Bodenfeuchteinformation am Signal, in Abhängigkeit von der „störenden" Vegetationsschicht. Zur Erfassung räumlich verteilter Bodenfeuchte mittels L-Band Radiometern ist es demnach essentiell Informationen über die räumliche Verteilung von Vegetationsparametern (z.B. Blattflächenindex – LAI, Pflanzenwassergehalt, Biomasse) bereitzustellen und in Modellrechnungen einzubeziehen.

Im Zusammenhang mit dem aufgezeigten Hintergrund bzgl. des Vegetationseinflusses auf das Mikrowellensignal behandelt das vorliegende Promotionsvorhaben die gemeinsame Analyse von flugzeug-getragenen L-Band Mikrowellenradiometerdaten (50 m geometrische Auflösung) und abbildenden Spektrometerdaten (1.5 m geometrische Auflösung). Flugzeug-getragene abbildende Spektrometerdaten verfügen über ein hohes Potential zur Vegetationsanalyse und enthalten aufgrund ihrer hohen räumlichen Auflösung (< 5 m) Informationen über die Subpixelheterogenität von Vegetationseigenschaften innerhalb räumlich geringer aufgelöster L-Band Daten. Die Ableitung der Bodenfeuchte im Rahmen dieser Arbeit erfolg-

te auf Getreideflächen (Wintergerste, Winterroggen) während der Fruchtentwicklungsphase. Eine besondere Charakteristik des Datensatzes ist die sehr geringe Bodenfeuchte (< 15 Vol. %) am Tag der L-Band Datenakquise, welche im Rahmen einer Feldkampagne in-situ gemessen und als Referenz verwendet wurde.

Die zentralen Zielsetzungen dieser Arbeit können demnach folgendermaßen zusammengefasst werden:

1. Besteht ein Zusammenhang zwischen sub-skaliger LAI Variabilität und der räumlich hochauflösenden „Strahlungstemperatur" passiver Mikrowellenfernerkundungsdaten des L-Bandes?

2. Ermöglicht der Einsatz von spektralen Vegetationsindizes die Charakterisierung des Vegetationseinflusses und damit die Ableitung von Bodenfeuchte aus L-Band Daten mittels „einfacher" empirischer Modelle innerhalb eines Getreidebestandes?

3. Wie beeinflusst die Temperaturinformation die Bodenfeuchteergebnisse bei der Verwendung des „land surface parameter retrieval model" (LPRM)?

4. Besteht ein Zusammenhang zwischen inner-schlagspezifischen Variationen der Vegetationsdecke und dem Rauhigkeitsparameter bei der Verwendung des „land surface parameter retrieval model" (LPRM)?

Die vorliegende Arbeit zeigt, dass auftretende Variabilitäten des LAI innerhalb eines Getreidebestandes das Mikrowellensignal nachweislich ($0.23 < R^2 > 0.90$) beeinflussen. Weiterhin können mittels einfacher empirischer Modelle unter Verwendung von hyperspektralen Vegetationsindizes sehr gute (RMSE = 0.82 Vol. %) Bodenfeuchteergebnisse erzielt werden. Der Vorteil dieser Datenkombination liegt in der sehr guten Charakterisierung der Heterogenität von Vegetationseigenschaften auch innerhalb eines Vegetationsbestandes. Die Ableitung von Bodenfeuchte mittels LPRM unter Verwendung eines „default" Wertes zur Rauhigkeitsparameterisierung erzielte keine zufriedenstellenden Ergebnisse. In Abhängigkeit von der verwendeten Temperaturinformation in LPRM wurden mittlere Unterschiede in den Bodenfeuchtergebnissen von bis zu 5.6 Vol. % nachgewiesen. Sehr gute Bodenfeuchtergebnisse wurden dagegen erzielt bei der Verwendung räumlich variierender Werte für die Rauhigkeit. Die räumlich variierenden Rauhigkeitswerte wurde durch eine Optimierung von LPRM mittels Monte-Carlo Simulation erzielt. Zwischen den optimierten Rauhigkeitswerten und NDVI (normalized difference vegetation index) Werten, berechnet aus den abbildenden Spektrometerdaten, wurde ein klarer Zusammenhang ($R^2 = 0.57$) gefunden. Die Ergebnisse der Arbeit zeigen insbesondere das hohe Potential der gemeinsamen Auswertung von passiven L-Band Mikrowellendaten und Vegetationsindizes, berechnet aus abbildenden Spektro-

meterdaten zur Ableitung räumlich verteilter Bodenfeuchte. Da der Einfluss von Vegetationseigenschaften räumlich stark variieren kann, besteht eine räumliche Variabilität in der Genauigkeit der Bodenfeuchteberechnung.

Die Integration von spektralen Vegetationsindizes zur Quantifizierung des Vegetationseinflusses an der L-Band Strahlungstemperatur verspricht operationelle Umsetzbarkeit. Die Kenntnisse über den Zusammenhang von Rauhigkeitsparameter und NDVI können verwendet werden um eine räumliche Optimierung der in physikalisch-basierten Modellen verwendeten Rauhigkeitswerte durchzuführen. In diesem Zusammenhang besteht die Anforderung an ein Monitoring des Verhaltens von Modellparameter (Rauhigkeit) zu Vegetationsparameter oder Vegetationsindizes in Abhängigkeit von der Art der Vegetation, der Phänologie und der damit verbundenen zeitlichen Dynamik innerhalb von Vegetationszyklen. Der Ausbau Bestehender sowie die Neueinrichtung terrestrischer Sensornetzwerke (z.B. TERENO) zur Bodenfeuchte- und Temperaturmessung oder dem Vegetationsmonitoring, ermöglichen die Bereitstellung von zeitlich hoch aufgelösten Referenzdaten zur Validierung aktueller und zukünftiger Fernerkundungsdatenprodukte wie z.B. SMOS, SMAP oder EnMAP.

1.   Introduction

1.1   Importance of spatial distributed soil moisture information

The soil moisture of the upper few centimetres plays an important role for many atmospheric and land surface processes related to meteorology, climatology and hydrology (Western et al. 2004). Global, continental and regional observations of soil moisture are particularly important for weather and climate forecasting (Huszar et al. 1999, Li et al. 2007). In meteorology soil moisture determines the partitioning of net radiation into latent or sensible heat components. Spatio-temporal dynamics of soil moisture are connected to hydrological processes like evapotranspiration, infiltration and surface runoff (Hupet et al. 2002). Soil moisture of the top few centimetres plays a key role in limiting evapotranspiration when the atmospheric demand is high (Ivanov et al. 2004). The response of natural catchments to precipitation depends on the spatial and temporal resolution of surface runoff generation which in turn is strongly related to the initial wetness condition (Vivoni et al. 2007). Spatio-temporal characteristics of surface soil moisture patterns provide information about the position of the water table (Troch et al. 1993). Soil moisture can vary significantly on diurnal basis, especially for short vegetation canopy. The widely applied Soil & Water Assessment Tool (SWAT) to predict the influence of land management practice on water, sediment and agricultural chemical yields in large complex watersheds requires soil moisture input data. Soil water models play an important role in terms of estimating water use, water allocation and water status at a specific spatial scale (Ranatunga et al. 2008). Their application is often hampered by the lack of specific soil moisture data for calibration to large areas or to assess temporal dynamics.

Therefore, improved information about spatial distribution of soil moisture is important for various applications and at field scale it may benefit:

-   agricultural practice and irrigation management (Bastiaanssen et al. 2000, Jackson et al. 1987, Wigneron et al. 1998)
-   early yield forecasting (Doan Minh et al. 2003, Engman 1991)
-   early drought prediction and monitoring (Jackson et al. 1987a, Sridhar et al. 2008)
-   solute transport and erosion analyses and management because of their influence on water flux patterns (Castillo et al. 2003, Jackson et al. 1987b)
-   flood forecasting though improved modelling of surface runoff and infiltration (Bindlish et al. 2009, Crow et al. 2005)

1.2   Methods to retrieve soil moisture

Various needs for soil moisture observations require different measurement techniques that can generally be distinguished in in-situ (point) measurements, soil-water models and re-mote sensing techniques.

The gravimetric technique, as a destructive field sampling, is the standard for the calibration of all other methods to determine soil moisture. The method consists of oven drying soil samples (105°C, ~48 h) until a constant weight. The amount of soil water content is usually expressed as volume percentage (Vol. %) by using a defined cylindrical tube. This method is technically simple but has a high effort on man power, field and laboratory equipment and is time consuming. Furthermore it is destructive and for temporal monitoring or large area soil moisture sampling circumstantial and extensive. For ground based soil moisture monitoring generally indirect measurement techniques are applied in which sensors are plunged in the soil or are permanently installed into the soil to record quasi continuous data. These methods make use of the impulse propagation of an electromagnetic pulse within the soil which is mainly dependent of the soil water conditions.

The neutron scattering method as a nuclear technique estimates the soil moisture content by measuring the thermal or slow neutron density (Belcher 1950). Neutrons with high energy are emitted by a radioactive source into the soil and are slowed down by nuclei of atoms and become thermalized. The collision with hydrogen can slow fast neutrons much more effec-tively than any other element present in the soil. Therefore, the density of the resultant cloud of slow neutrons is a function of the moisture content in the soil. The number of slow neu-trons returning to the detector is counted per unit time and the soil moisture content is de-termined using a known calibration curve of counts versus volumetric water content.

Electromagnetic techniques, such as frequency domain reflectometry (FDR) and time do-main reflectometry (TDR) depend upon the effect of soil moisture on the dielectrical proper-ties of the soil. Dry soil has a dielectric constant near 5 whereas that of water is 80. Capacit-ance or resistivity between electrodes in a soil is measured for soil moisture. Using TDR devices high frequency electromagnetic waves are transmitted and the dielectric permittivity is determined by measuring the time it takes for an electromagnetic wave to propagate along a transmission line that is surrounded by the soil. The information required is obtained from a reflection vs. frequency graph and transferred to soil moisture values using a calibration function. Tensiometer measures the capillary tension or the energy with which water is held (suction) by the soil. Breakdowns appear mainly during dry conditions and a regular mainte-nance is required.

Soil water models play an important role in agricultural water management and vary much in their complexity (Ranatunga et al. 2008). Soil water models include soil water flow equations and are based upon the conservation of mass to determine soil moisture at any time. Such models can be used to estimate soil moisture at various depth and different spatial and temporal resolutions. TOPMODEL is a widely used rainfall-runoff model to predict soil moisture distribution within catchments (Beven et al. 1979). These models usually require extensive meteorological and site specific input parameterization. Data assimilation using remote sensing derived spatial distributed near surface soil moisture information can be applied in such models for calibration purpose and to provide soil moisture information at much greater depth (Houser et al. 1998, Walker et al. 2001).

Remote sensing techniques to retrieve soil moisture are performed using portions of the visible ($0.4 – 0.7$ μm), near ($0.7 – 1.4$ μm), shortwave ($1.4 – 3.0$ μm), thermal infrared ($8.0 – 15$ μm) and microwave (1 mm $– 1$ m) electromagnetic spectrum. Dependent on the specific sensors remote sensing offers the opportunity to estimate soil moisture and appearing spatial patterns at various spatial scales (field to global scale).

Penetration depth with optical remote sensing is significantly lower compared to microwave sensors. Reflected solar energy within the visible spectrum responds to only the top few centimetres of the soil profile (Idso et al. 1975). Increasing soil moisture up to a specific level entails a decrease in reflectance values in the visible and short wave infrared. Surface covariates to account for during soil moisture analyses are soil texture, surface roughness, organic matter, crust and vegetation cover (Capehart et al. 1997). Using the visible region of the electromagnetic spectrum, the soil moisture retrieval is based on measurements of the surface albedo (Jackson et al. 1976). The normalized soil moisture index (NSMI) is proposed to assess near surface soil moisture directly in the field using spectrometer measurements of the shortwave infrared at 1800 nm and 2119 nm (Haubrock et al. 2008a). However, the found coefficient of determination was not outstanding with $R^2 = 0.61$. Nevertheless, the NSMI was applied and validated over a lignite mining area with a coefficient of determination of $R^2 = 0.82$ using airborne imaging spectrometer data to quantify multi-temporal surface soil moisture (Haubrock et al. 2008b). The most constraining criterion for the use of optical remote sensing data are the limited applicability to non- or very low vegetated soils and the requirement of optimal solar illumination conditions, therefore limiting the observations to day time and to areas with no cloud cover.

Soil moisture retrieval using thermal infrared (TIR) data are based on the effect of water on the thermal properties (heat capacity, thermal conductivity) of the soil. In turn, thermal properties effect the surface radiant temperature and the soil resistance to diurnal changes of

temperature caused by external (solar radiation, air temperature, relative humidity, cloudiness) meteorological influences (Schmugge et al. 1980, Van de Griend et al. 1985). Good correlations were found between the diurnal range of soil temperature and soil moisture. Although, no unique relationship exist between temperature determined from TIR data and soil moisture for vegetation covered soils. Since for vegetated soils the surface temperature is an integrated value, including temperature effects of the vegetation layer and the soil the vegetation contribution has to be considered for soil moisture analyses.

Remote sensing using microwave sensors measure the electromagnetic radiation in the microwave domain between 0.75 and 100 cm, corresponding to frequencies between 40 GHz and 0.3 GHz. This microwave region is subdivided into specific bands, which are generally referred to by a lettering system (see table 1). Microwave remote sensing signals over bare soil targets are very sensitive to soil water content as it is directly linked to the soils dielectric constant which increases with increasing water content (Schmugge 1978, Ulaby 1986). For soil moisture retrieval studies the most important frequency bands are the L-, C- and X-band.

Table 1-1.   Microwave bands (Lillesand et al. 1994)

Band	Wavelength [cm]	Frequency [GHz]
Ka	0.75 – 1.10	40.0 – 26.5
K	1.10 – 1.67	26.5 – 18.0
Ku	1.67 – 2.40	18.0 – 12.50
X	2.40 – 3.75	12.5 – 8.0
C	3.75 – 7.50	8.0 – 4.0
S	7.50 – 15.0	4.0 – 2.0
L	15.0 – 30.0	2.0 – 1.0
P	30.0 – 100.0	1.0 – 0.3

The basic approaches in microwave remote sensing are distinguished into two categories: active and passive. Both, the radar backscattering coefficient and the brightness temperature measured by microwave radiometers depends on the incidence angle, frequency, wavelength, polarization and dielectric properties of the soil. Furthermore the sensitivity of both data products to soil moisture is hampered by surface roughness and vegetation.

Active sensors make use of a radar antenna, which transmits specific wave pulses and receives a return signal (reflectivity) whose intensity varies with the characteristics of the observed target. The signals send and received by a radar are usually polarized horizontally or vertically. The relationship between radar backscatter and dielectric constant is highly non-

linear. Using either, empirically and physically based soil moisture retrieval algorithms site specific successful results ($R^2 > 0.9$ between observed and modelled soil moisture) may be obtained for bare soils and vegetated soils at macro- scale (Bindlish et al. 2000, Srivastava et al. 2009). The model performance was generally found to be lower for vegetation covered soils as the backscattering coefficient of the soil is attenuated by the vegetation layer (Ulaby et al. 1982). Some studies found that the correlation between radar backscatter at C-band and soil moisture was poor at field scale and higher correlation where found at catchment scale where site specific effects seemed to average out (Alvarez-Mozos et al. 2005, Cognard et al. 1995). The vegetation effect on C-band may be even as significant as it is applicable for vegetation biomass retrieval (Mattia et al. 2003, Wigneron et al. 1999). The advantage in using mapping radar techniques compared to microwave radiometers is the higher spatial resolution. Therefore radar data is also proposed to support soil moisture studies within dis-aggregation procedures using passive L-band data (Narayan et al. 2006, Piles et al. 2009).

The first experiment to estimate soil moisture from microwave radiometers was performed in the 1970s (Schmugge et al. 1974). L-band penetrates vegetation better than C-band and X-band. Consequently passive microwave remote sensing of soil moisture at L-band is found as the most promising technique for global soil moisture monitoring except over dense forests (Prigent et al. 2005, Wagner et al. 2007, Wigneron et al. 2003). The background of this technique is the effect of the dielectric properties of the soil on the natural microwave emission from the soil (Schmugge et al. 1980). The dielectric constant can be calculated as a function of soil moisture and other soil parameters such as soil texture, soil salinity and bulk density. The most widely used dielectric models within the low frequency range (1-20GHz) are the Dobson Model (Dobson et al. 1985) and the Wang-Schmugge Model (Wang et al. 1980).

The brightness temperature T_B at L-band over a smooth bare soil measured by a radiometer is given by

$$T_B = e_P \cdot T_s, \tag{1.1}$$

where e_p is the soil emissivity at a specific polarization p (horizontal or vertical) and T_s the soil temperature. The equation (1.1) is determined from Plank's blackbody law through the Rayleigh-Jeans approximation for microwave frequencies (Schmugge 1985). Kirchhoff's reciprocity theorem relates the emissivity to the reflectivity r_s by

$$e_P = 1 - r_s. \tag{1.2}$$

The value range of soil emissivity exhibits from around 0.95 for dry soil (~ 5 Vol. %) to around 0.6 for wet soil (~ 40 Vol. %). Furthermore the soil layer depth contributing to the

soil emission depends on the soil moisture itself (Jackson et al. 1996, Schmugge 1983). If the soil is very wet, the soil emission originates mainly from layers at the soil surface. Conversely, for dry soils the emission contributing soil layer at L-band is deeper (e.g. more than 1 m for dry sand). In other words, the soil moisture retrieval using passive L-band data is typically dynamic in depth, as the soil goes from moist to dry, the depth to which the soil moisture estimate corresponds increase, since the depth over which the microwave emission originates increases. The impact of surface roughness on the soil emissivity is probably the most discussed parameter in soil moisture studies at L-band. In Wigneron et al. 2007 the roughness parameter is defined "as an effective parameter that accounts for (i) "geometric roughness" effects, in relation with spatial variations in the soil surface height, and (ii) "dielectric roughness" effects in relation with variation of the dielectric constant at the soil surface and within the soil which can be caused by non-uniformities in the soil characteristics". For rougher surfaces, the emissivity increases and the sensitivity to soil moisture decreases (Newton et al. 1980, Wang 1983). This effect may be interpreted as an increasing in soil surface area increases the emissivity. The roughness effect itself depends on the observation configuration, in terms of polarization and incidence angle and the soil moisture conditions. Above the soil, vegetation emits microwave radiation, whilst it absorbs and scatters the radiation coming from the soil (Jackson et al. 1996, Van de Griend et al. 1985). Therefore, the sensitivity of the passive L-band microwave signals to soil moisture changes depending on the characteristics of the soil coved vegetation. A more detailed discussion about vegetation specific influence on the L-band brightness temperature is provided in section 1.3 since it represents a major topic of this study.

Furthermore, in preparation of satellite missions and to support studies related to hydrology and climate numerous airborne L-band radiometer campaigns were performed during the last two decades. The probably most important experiments and basis for important studies related to soil moisture retrieval are collected in table 1.2.

Table 1-2.   Overview of important L-band radiometer campaigns.

campaign	spatial resolution	reference
HAPEX, FIFE, MONSOON '90	~ 100 m	Schmugge 1992, Wang et al. 1990
PORTOS'91, PORTOS'93	not defined (field scale, several rows)	Wigneron et al. 1993, Wigneron et al. 1995
Washita'92	coarse scale (200 m)	Jackson et al. 1995
Southern Great Plains'97	coarse scale (800 m)	Jackson et al. 1999
Southern Great Plains'99	coarse scale(> 100m)	Njoku et al. 2002
EuroSTARRS 2001	multiple scales (< 100m)	Saleh et al. 2004
SMEX'02	400 m	Narayan et al. 2006
SMEX'03	not defined	Ryu et al. 2007
SMEX'04	2 km, 3 km	Jackson et al. 2005
NAFE'05	1 km – 62.5 m	Panciera et al. 2008
NAFE'06	1 km	Merlin et al. 2008
SMAPVEX'08	1 km, 2.1 km, 4.2 km	Majurec et al. 2009

On November 2nd 2009 the European Space Agency's SMOS (Soil Moisture and Ocean Salinity Mission) satellite was launched as a first satellite using L-band specific for global soil moisture observations (Kerr et al. 2001). SMOS aims to provide global soil moisture maps with an accuracy better than 4 Vol. % every 3 days and a spatial resolution of ~ 40 km. The NASA's Soil Moisture Active and Passive Mission (SMAP) is planned to be launched in 2013 (Entekhabi et al. 2010). SMAP combines L-band radar and L-band radiometer, allowing simultaneous active and passive microwave observations of the same land surface target. By combining the radar and radiometer measurements in a joint retrieval algorithm, fine resolution (10 km) soil moisture maps will be provided.

1.3   Vegetation influence on passive L-band data

The retrieval of soil moisture and biomass are the fundamental applications of passive microwave remote sensing. Estimations of soil moisture from thermal microwave radiation are significantly affected by the soil's vegetation cover. For L-band microwave emission, the optical depth τ, defined as a one-way canopy absorption factor, is applied to parameterize the attenuation effect of the overlaying vegetation (Kirdyashev et al. 1979). Under most vegetation and soil conditions, the radiometric soil moisture sensitivity decreases approximately exponentially with increasing optical depth τ (Du et al. 2000). The scattering and absorption effects of L-band within a canopy are mainly affected by vegetation dielectric and geometrical characteristics.

Vegetation optical depth τ at L-band is well correlated to the dielectric properties and the vegetation water content (vwc) and increases with increasing water content (Jackson et al.

1982). Vegetation water consequently reduces the transmission of the soil brightness temperature. In several studies found in literature the optical depth τ is linearly related to the vegetation water content (Jackson et al. 1991, Panciera et al. 2009, Van de Griend et al. 2004). The effect of vegetation structure plays a significant role on the optical depth of standing vegetation (Saleh et al. 2006, Wigneron et al. 2007). Microwave emissivity at L-band is well correlated with soil moisture as the vegetation optical thickness is low for narrow vegetation layers and low biomass (Ferrazzoli et al. 2000, Jackson et al. 1991). Whereby, the vertical polarization suffers more vegetation effects than the horizontal polarization. However, if vegetation effects are considered in soil moisture studies, the vertical polarization is less sensitive to soil roughness variations and may be preferred for soil moisture estimations from soils with unknown roughness characteristics. Emissivity at L-band horizontal polarization over a whole wheat growing cycle showed an increase during the crop growing and decrease during crop drying (Ferrazzoli et al. 2000). This phenomenon is generally interpreted according to a very low scattering in the upper hemisphere of a wheat crop as a result of the near-vertical orientation of the stems and ears. Therefore, wheat behaves similarly to an absorbing layer. Furthermore the optical depth τ is strongly influenced by the incidence angle of the observation. The horizontal polarized brightness temperature suffers more attenuation through the vegetation at lower incidence angles. Therefore, generally higher incidence angles (incidence angle > 20°) are applied for soil moisture retrieval.

Vegetation effects on observed brightness temperature can be approximated well by a radiative transfer equation. The emission of vegetation canopy at L-band is usually expressed by the so called $\tau - \omega$ model which is a zero-order solution of the radiative transfer equation proposed by Mo et al. 1982 and applied in numerous studies (Brunfeldt et al. 1984, Brunfeldt et al. 1986, Jackson et al. 1991, Mo et al. 1982, Van de Griend et al. 1996, Wigneron et al. 1995). The zero-order solution assumes that the vegetation scattering phase matrix can be neglected for L-band. This model based on the optical depth τ and the single scattering albedo ω, which are used to account for the vegetation attenuation properties and the scattering effects within the vegetation canopy.

Beside incidence angle and polarization, in real application the vegetation influence varies from pixel to pixel, with the spatial resolution of the observation and with the phenological stage. Therefore, achieved relationships between the optical depth τ and a specific vegetation parameter (e.g. LAI or vwc) are valid only for a very specific phenological stage and site characteristics (e.g. soil type). For instance, model parameters evaluated e.g. for winter wheat during tillering are not consequently appropriate for applications at another phenological stage because of the high variation of vegetation water content and biomass during the growing cycle. Furthermore, model parameters retrieved on a specific spatial

scale (e.g. 200 m pixel resolution) using specific observation characteristics (polarization, incidence angle) can not simply applied on data sets having other observation characteristics. For example using the soil moisture retrieval algorithm proposed by Jackson et al. (1999) for 800 m TB observations Uitdewilligen et al. (2003) had to redefine the parameters for the data with a pixel resolution of 200 m in cause of underestimation. The higher resolution data required more site specific calibration.

At coarse scale (e.g. SMOS with ~ 40 km spatial resolution) significant spatial heterogeneity of soil moisture and vegetation cover appears (Panciera 2009). The effect of vegetation optical depth τ heterogeneity (0 – 0.6) was found to be significant with 6.1 Vol. % for computed soil moisture using simulated data for SMOS observation characteristics (Davenport et al. 2008). Therefore, the SMOS soil moisture retrieval algorithm account for the sub-pixel heterogeneity of land surface conditions by dividing the pixel into fractions determined using high resolution land use maps. As the influence of sub-pixel heterogeneity varies with the spatial footprint, scale dependent parameterizations of vegetation conditions are required. Therefore, a major research interest is the analyses and interpretation of vegetation effects on a sub-pixel scale level for different spatial resolutions to reduce the error in soil moisture estimates.

In general studies dealing with the problem of land surface heterogeneity on L-band soil moisture products can be categorised in i) analytical studies, ii) simulation experiments and iii) experimental data analyses. An overview about studies on sub-pixel heterogeneity is presented in table 1-3. In due to the physical nature of microwave radiometry at L-band the most analyses are performed on coarse scale data that represents spatial resolutions > 100 m within this thesis. The advantage of using analytical studies or simulated data sets is the great potential in analysing many different signal influencing factors at the same time and under controlled conditions (e.g. incidence angle, temperature fields). Simulation experiments apply more realistic connections of value ranges (e.g. for LAI, vwc, soil moisture, soil temperature) between different land surface factors. Ancillary data is generally derived from land surface process models. For example, the simulation experiment performed by Loew and Mauser (2008) showed strong scale dependent soil moisture retrieval errors on different coarse scales.

Table 1-3. Overview of analytical studies, simulation experiments and experimental studies according to sub-pixel influence of various surface parameters.

Analytical studies		
factor	*spatial scale*	*reference*
soil moisture, soil temperature, vegetation	not defined	Njoku 1996
soil type		Galantowicz et al. 2000
perturbation around mean soil moisture values, soil temperature, soil texture, NDVI (as proxy for vwc)	800 m	Bindlish et al. 2002
soil moisture, soil surface roughness, vegetation optical depth, (single and multi-angle data)	not defined	Davenport et al. 2008
multi-angle data	30 km	Van de Griend et al. 2003
land cover specific vwc	50km	Burke et al. 2004
Simulation experiments		
multi-angle, bi-polarised, soil texture, land cover, vwc, soil moisture	1km, 40 km	Loew et al. 2008
Experimental studies		
vwc, soil texture, soil moisture	see SGP'97 (table 1.2)	Burke et al. 2003
soil hydraulic conductivity, landuse, NDVI	see SGP'97 (table 1.2)	Bindlish et al. 2002
soil moisture, vegetation cover, soil temperature, soil texture, surface roughness	see NAFE'05 (table 1.2)	Panciera 2009

Nevertheless, in reality the quantities of surface parameters and the intermixture of land surface patches varies and consequently hamper the transfer of parameter values, proposed correlations and methods. Obviously there is a lack of information based on experimental data to address the effect of vegetation on high spatial resolution brightness temperature observations at L-band within a vegetation canopy previously have been assumed homogeneous (e.g. agricultural fruits).

1.4 Research objectives and thesis organisation

Given the deficit mentioned above, the aim of the study is the assessment of surface soil moisture below a crop representing a vegetation canopy that previously had been assumed to be homogeneous. Therefore the thesis deals with the analyses of experimental high spatial resolution L-band radiometer data according to i) its vegetation influence and ii) its sensitivity for soil moisture retrieval over crops during dry conditions. The key questions of the study are as follow:

1)   Is there a unique relationship between LAI and high spatial resolution L-band brightness temperature at sub-pixel level?

2)   Does the combined use of L-band data and hyperspectral vegetation indices provide reasonable estimates of surface soil moisture using empirical models?

3)   How strongly does the temperature information affect the soil moisture estimates using the land surface parameter retrieval model (LPRM)?

4)   Is there a relationship between within field variations of the vegetation canopy and the roughness parameter used with the land surface parameter retrieval model (LPRM)?

Therefore, the study involves:

-    collection of airborne L-band radiometer and imaging spectrometer data

-    collection of ground truth data

-    assessment of the effect of inner-field heterogeneities of a "pseudo"- homogeneous vegetation layer on the microwave emission

-    understanding the link between vegetation characteristics and spatial dynamic of L-band brightness temperature observations

-    testing empirical models for soil moisture estimation using spectral narrow band vegetation indices to account for the spatially changing optical depth

-    testing of the land surface parameter retrieval (LPRM) approach as a physically based model to retrieve soil moisture below a crop canopy

Chapter 2 provides information about the experimental data set and test site characteristics. Campaign specific information about the characteristics and data handling for the airborne passive microwave data and applied imaging spectroscopy data is given. The field data sampling of soil moisture and vegetation characteristics is described. A correlation analyses between LAI and brightness temperature observations and calculated emissivity for crops is performed in Chapter 3. Within Chapter 4 a combined empirical analyses of L-band radiometer data and spectral vegetation indices for surface soil moisture retrieval is presented. Chapter 5 evaluates the performance of the land surface parameter retrieval (LPRM) to compute soil moisture for the test sites and occuring soil moisture conditions. Chapter 6 gives a general conclusion and recommendation for future work. A summary about the complete thesis is presented in Chapter 7.

The chapters of this thesis, apart from the introduction (Chapter 1), the general conclusion (Chapter 6) and summary (Chapter 7), have been written as stand alone manuscripts to be submitted for peer reviewed scientific journals. Hence, Chapter 3, 4 and 5 can be read separately from the rest of the thesis. As a result, overlaps occur mainly in the chapters "Introduction" and "Data".

2. Test site and data set

The investigations carried out within this study were focussed on crops, namely winter barley (~27 ha) and winter rye (~37 ha). The test sites are located in south-east Germany near the city Leipzig (see figure 2-1). Land use in the area is dominated by agricultural crop production. The specific selection of the two test fields was determined by factors such as accessibility and the fact that the sites are within a catchment which is well monitored in terms of water and nutrient fluxes. The topography is gently sloping and the fields consist of loamy sand with ~ 52 % sand and ~ 11 % clay.

The airborne remote sensing and field data collected within this study belongs to very early TERENO (Terrestial Environmental Observatories, Bogena et al. 2006) activities within the Harz/Central German Lowland observatory which is coordinated by the Helmholtz Centre for Environmental Research – UFZ in Leipzig. Within TERENO, these data are part of the long term monitoring concept for hydrological process studies of the local and regional scale.

Within this chapter, section 2.1 and section 2.2 give information about the airborne remote sensing data, main sensor characteristics and data specific processing steps respectively using an L-band radiometer and an imaging spectrometer. Note that each of the two remote sensing data products is available for only one day with a time shift of 15 days between the passive microwave and imaging spectrometer data. Section 2.3 provides information about the field data collected during the whole growing cycle from the specific test sites in the year 2008.
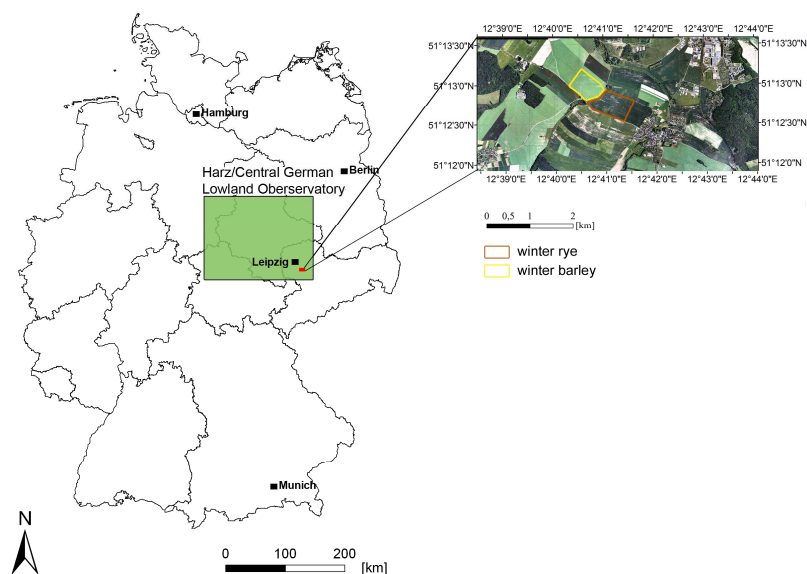
Figure 2-1.   Location of the two crop sites within Germany and the Harz/Central German Lowland observatory of TERENO.

2.1 Airborne L-band microwave radiometer data

The passive microwave data was achieved with the Polarimetric L-Band Multi-beam Radiometer (PLMR) developed by ProSensing (ProSensing Inc. USA) and owned by an Australian scientific consortium. For the flights in Germany, the sensor was fitted to the Enviscope Partenavia PA68 D-GERY. On May 26, 2008 (DOY 147) four test areas within the TERENO Harz/Central German Lowland observatory were flown (see figure 2-2) to collect passive microwave brightness temperature data. The background for the initialization of the campaign was the evaluation of the PLMR sensor for long-term soil moisture monitoring in TERENO. Consequently the L-band data is available at only one day and for the adjacent soil and vegetation conditions (see section 2-3) because there was a temporal scope of demand.
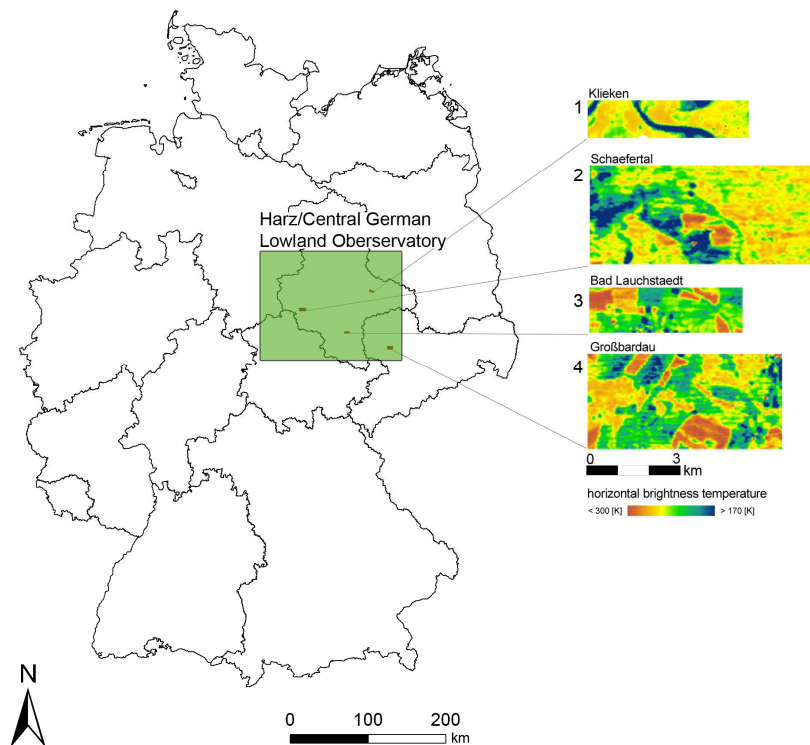
Figure 2-2.   Location of the four test sites flown with the PLMR on May 26, 2008 as part of the TERENO Harz/Central German Lowland observatory. (Note that soil moisture and vegetation analyses were performed only for the data set Grossbardau.)

All analyses within this study related to the outlined issues (see section 1.4) are performed using the Grossbardau data because of its site characteristics and the availability of appropriate ground truth data. The PLMR observations for Grossbardau were obtained between 9 and 10 am in the morning.

PLMR is a dual-polarized L-band radiometer which uses six pushbroom patch array receivers with incidence angles of 7°, 21.5° and 38.5° (see figure 2-3). Vertical and horizontal brightness temperature is measured for each beam position using a polarization switch. The six beams were orientated across track to provide an image. A reduced antenna beam width and a specific flight plan, flying low and slow, ensured a final pixel size of 50 m. All radiometric and geometric pre- and post flight calibration were performed by Airborne Research Australia (Adelaide/Australia).
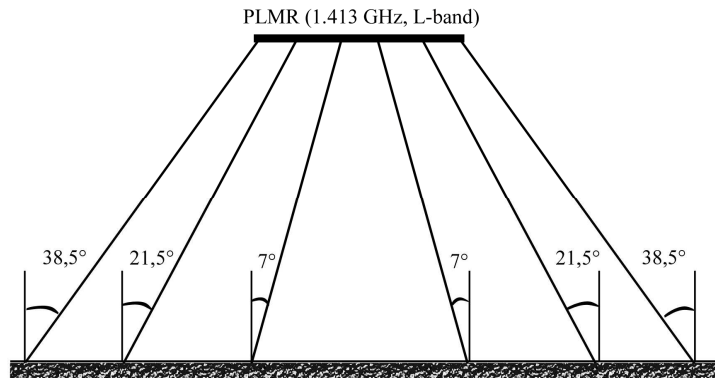
Figure 2-3.   PLMR viewing angles.

During the campaign warm (blackbody) and cold (sky) point calibrations were performed before and after each flight. Figure 2-4 presents the PLMR sensor during cold point calibration. Each target (blackbody or sky) was observed for 15 minutes. Beam specific calibration coefficients of the brightness temperature at both polarizations were retrieved by averaging pre- and post-flight coefficients. The radiometric calibrated PLMR data were georectified taking into consideration the geographical position and inertial navigation information (roll, pitch, yaw) recorded for each measurement. The beam centres were projected on a 90 m digital elevation model of the study sites.

Figure 2-4.   PLMR during cold point calibration orientated to the sky. The picture was made during another campaign in Narranda, Australia in December 2009.

Over homogeneous bare soil target, the measured TB is affected by the viewing angles (Ulaby 1986). The angular variations on observed horizontal and vertical brightness temperature can be described by the Fresnel equations and differ depending on the land surface characteristics and conditions and have to be considered during data analyses. Previous studies using similar instruments applied normalization procedures to mixed land covers (Jackson 2001, Jackson et al. 1999). This procedure assumes that the deviation between beam positions is due to the Fresnel effect and that for individual beams the calibration errors are constant for a range of soil moisture and vegetation conditions. Using single flight lines for this correction can lead to errors if the land surface heterogeneity is strong. Therefore, mostly daily averages of viewing angle dependent TB data were used to calculate correction terms for the individual beam positions. This assumption should be not valid in the TERENO study area and for the collected PLMR data, since the test sites show high variations in their land surface characteristics that result in different microwave response as can be seen on the value range of the horizontal TB data in figure 2-2. Hence, for the data used in this study, no campaign averages of the TB data were used to calculate correction terms for viewing angle normalization. Therefore, only flight line sections were applied to calculate correction terms. These were selected individual for each test site over an area with known and homogeneous land surface conditions. As the applied procedure is part of a further section, more detailed and site specific information is provided in chapter 4.3.1 and 4.4.1. Nevertheless, as the viewing angle influence visually appears as a stripe effect, an example of pre- and post correction is presented in figure 2-5. As can be seen, the results differ depending on the polarization and the horizontal TB image appears smoother.

horizontal polarization

vertical polarization

without viewing angle normalization

viewing angle normalization to 38.5°

brightness temperature [K]

300   170
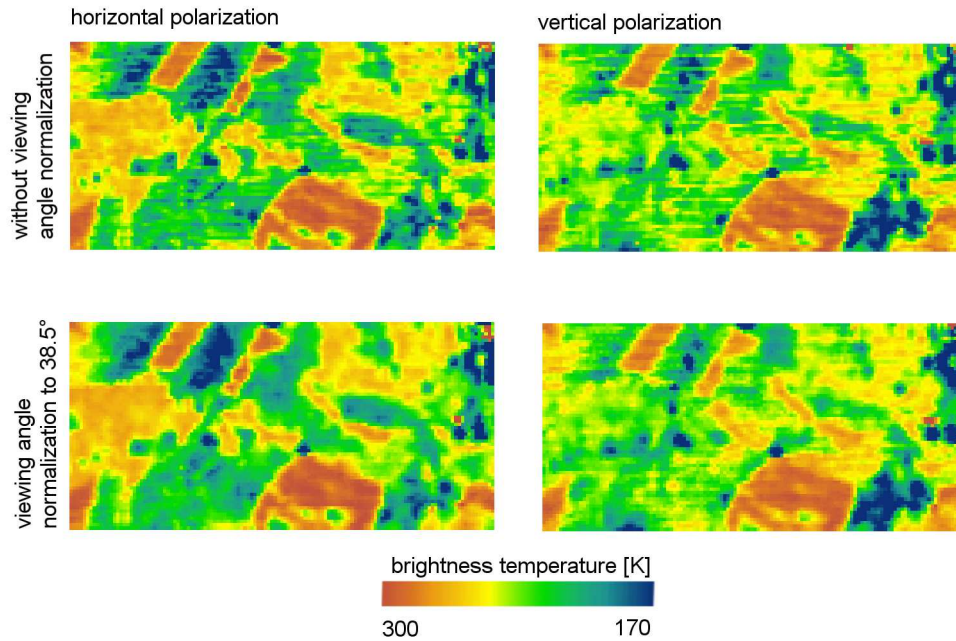
Figure 2-5.   PLMR brightness temperature of horizontal and vertical polarization before and after viewing angle normalization.

To obtain surface soil moisture estimates from passive microwave observations, knowledge about the soil effective temperature is required as the emission at L-band is a function of the physical temperature of the emitting layer. It is not possible to measure soil temperature below a vegetation canopy using satellite or airborne remote sensing techniques. However, the acquisition of TIR observations together with the L-band passive microwave data provides composite information about vegetation and soil surface temperature. Furthermore, those data can provide excellent estimates of the spatial distribution of land surface temperature since the measurements are already spatially integrated. Therefore on all PLMR flights also an InfraTec thermal imager was also operated to provide land surface temperature data T_{TIR} (see figure 2-6). The camera detects thermal infrared radiation of a spectral range between 7.5 – 14 μm and the emissivity was set to 0.98.

TIR land surface temperature

290 [K] 297
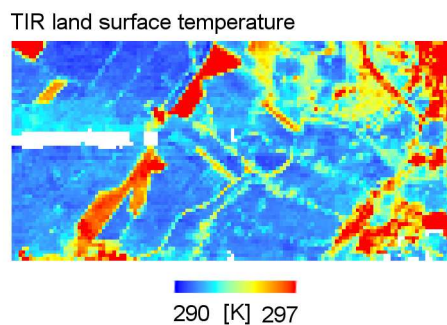
Figure 2-6.   TIR land surface temperature image of the test area Grossbardau.

The TIR data was used to calculate surface emissivity at L-band as it is given by equation (1.1). Figure 2-7 presents a spatial image of calculated emissivity for the two polarizations. As expected from theory the emissivity for the vertical polarization is higher than for the horizontal data normalized to the outer beam positions. The effect can be explained by an increasing of the optical depth τ for the vertical polarization with increasing viewing angle.
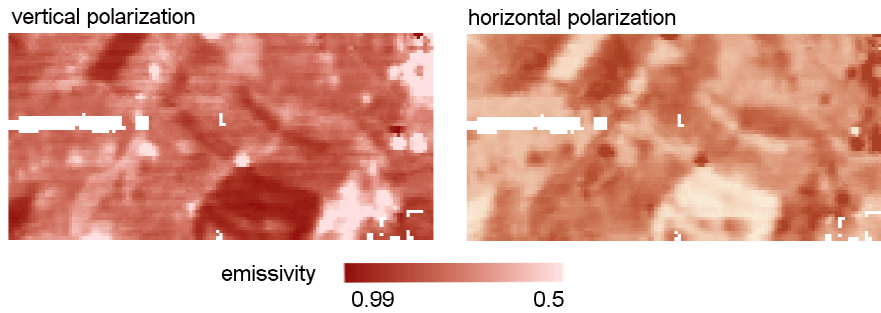
Figure 2-7.   Spatial images of calculated emissivity from horizontal (right) and vertical (left) PLMR brightness temperature (normalized to 38.5°) using TIR temperature data.

2.2   Airborne imaging spectrometer data

Vegetation conditions play a crucial role in the retrieval of soil moisture from passive L-band microwave data. Since vegetation absorbs, emits and scatters microwave radiation, the vegetation influence on observed brightness temperature observations varies spatially and temporally with the vegetation conditions. Therefore, a "perfect" case would be a contemporary acquisition of L-band data and an optical remote sensing data product (multi or hyperspectral) of similar or even finer spatial resolution to provide real-time information about the soil covered vegetation.

In the framework of this study AISA Eagle (Airborne Imaging Spectro-Radiometer for Application, SPECIM – Spectral Imaging Ltd. 2007, Finland) airborne imaging spectrometer data within the visible and near infrared range of the solar spectrum from 400-970 nm was collected. As the acquisition of hyperspectral data requires clear skies (no clouds), a flight could only be performed at June 10, 2008 (DOY 162). For the campaign the AISA-EAGLE sensor, together with a GPS/INS unit RT3100 (Oxford Technical Solutions LTD., UK) was fitted to the Microlight aircraft (Trike, D-MUFZ) owned by the Helmholtz Centre for Environmental Research UFZ in Leipzig, Germany (see figure 2-8).

Figure 2-8.   Microlight aircraft (Trike, D-MUFZ) owned by the Helmholtz Centre for Environmental Research UFZ in Leipzig, Germany

AISA comes with the operating software RS Cube to set campaign specific frame rate, exposure time and binning and monitor the GPS and INS status as well as the image quality e.g. in terms of saturation effect. Campaign specific settings are presented in table 2-1. During image acquisition the raw image file and header file, dark image data stored together with the raw image file, the navigation file containing GPS/ INS data and a log file containing information about the missing frames are recorded and stored. Radiometric calibration and geo-rectification is performed using CaliGeo software provided from SPECIM which runs as an ENVI/IDL plug-in. The data is proposed to achieve a Signal-to-Noise Ratio of 350:1 – 500:1 depending on the spectral settings.

Table 2-1.   Applied AISA Eagle specifications

parameter	campaign specific setting
spectral binning	2x
spectral bands	252
spectral sampling	2.3 nm
focal length	9 mm
FOV (field of view)	62.1°
spatial ground resolution	1.5 m
image rate (fps – frames per second)	30

Atmospheric correction was performed using ENVI FLAASH which cooperate the MOD-TRAN-4 radiation transfer code. The atmospheric model applied was Mid-Latitude-Summer. The water vapour factor was set to 1. The ground visibility was greater than 40 km during data acquisition and the no aerosol retrieval was applied. In figure 2-9 a spatial subset of the AISA data set over winter rye is presented.
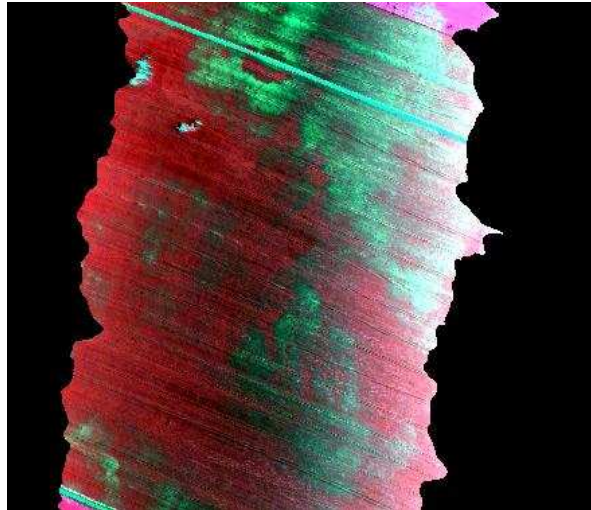
Figure 2-9.   Colour infrared image of an AISA Eagle swath collected over winter rye on
June 10, 2008.

2.3   Field data sampling

To provide information about inner-field vegetation and surface soil moisture heterogeneity
as basic ground truth assumption for the remote sensing data analyses field campaigns were
performed during the airborne data acquisition on DOY 147 (AISA flight) and DOY 162
(PLMR flight). Additionally, information about the temporal behaviour of vegetation char-
acteristics and surface soil moisture is provided from field campaigns during the whole
growing cycle. Therefore, 43 sampling points on the winter barley and 47 on the winter rye
site were used as ground truth points (see figure 2-10) and measured in a regular 14-days-
interval. The sampling point coordinates were located using a handheld GPS device (Leica
GS20 Professional Data Mapper, Leica Geosystems). The sampling profiles were placed 1.5
m parallel to the machine tracks and along the complete field. This procedure avoid damage
within the vegetation canopy and realizes the collection of within row measurements since
the canopy very close to the machine track appears generally more dense. The differences
can be due to slight differences in water supply, seed density and agricultural machining or
the amount of incoming radiation.
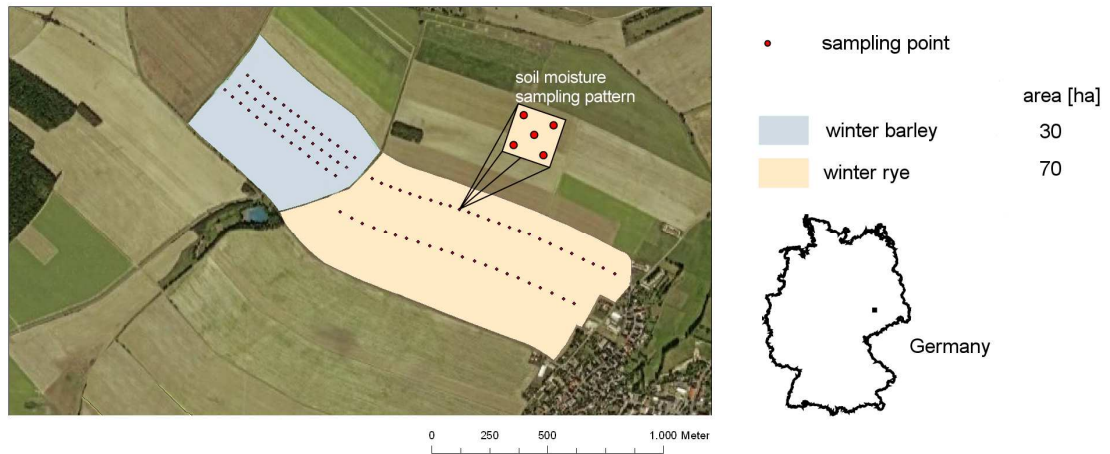
Figure 2-10.   Aerial photograph of the winter barley and winter rye test sites and ground sampling pattern located in south-east Germany. The smaller patch indicates the five single soil moisture measurements.

Field surface soil moisture data was measured at eight field campaigns during DOY 86 and DOY 189 in 2008. The measurements were performed using ThetaProbe ML2x Probes (Delta-T Devices, Ltd., Cambridge, UK). The probe length of 6 cm provided average moisture content of the upper soil layer that is representative for the signal contributing soil layer at L-band (Schmugge 1983). The temporal soil moisture dynamic for the growing cycle 2008 of the two test sites is presented in figure 2-11. Around the peak of the biomass increasing phase (see figure 2-13 (e) and (f)) at DOY 134 and 147 the soil moisture conditions were very dry and the field mean soil moisture did not exceed 15 Vol. %. During this time period the soil surface appeared as a solid crust as a result of a longer drought. Because surface soil moisture appears highly variable during the day at the acquisition of the passive microwave data (DOY 147) soil moisture was measured $\pm$ 1 h of the flight.
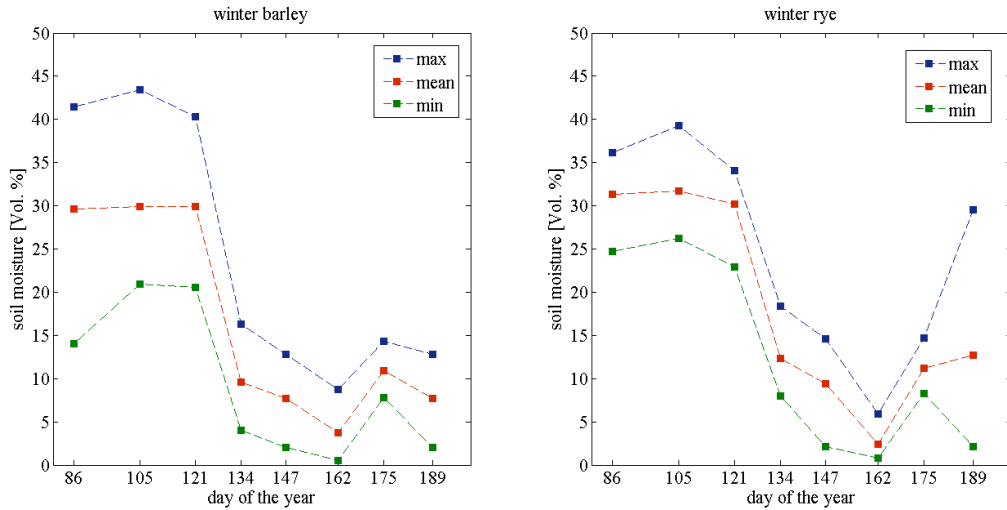
Figure 2-11.   Temporal behaviour of ground measured surface soil moisture of the top 6 cm for the winter barley (left) and winter rye (right) test site.

Each soil moisture value was achieved by averaging five single measurements at each sampling point location to represent soil moisture ground truth. The number of samplings is a compromise between operational effort and the fact of minimizing the error of the representative mean soil moisture value. For the soil moisture sampling on DOY 147 (PLMR campaign), the standard error of the mean (SEM_{sm}) was calculated by

$$SEM_{sm} = \frac{s}{\sqrt{n}}$$ (1.3)

where s is the standard deviation of the soil moisture measurements and n is the number of the soil moisture samples. The average SEM_{sm} is 0.63 Vol. % and the relationship of the single SEM_{sm} values to the mean soil moisture value at each sampling point for DOY 147 is shown in figure 2-12.
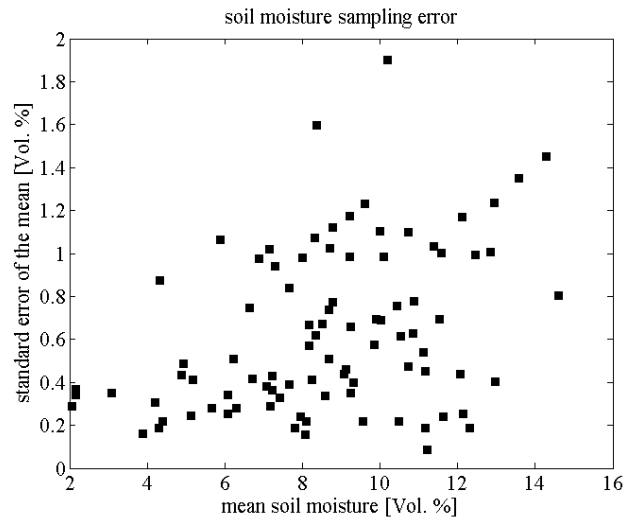
Figure 2-12.   Scatter plot of the standard error of the mean vs. the mean soil moisture value for the soil moisture field sampling on the winter barley and winter rye site on DOY 147.

The monitoring of inner-field vegetation canopy characteristics were performed on six field campaigns for winter barley (DOY 105 – 175) and seven for winter rye (DOY 105 – 189). The differences in the number of campaigns are due to an early harvest of winter barley. Parallel to airborne remote sensing campaigns (DOY 147 and 162) leaf area index (LAI) and canopy height were measured at every sampling point. For all other dates, only data of every second sampling point was collected due to limited personal capacities.

LAI is a dimensionless value representing the ratio of total upper leaf surface of a vegetation canopy divided by the land surface area on which the vegetation grows. LAI was measured using a LI-COR, Inc. (Lincoln, Nebraska, USA) LAI-2000 Plant Canopy Analyzer, which is a handheld technique and a quite rapid method for field applications. The measurement principle relies on the strong dependency between canopy structure and gap fraction of the canopy. The gap fraction corresponds approximately to the transmittance of radiation of those wavelengths were the scattering by foliage can be neglected. As the measurements have to be performed under diffuse light conditions the data sampling was generally conducted at dawn or under clouded sky during the day. The measuring technique compares sky brightness above the canopy with the below-canopy light level while the sensor is viewing skywards. Light levels are detected in five conical rings, with the view zenith angle ranging from 0 to 75°, to infer LAI (Welles et al. 1991). To exclude the effect of varying measurement orientation the below and above measurements were carried out with the same azimuth direction and the same observation height. At each sampling point location, three LAI measurements got sampled where each single value is an average of six observations. Its seasonal trend for winter barley and winter rye can be seen in figure 2-13 (a) and (b). Canopy height

was simply measured using a foot rule by averaging ten single measurements (see figure 2-13 (c) and (d)).

Destructive biomass sampling was performed to retrieve fresh biomass and vegetation water content (vwc) in a unit of kg per m² using weighing method. Therefore, a defined frame of one square meter extent and divided in four sub-squares was put on the sampling point location and three plants were taken out of two sub-squares. The plants were cut directly above the ground. To retrieve the stand density per m² all single plants were counted inside four sub squares of the frame and calculated by averaging the single counts. Because of field data sampling in regular intervals on the test sites, no complete square meter samples of biomass could be taken. The plant samples were packed in plastic bags, transported to the laboratory and weighed. After oven drying at 105° C until constant weight (~ 24 h) the plants were weighed again to calculate vwc as defined as the difference between fresh and dry biomass.
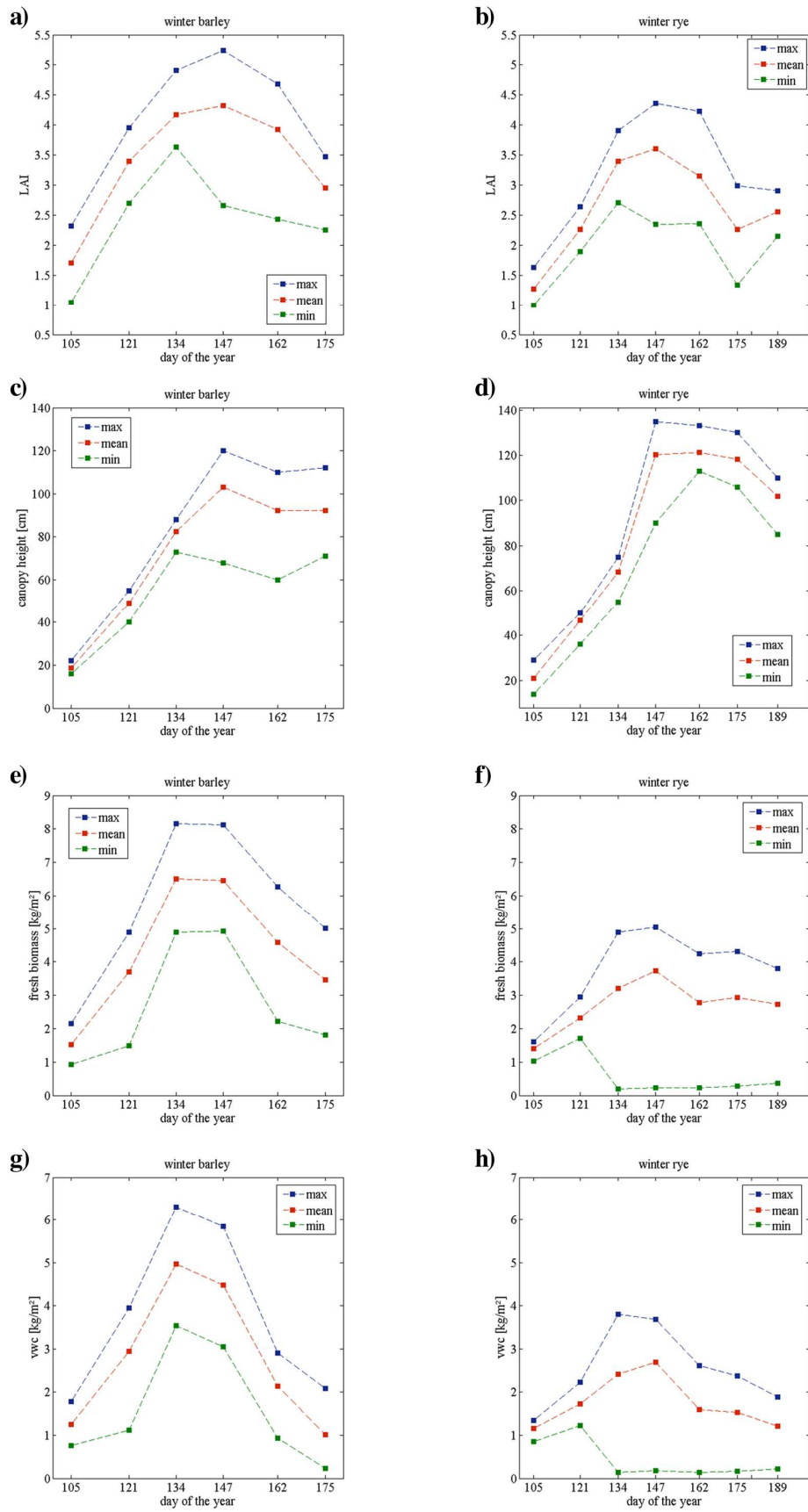
Figure 2-13.   Temporal behaviour of vegetation parameters of winter barley and winter rye for the growing season 2008.

The vegetation monitoring also included the sampling of proxy for vegetation canopy "greenness". The motivation for this was the analyses of optical remote sensing data products for fresh (green) biomass monitoring which is not part of this thesis. Nevertheless, the temporal dynamic of the leaf chlorophyll content was observed using a handheld Chlorophyll-Meter SPAD-502 (Minolta) (see figure 2-14). The SPAD-502 measures the transmittance of plant leaves in the red and near-infrared spectral regions. The ratio of these two transmittances is proportional to the total leaf chlorophyll content. Ten single measurements were averaged at each sampling point, whereby the single measurements were collected from the uppermost leaves of various plants.
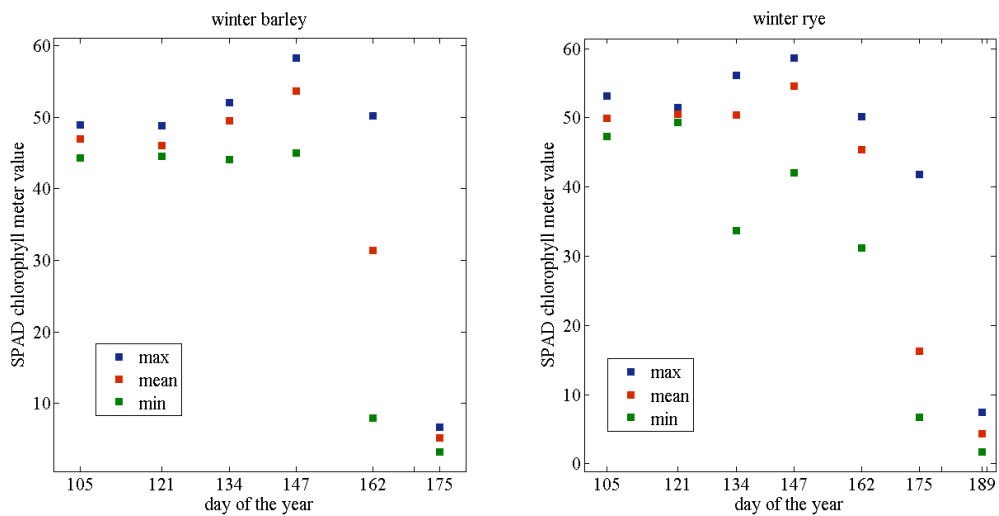
Figure 2-14.   Temporal behaviour of leaf chlorophyll content represented by SPAD chlorophyll meter measurements.

The airborne remote sensing and field data described provide the basis for the analyses presented in the following chapters. Note that the L-band soil moisture campaign was performed only once over the test site and the soil moisture conditions at the day of the experiment were very dry (~ 9 Vol. %). There was no study found in literature analysing passive L-band data for soil moisture retrieval under such extreme conditions and narrow value range (standard deviation 2.8 Vol. %).

3. Vegetation influence on high spatial resolution airborne L-band brightness temperature observations on homogeneous land cover

Vegetation structural parameter such as leaf area index (LAI) are well known for exhibiting significant control over passive microwave signals e.g. during the retrieval of land surface soil moisture conditions. Within this chapter, the functional relationship between LAI as a vegetation structural parameter and high spatial resolution (50 m) airborne L-band brightness temperature observations at two polarizations (h, v) and two viewing angles (7°, 38.5°) are investigated. L-band brightness temperature and airborne imaging spectrometer data as well as local scale leaf area index (LAI) measurements were obtained from two test sites, a ~27 ha winter barley and a ~38 ha winter rye field located in south-eastern Germany. Regression analysis between narrow band spectral vegetation indices and local scale LAI observations allowed field-wide mapping of LAI at a 1.5 m resolution, thus providing information about sub-pixel heterogeneity of plant structural conditions within the passive microwave pixel. The results show an obvious dependency of the microwave signal dependent on i) the PLMR pixel average LAI, ii) sub-pixel variability of LAI, and iii) the angle of normalization within field scale.

3.1 Introduction

Low-frequency passive microwave radiometers (L-band) have been found to be the most promising remote sensing method for monitoring surface soil moisture patterns due to the direct link between microwave radiation and dielectric properties, its deeper penetration into vegetation and its negligible atmospheric attenuation (Jackson et al. 1999, Schmugge, T. 1983, Wagner et al. 2007).

L-band brightness temperature (TB) has a nearly linear relationship to surface soil moisture, given homogeneous vegetation and soil characteristics. However, in practice, the vegetation influence changes spatially and has a major influence on final soil moisture products since it reduces the sensitivity of the observed TB to soil moisture changes (Jackson et al. 1996, Van de Griend et al. 1985). The vegetations optical depth characterizes the physical connection between vegetation cover (optical depth) and soil moisture while depending on vegetation dielectric properties and geometrical plant characteristics. The so called 'τ-ω' model is a widely used approach making use of the optical depth and the single scattering albedo to characterise the absorption and scattering of the soil signal through the vegetation canopy

(Mo et al. 1982). The optical depth for the microwave emission at L-band is very sensitive to vegetation water content in due to its direct link to the dielectric properties and can be expressed as a linear function of vegetation water content for L-band applications (Jackson et al. 1982, Wigneron et al. 1993). Therefore, it is validly recommended to provide information about vegetation water content during L-band soil moisture observations over vegetated areas.

Since vegetation water content measurements are impractical from an operational viewpoint due to the requirements of destructive plant sampling and laboratory analyses other vegetation parameters or proxy in terms of vegetation indices are applied in soil moisture retrieval studies using L-band data. Parameters used to account for the optical depth are commonly estimated empirically and are validated for specific vegetation type and occurring phenological characteristics (Jackson et al. 1991, Jackson 1993, Njoku 1996). The application of vegetation indices retrieved from land surface models (leaf area index - LAI) or optical remote sensing data (spectral vegetation indices) showed reasonable relationships to optical depth and to account for the vegetation influence on passive L-band microwave observations (Jackson et al. 2004, Jackson et al. 1999, Saleh et al. 2006).

Experimental studies to investigating the effect of vegetation on soil moisture retrieval were performed with varying but generally coarse (> 100 m) spatial resolution (Burke et al. 2003, Jackson et al. 1999, Ryu et al. 2007, Saleh et al. 2004). Since the effective optical depth of a mixed pixel is known to be scale dependent and generally decreases with coarser spatial resolution, information is therefore not generally transferable between spatial scales. Accordingly, a lack of information exists for the application of high spatial resolution L-band data (< 100 m) for small scale analyses with the assumption of heterogeneity within a homogeneous land use target (e.g. agricultural crops).

Therefore, the investigation of this paper is applied on field scale and focused on LAI as it represents a structural vegetation factor characterising the optical depth. The influence of LAI on L-band brightness temperature observations (50 m x 50 m) at horizontal and vertical polarization is thereby analysed on a sub-pixel level using pixel average values for LAI. Spatial high resolution (1.5 m x 1.5 m) data about LAI was achieved from regression models using field measurements and spectral narrow band vegetation indices. The latter were calculated from airborne imaging spectrometer data collected over the test sites. The achieved grid maps of LAI produced were treated as ground truth. To investigate the viewing angle effect according to the mentioned issue of this study, the observed TB data was normalized to 7° and 38.5° viewing angles. Regression analyses with LAI as independent variable were finally performed for the two polarizations, a microwave polarization index and calculated emissivity on uncorrected and viewing angle normalized TB data (dependent variables). The

microwave data was achieved from flight campaigns with the polarimetric L-band micro-wave radiometer PLMR over a test site of TERENO (Terrestial Environmental Observatories, www.tereno.net) (Bogena et al. 2006) in Germany.

Section 3.2 gives an overview about data characteristics and section 3.3 presents the results analyzing the relationship between LAI and the L-band brightness temperature data. This is followed by a discussion and conclusion in section 3.4.

3.2   Data

The data used for the presented study belongs to the TERENO/ PLMR soil moisture experiment performed in May 26th 2008 over the Harz/Central German Lowland observatory. For the study presented here, only field and airborne data achieved from two crop sites is used (see figure 3-1).
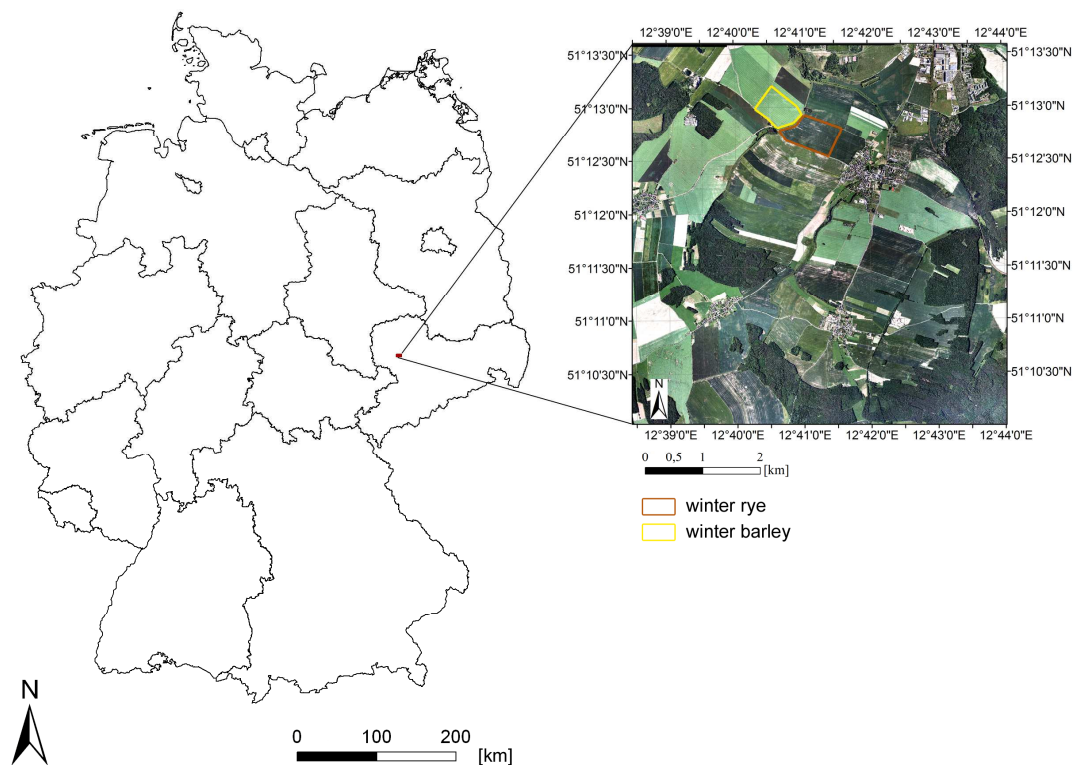
Figure 3-1.   Location of the two crop sites within Germany.

3.2.1   L-band brightness temperature data

PLMR (frequency = 1.413 GHz) utilizes six pushbroom patch array radiometer receivers with observation angles of ±7°, ±21.5°, and ±38.5° (Panciera et al. 2008). Together with the

TB observations, surface temperature (T_{TIR}) information was collected by a thermal infrared sensor flown together with the PLMR. The PLMR and T_{TIR} data were pre-processed by Airborne Research Australia (ARA) for aircraft movement and attitude. Pre-flight and post-flight calibration data were used at that stage. The PLMR data was provided with a ground resolution of 50 m.

Since the microwave brightness temperature observations are affected by the observation angle (Ulaby 1986), a viewing angle normalization was performed by correction term calculations (Jackson 2001, Jackson et al. 1995). In contrast to Jackson et al. 1995 only a flight line section was selected from the whole PLMR data set to calculate the correction terms since the completely flown area is very heterogeneous. Therefore, the flight line section was selected within a homogeneous land surface target covering all six beam positions.

To analyse the vegetation influence on the TB data dependent on different observation angles the normalization procedure was applied to two beam positions. Therefore the PLMR TB data of the horizontal and vertical polarization was normalized to the 7° and to the 38.5° viewing angle position:

$$TB_{ij}^N = TB_{ij} + (\overline{TB_{ij}} - \overline{TB_{ijREF}}) \qquad\qquad (3.1)$$

j = viewing angle (7° or 38.5°)

i = polarization (v - vertical or h - horizontal)

$\overline{TB_{ij}}$ and $\overline{TB_{ijREF}}$ are the averages of the flight line sections selected for the viewing angle correction whereby the latter is the viewing angle taken as reference.

Three processing stages; i) uncorrected TB, ii) 7° corrected TB and iii) 38.5° corrected TB of the PLMR horizontal and vertical polarization were finally used to calculate a microwave polarization difference index (MPDI) and microwave emissivity e at L-band.

The microwave polarization difference index (MPDI) is defined as the normalised difference between vertical and horizontal polarization and is proposed to account for the vegetation influence on the L-band signal. In this study it was calculated for all three processing stages from PLMR data:

$$MPDI = \frac{(TB_{vj} - TB_{hj})}{(TB_{vj} + TB_{hj})} \cdot \qquad\qquad (3.2)$$

The index j reefers to the processing stage. Surface temperature T_{TIR} data was used to calculate the emissivity for the two polarizations and three processing stages:

$$e_{ij} = \frac{TB_{ij}}{T_{TIR}}$$
(3.3)

3.2.2 Vegetation parameter information

To avoid influence dependent on vegetation type on the analysed correlations and focus the study as much as possible on leaf area index, a homogeneous land surface target was selected using winter barley (~27 ha) and a winter rye (~38 ha). At the day of PLMR data acquisition (May 26, 2008) the main phenological stage of the two crop types was flowering (main shoot). Whereby for winter barley the flowering was more pronounced and fruit sets were mostly visible. Average vegetation water content for winter barley and winter rye was approximately 2-3 kg m^{-2} respective to the apparent phenological stage and confirmed by random field samples.

Field LAI data was used to generate bi-variate regression models using spectral narrow band vegetation indices as independent variables for spatial empirical modelling of LAI. Therefore high spatial resolution (1.5 m) imaging spectrometer data from an AISA (airborne imaging spectro-radiometer for application) flight campaign and field data from the June 10th 2008 were used. Spatial distributed field LAI data was provided from measurements using a LI-COR, Inc. (Lincoln, Nebraska, USA) LAI-2000 Plant Canopy Analyzer. Finally, derived bi-variate regression models were used to generate LAI maps of 1.5 m resolution that serve as spatial distributed ground truth for LAI with 1.5 m spatial resolution (see figure 3-2). For winter barley, the Plant Senescence Reflectance Index PSRI (Merzlyak et al. 1999) and for winter rye the Modified Triangular Vegetation Index MTVI-2 (Haboudane et al. 2004) showed best results (R²=0.58 and 0.67 respectively) for estimating LAI. The time shift of 15 days between PLMR and AISA data acquisition is thoroughly critically, however, the further analyses presented in this study still proving their applicability.
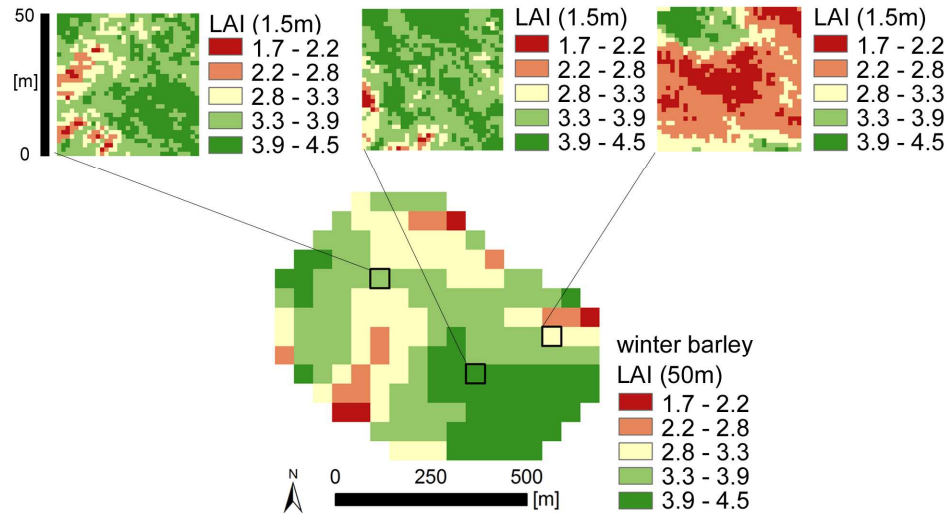
Figure 3-2.   Visualization of sub-pixel heterogeneity of LAI for winter barley within three examples of 50 m x 50 m PLMR pixel.

3.3   Zone statistics and regression analyses

110 pixels from the winter barley and 152 pixels of the winter rye field from the PLMR data set were used for analysing the influence of LAI to i) L-band brightness temperature TB at horizontal and vertical polarization, ii) to emissivity at L-band at the two provided polarizations and iii) to the microwave polarization ratio MPDI. All analyses were performed for the uncorrected data and the two processing stages for the viewing angles. Between the two crop types slight differences of the mean values and standard deviation within each data set occur (see table 3-1). The correlation between PLMR observations and LAI were investigated using bi-variate regression and compared by its coefficient of determination (R^2) which are given for the TB data in the result figures 3-5 and for the emissivity in table 3-2.

Table 3-1.   Value ranges, mean values and standard deviation of analyzed PLMR data and associated MPDI and emissivity for the winter barley and winter rye site (h – horizontal polarization, v – vertical polarization, un – no viewing angle normalization applied, 7° - normalized to 7° beam position, 38.5° - normalized to 38.5° beam position).

PLMR observation	winter barley				winter rye			
	min	max	mean	std	min	max	mean	std
TB h 38.5° [K]	237	256	244	3.62	240	268	252	7.1
TB v 38.5° [K]	257	274	268	3.39	260	280	273	4.3
TB h 7° [K]	242	262	250	3.83	244	271	256	6.69
TB v 7° [K]	254	268	263	3.01	255	275	268	4.65
TB h un [K]	238	261	248	4.7	241	272	254	7.13
TB v un [K]	254	271	264	3.76	255	277	269	5.02
MPDI 38.5°	0.03	0.06	0.05	0.01	0.02	0.05	0.04	0.01
MPDI 7°	0.01	0.04	0.03	0.01	0.01	0.04	0.02	0.01
MPDI un	0.02	0.06	0.03	0.01	0.01	0.05	0.03	0.01
e h 38.5°	0.8	0.87	0.83	0.01	0.81	0.91	0.86	0.02
e v 38.5°	0.87	0.93	0.91	0.01	0.88	0.95	0.93	0.01
e h 7°	0.83	0.89	0.85	0.01	0.83	0.92	0.87	0.02
e v 7°	0.87	0.92	0.9	0.01	0.87	0.94	0.91	0.02
e h un	0.81	0.9	0.85	0.02	0.83	0.94	0.87	0.02
e v un	0.87	0.92	0.9	0.01	0.87	0.94	0.92	0.01

The applied method for correction term calculation results in a linear shift of the TB data for the individual corrected beam position (viewing angle). As shown in table 3-1, the absolute values of the TB data changes much (up to 20 K) dependent on the selected beam position as normalization reference. However, as can be seen in figure 3-3, the general spatial patterns remain visible in all three processing stages. Nevertheless, the TB value change through normalization has finally obvious influence on analysed correlations as shown and discussed in the following.
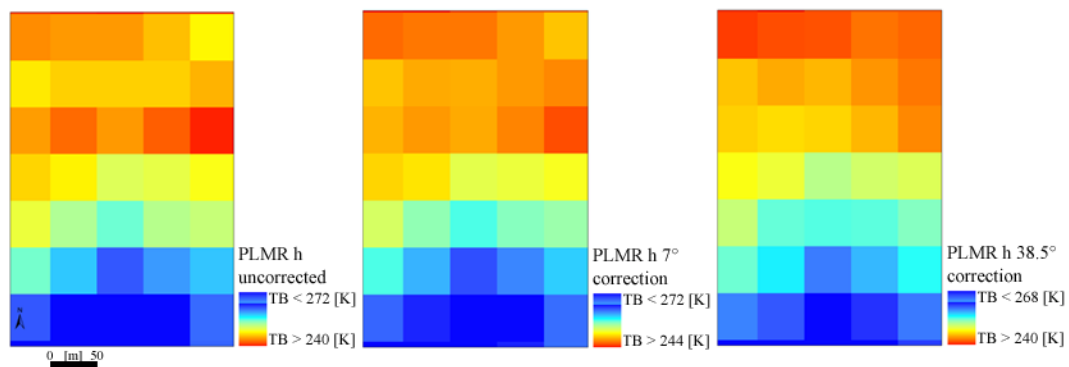
Figure 3-3.   Visualization of spatial patterns for observed and normalized TB data on a subset of the winter rye data.

Each 50 m x 50 m PLMR pixel includes approximately 1111 LAI pixels (see figure 3-2) of 1.5 m x 1.5 m spatial resolution. Average values and standard deviation of LAI were calculated inside each 50 m PLMR pixel. To make the results more clear in terms of interpreta-

tion, all PLMR observations (see table 3-1) were classified to values of whole-numbers. This classification procedure results in changing numbers of "sampling points" between the different PLMR observation data sets because of differences in the data range and values.

An obvious relationship between horizontal or vertical TB and LAI within field scale exists as it is shown in figure 3-4. TB decreases with increasing LAI. As expected based on theory, the correlation decreases slightly with increasing viewing angle for the horizontal polarization. From theory a higher correlation of the vertical polarized data to LAI may be expected because of higher attenuation introduced by vertical stems and leaves within a crop canopy. For winter barley the correlation of the horizontal TB (see figure 3-4 *(b)*) is very strong (e.g. $R^2 = 0.90$ for 7° viewing angle) which can be interpreted as a very good estimation of the optical depth by the LAI map achieved from AISA data. For winter rye the correlation is also obvious visible but is less linear at those time of data "snap shot". In return, the correlation of the vertical TB (see figure 3-4 *(d)*) and LAI for the winter barley data is very weak (e.g. $R^2 = 0.30$ for 7° viewing angle) compared to others (e.g. $R^2 = 0.72$ for 7° viewing angle and winter rye), which is unexpected because from further studies the vertical polarised data is proposed to be more sensitive to vegetation structural changes. Since with increasing viewing angle the stems become more prominent and increase the effect of vertical polarization. For winter rye, the correlation with the vertical TB (see figure 3-4 *(c)*) data is general stronger than for winter barley, which might be influenced by differences in the canopy height. The winter rye, canopy was approximately 20 cm higher than the winter barley canopy at the day of PLMR data acquisition. However, regarding the correlation of pixel average standard deviation (see figure 3-5) and vertical TB, for winter barley the variability of LAI within field scale is obviously connected to the passive L-band observation. A high coefficient of determination with $R^2 = 0.81$ for the winter rye data and vertical TB at 38.5° viewing angle was found. Generally, the correlation of the LAI variability within a PLMR pixel and represented by the pixel average standard deviation is slightly stronger at the outer viewing angle (38.5°). The standard deviation consequently increases with increasing TB. For the horizontal polarization the coefficients of determination are more weak and do not exceed values of $R^2 = 0.5$.
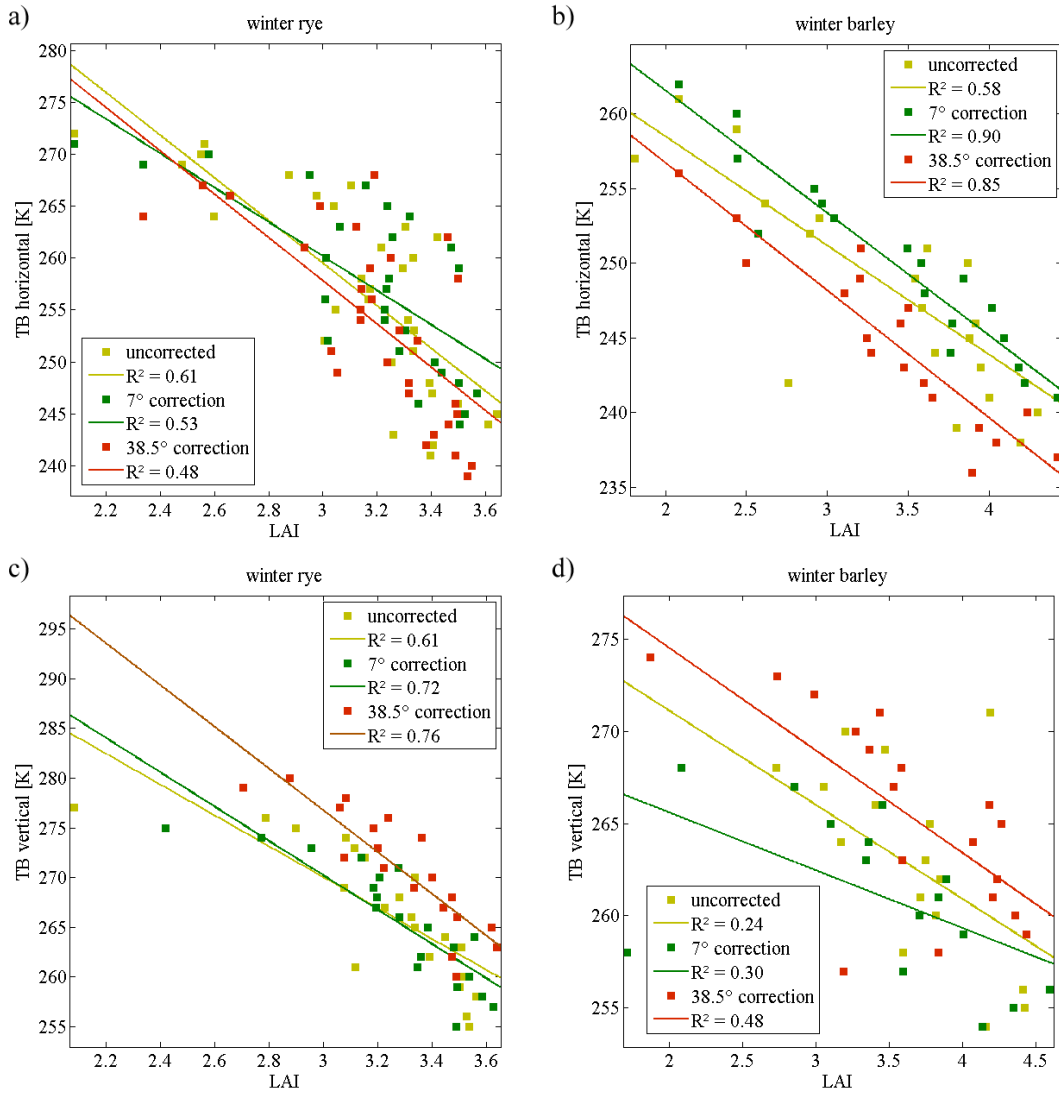
Figure 3-4.   Three processing stages (uncorrected, 7° correction, 38.5° correction) of PLMR horizontal (a and b) and vertical (c and d) TB plotted against average LAI on the sub-pixel level for winter rye (a and c) and winter barley (b and d) data. Linear regression line and coefficient of determination R^2 plotted for each data pair.
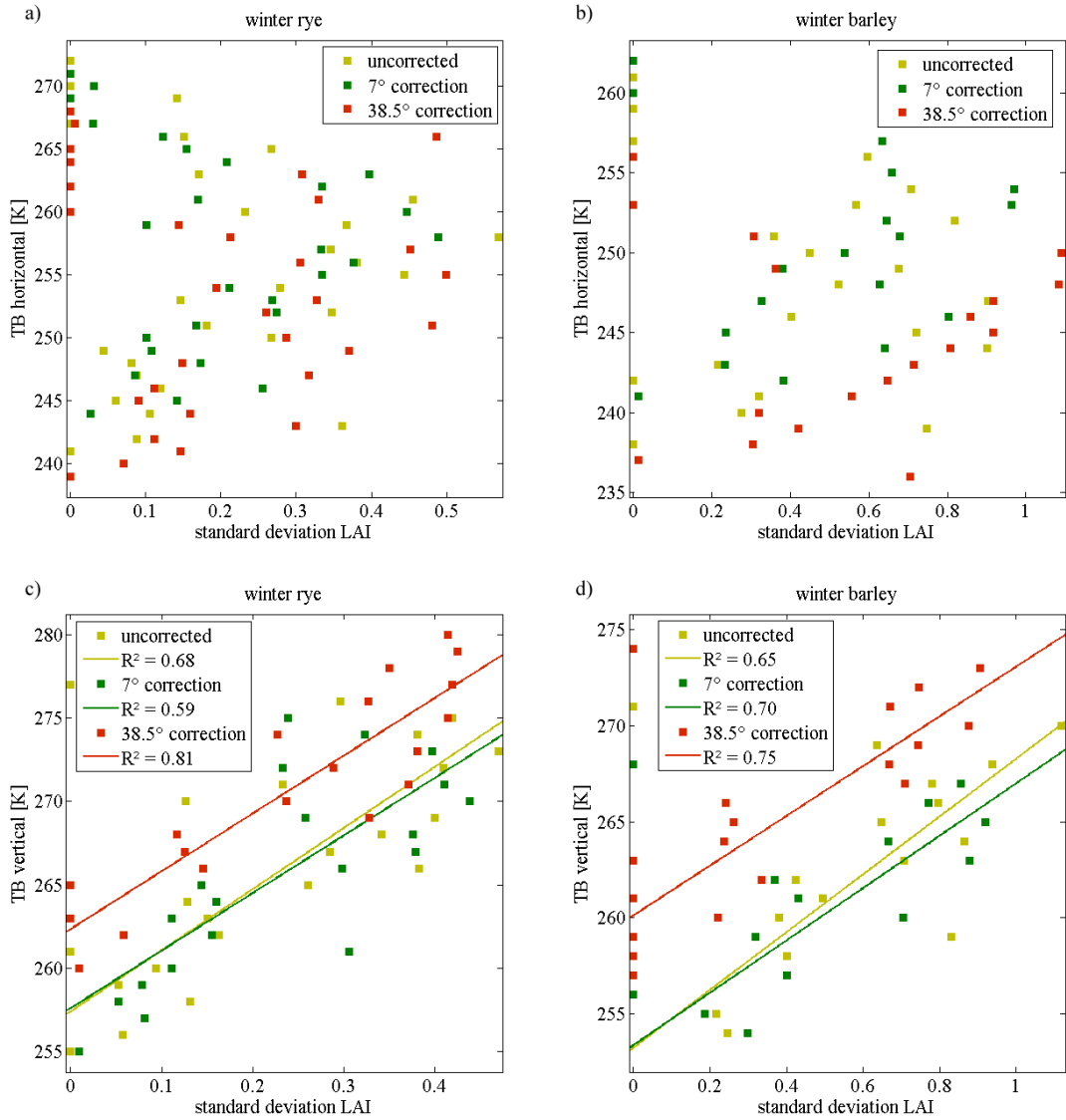
Figure 3-5.   Three processing stages (uncorrected, 7° correction, 38.5° correction) of PLMR vertical TB plotted against the standard deviation of LAI for the sub-pixel level for winter rye (a and c) and winter barley (b and d) data. Plotted linear regression calculated without the zero values for the standard deviation of LAI within sub-pixel level for the vertical polarization.

Compared to the single polarization PLMR observations, the coefficient of determination between the MPDI and LAI is weak (see figure 3-6). Because the MPDI is proposed to account for the vegetation influence on the L-band microwave signal, stronger correlations were expected (Owe et al. 2001). It is proposed that MPDI increases with vegetation growth, as represented in this study by LAI a slight bias can be seen as with increasing LAI the MPDI increases. Comparing the winter rye and winter barley data sets, very different characteristics in the relationship of MPDI vs. LAI are observed.
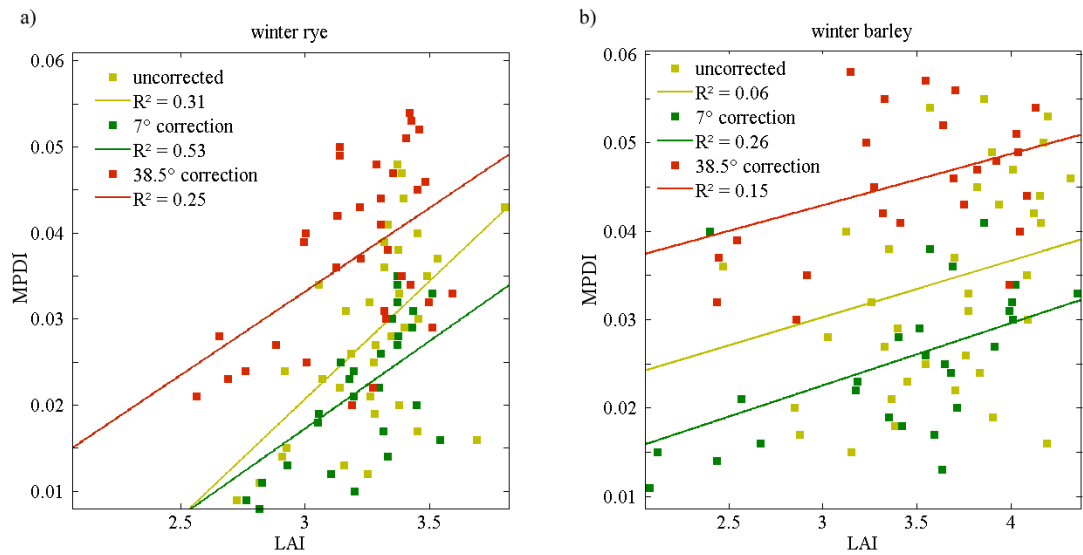
Figure 3-6.   Three processing stages of PLMR polarization difference index (MPDI) plotted against average LAI on the sub-pixel level for winter rye (left) and winter barley (right) data.

Since the relationship between emissivity and TB is linear (see figure 3-7) the correlation of emissivity to LAI is quite similar if using TB. TB and emissivity decreasing with increasing LAI as is shown in figure 3-8. Therefore, the decreasing trend could be due to an increasing attenuation effect by the vegetation biomass, as represented by LAI. The increasing LAI may lead to higher scattering effects and thus lower emissivity at locations with higher LAI. A bias between TB h and vegetation canopy obviously exists where the emissivity decreases with increasing LAI. Higher LAI causes potentially more vegetation water content at the appropriate phenological stage. Thus, LAI can be regarded as an applicable proxy for vegetation influence on microwave emission.
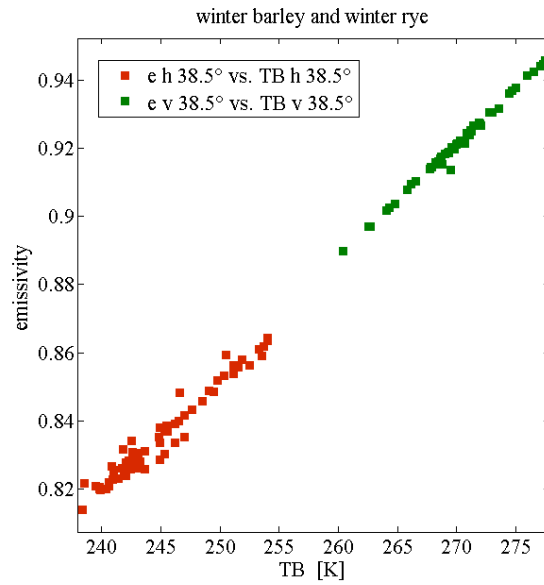
Figure 3-7.   Linear relationship between TB data and emissivity at horizontal polariza-
tion. Example plotted for ground truth locations at the winter barley and
winter rye site.
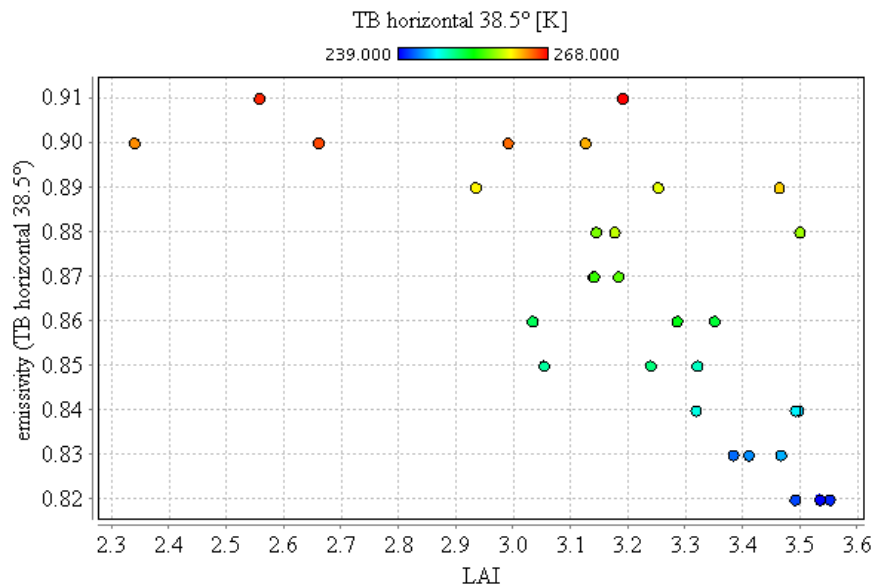
Figure 3-8.   Surface emissivity e of the horizontal polarization at 38.5° viewing angle
plotted against LAI (winter rye data) whereby the colour scheme represent
the appropriate TB data.

The analysed linear relationships between emissivity and LAI are frequently weaker than
before the normalization of TB observation using the provided surface temperature. That
effect could be interpreted as a decreasing vegetation influence on the retrieved emissivity as
the used surface temperature data contains information about the soil layer contributing to
the microwave emission.

Table 3-2.   Coefficients of determination (R²) for linear regressions of LAI and emissivity (e) data at different viewing angles and horizontal (h) and vertical (v) polarization.

LAI vs.	winter barley R²	winter rye R²
e h 38.5°	0.4	0.4
e v 38.5°	0.28	0.5
e h 7°	0.38	0.38
e v 7°	0.1	0.58
e h un	0.33	0.33
e v un	0.4	0.26

3.4   Discussion and Conclusion

To better understand the effect of LAI on observed brightness temperature at L-band, a simple analysis is performed analysing its relationship to pixel average LAI and its standard deviation. Weak to strong influence of LAI on the L-band observations were examined in this study, which proves this structural vegetation canopy parameter as valuable estimator to account for the optical depth for high spatial resolution passive L-band microwave data. Even variations within a small value range ($2 < LAI > 4$) in a crop field were found to have major influence ($0.23 < R^2 > 0.90$) on the retrieved high resolution TB observations. However, the observations do not agree with findings from Ferrazzoli et al. 2000 where the emissivity increases in due to vegetation growth during a whole growing cycle. Vegetation growth might be represented by LAI in this study but gives no direct information about the vegetation dielectric properties as can be estimated from vegetation water content data. The found correlations confirm results of the study from Saleh et al. 2004 were a decrease in vertical TB was found with increasing biomass which may lead to higher scattering effects. However, their dry biomass data was achieved from regression analyses using the stand age as independent variable and represent a different level in detail regarding the vegetation influence compared to this study. In this study the effect of decreasing brightness temperature and emissivity with increasing biomass as represented by LAI has been shown for the horizontal and vertical polarization and different viewing angles within a crop canopy. The observations have demonstrated a high potential for differences in the correlation between L-band observations and LAI within a vegetation canopy previously assumed homogeneous. Since the top canopy is a geometrically complex structure that is strongly influenced by rain and wind, such variations may be explained in addition to occurring phenological variations.

The derivation of several data sets in terms of different processing stages represented by different viewing angles and calculated from the same data source promise information about the vegetation contribution to the detected microwave emission and can be used to account for the vegetation influence in soil moisture algorithms. Furthermore, high resolu-

tion L-band experiments over crops at several phenological stages within TERENO are required to generalize the outcomes and support the parameterization of the optical depth within physically based soil moisture retrieval algorithms.

4.   Soil moisture retrieval using airborne L-band brightness temperature and imaging spectrometer data

The monitoring of spatially distributed soil moisture fields is an essential component for a large range of hydrological, climate and agricultural applications. Soil moisture information is needed for modelling studies as direct boundary conditions are used in the model calibration process or can be assimilated in order to reduce the uncertainties of any model prediction. While direct measurements are expensive and limited to small spatial domains, the inversion of airborne L-band radiometer data has shown the potential to provide spatial estimates of surface soil moisture up to the meso-scale. However, when using airborne L-band radiometer for soil moisture retrieval, a major limitation is the attenuation of the microwave signal by the vegetation, hampering the signal inversion and thereby making spatially distributed plant information necessary. In order to address vegetation influence, in this study combined analyses of airborne L-band microwave data and imaging spectrometer data is performed over crop sites in Germany. Intensive field campaigns coinciding with the sensor overpass provided fundamental information on surface soil moisture and vegetation canopy parameters. Results show strong improvements ($R^2 \sim 0.2$) on all models adding spectral vegetation indices to the independent variable set for final soil moisture retrieval. More importantly, the results demonstrate that reasonable estimates of surface soil moisture on field scale are possible using multi-variate regression or neural networks without in-situ measurements.

4.1   Introduction

Soil moisture is one of the dominant controls for the partitioning of water and energy fluxes at the land surface including the splitting of rainfall into surface runoff, infiltration and evapo-transpiration, as well as the redirection of incoming solar radiation into albedo, thermal radiation, sensible and latent heat fluxes. Information about spatial surface soil moisture is therefore an important boundary condition for process based hydrological, climate or ecological models ranging from the field scale up to the global scale and its knowledge is essential in order to improve operational hydrological, climate and weather predictions including flood forecasting, drought monitoring or eco-climatological projections via calibration or data assimilation techniques.

Soil moisture patterns are not stable over time (Grayson et al. 1998) and require precise detection and monitoring. Soil moisture accounting schemes are applied for estimations at catchment scale using climate data (Merz et al. 2004, Robinson et al. 2008). For plant

growth models and fertilization application on agricultural sites, spatial distributed soil moisture on field scale is a main input for model calibration (Bouma et al. 1999). In-situ soil moisture measurements, using gravimetric samples, frequency or time domain reflectance measurements provide reasonable estimates, but they are point measurements. It is very difficult to estimate extensive spatial soil moisture distribution based on point measurements because of the high spatial variability at field scale. The inversion of microwave radiometer data has shown the potential to provide spatial estimates of surface soil moisture up to the meso-scale.

The retrieval of surface soil moisture from L-band radiometers (frequency f=1-2 GHz, wavelength λ=30-15cm) from aircraft and satellite platforms received a significant upturn during the last 10 years (Blyth 1993, Kerr 2007, Wagner et al. 2007). Particularly the European Space Agency's (ESA) Soil Moisture and Ocean Salinity mission SMOS initialized a high number of high resolution airborne L-band radiometer campaigns to analyse scale dependent soil moisture sensitivities (Delwart et al. 2008, Panciera et al. 2008). L-band brightness temperature (TB) data offers a nearly linear relationship to surface soil moisture, given uniform vegetation and soil characteristics (Jackson et al. 1984). Furthermore, TB from L-band radiometers is less sensitive to parameterization of surface roughness and vegetation canopy characteristics compared to radar applications. Hence, it seems to provide a monitoring method for surface soil moisture on various spatial scales.

The large amount of research on estimating soil moisture from L-band radiometers resulted in a consensus on major factors that should be incorporate in data analyses (Jackson et al. 1991, Schmugge et al. 2002, Wagner et al. 2007). Unfortunately, operational methods to apply such data and products quickly to the end user are still not available. The signal's soil moisture sensitivity changes spatially with soil, vegetation and terrain characteristics. In order to estimate soil moisture regimes under a vegetation canopy it is essential to provide spatial distributed information about vegetation characteristics since it contributes an own microwave emission to the signal. To apply airborne L-band radiometer data in more operational applications, it remains a major challenge to provide ancillary data to run complete physically based models. Therefore, the largely empirically retrieved model parameters are very site dependent and vary at low scale to a large degree (Wigneron et al. 2007). Hence, it is necessary to make assumptions, chose a proper model algorithm and focus on reasonable key factors dependent on the study site and subject of the study.

The Helmholtz Association in Germany recently launched an extensive investigation into the long-term effects of climate change at the regional level called TERENO (TERrestrial ENvironmental Observatories). TERENO consists of three long-term observatories in Germany to study how climate change affects both the local ecosystems and the local economies

(Bogena et al. 2006). In the context of TERENO, one major interest is the detection and monitoring of spatial distributed surface soil moisture. Hence, in May 26, 2008 a flight campaign with the Polarimetric L-Band Multibeam Radiometer (PLMR) was realized by TERENO and Airborne Research Australia (ARA). This airborne campaign was designed to investigate the utility of the PLMR sensor for TERENO soil moisture monitoring at field and regional scale.

The angular characteristics of multi-beam radiometers directly influence the observed TB values. Theoretically, the angular variation can be explained by the Fresnel equation, which describes a linear viewing angle effect on the TB over homogeneous land cover target. The calculation of correcting terms for normalization to a defined beam position should therefore be applied over homogeneous land cover sites. Furthermore, the availability of proper spatial information about vegetation canopy is rarely be obtained from field campaigns since these are time consuming and require special measurement infrastructure. Therefore, the integration of information from optical remote sensing (visible and near infrared spectrum) data products promises reasonable proxies for vegetation conditions and their spatial variability.

This study describes the data analyses from the TERENO PLMR campaign performed on May 26, 2008 in the Harz/Central German Lowland Observatory of TERENO. The nadir normalization of the TERENO PLMR data is described and discussed. Furthermore, PLMR soil moisture sensitivity was analysed in detail over barley and rye crops for one TERENO test site. Information about in-situ soil moisture and ancillary vegetation characteristics was provided from ground truth campaigns. Additional narrow band spectral vegetation indices (VI) from airborne imaging spectrometer data were analysed together with the passive microwave data. Multi-variate regression and neural networks were applied with statistical cross-validation to explore empirical models for soil moisture retrieval from different sets of independent variables.

4.2 Study sites and data

The TERENO Harz/Central German Lowland observatory features low mountain forests, lowland riparian forests, extensive agricultural areas, urban and industrial areas as well as open pit mines. Within the area four different sites, flights were carried out on May 26, 2008 as shown in figure 4-1. Grossbardau is an agricultural used site where studies are focussed on agricultural issues. Schaefertal and Klieken were recently equipped for long term monitoring of hydrological processes and nutrient fluxes. Bad Lauchstaedt is a long term agricultural fertilization test site.

Ground data were sampled within the time period of the sensor's overpass. For logistical and application orientated reasons, the ground teams operated independently with different ground sampling methods. In this study, the normalization of PLMR TB data was performed for all four monitoring sites. The analyses concerning the soil moisture retrieval were performed only over the crop sites around Grossbardau because of the availability of airborne imaging spectrometer data. All data used in this study is provided from a TERENO pre-study because the final instrumentation is not finished yet.
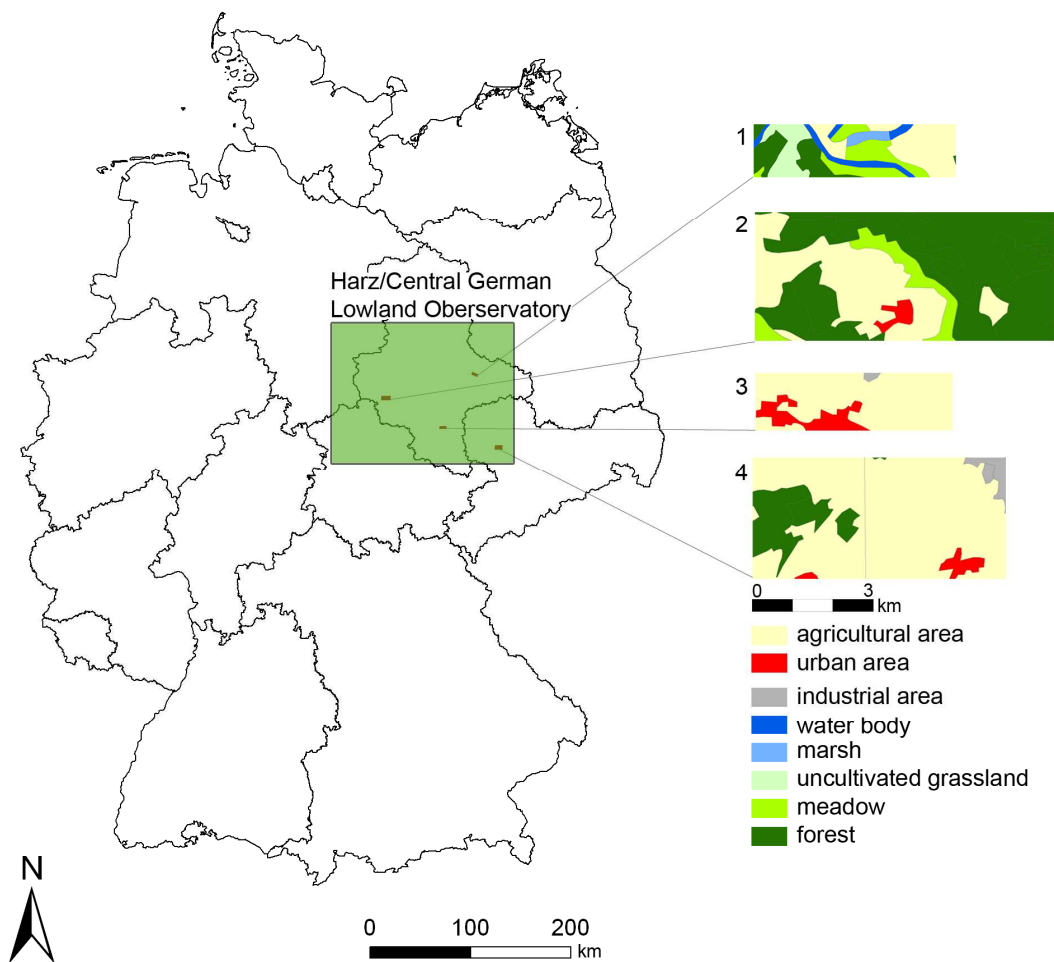
Figure 4-1.   Location of the four soil moisture monitoring test sites and general land cover information from CORINE 2000 data; 1) Klieken, 2) Schaefertal, 3) Bad Lauchstaedt, 4) Grossbardau.

4.2.1   Field data

In Grossbardau the field data sampling was focussed on a winter rye (70 ha) and winter barley (30 ha) field at known geo-referenced sampling points which were installed for whole seasonal vegetation monitoring in 2008. The sampling points were located between 2 m and

2.5 m from the machine tracks in order to achieve representation within field measurements. For winter rye there were 47 and for winter barley 43 ground truth points sampled. At the day of field data acquisition the main phenological stage was flowering (main shoot). It should be noted that for winter barley the flowering was more pronounced and fruit sets were mostly visible.

Soil moisture measurements of the 0-6 cm layer were performed using mobile FDR (frequency domain reflectrometry) probes. Each measurement represents an average of five single measurements. Coincident with FDR measurements soil temperature data of the first 6 cm layer was collected using field thermometers. To rapidly determine field measurements of leaf area index (LAI) a LI-COR, Inc. (Lincoln, Nebraska, USA) LAI-2000 Plant Canopy Analyzer was applied. This compares above- and below-canopy light levels detected in five conical rings, with the view zenith angle ranging from 0 to 75°, to infer LAI (Welles et al. 1991). At each sampling point location three LAI values got sampled where each single value is an average of six observations. Canopy height was simply measured by a foot rule. A Chlorophyll-Meter SPAD-502 (Minolta) was used to provide rapid and reasonable estimates of leaf chlorophyll characteristics (Markwell et al. 1995). The SPAD-502 measures transmittance of plant leaves in the red and near-infrared spectral regions. The ratio of these two transmittances is proportional to the total leaf chlorophyll content. Table 4-1 provides a summary about the measured value ranges.

Table 4-1.   Soil moisture and vegetation parameter characteristics for the test fields Grossbardau.

winter barley				
parameter	*average*	*min*	*max*	*standard deviation*
surface soil moisture [Vol. %]	7.8	2.1	12.9	2.7
LAI	4.3	2.7	5.2	0.5
canopy height [cm]	99.7	10.0	120.0	17.9
chlorophyll meter value (SPAD)	54.0	45.0	58.0	2.7
soil temperature [°C]	14.5	13.0	18.0	1.1
winter rye				
surface soil moisture [Vol. %]	9.3	2.2	14.6	2.7
LAI	3.6	2.3	4.5	0.4
canopy height [cm]	120.0	90.0	135.0	7.7
chlorophyll meter value (SPAD)	55.0	42.0	58.0	2.7
soil temperature [°C]	14.33	13.0	16.0	0.72

4.2.2   L-band microwave radiometer data

For the TERENO flight campaigns the PLMR (ProSensing) sensor was fitted to an Enviscope Partenavia PA68 D-GERY aircraft. Data acquisition over the four test sites took place between 9 am. and 2 pm. on May 26, 2008.

PLMR (frequency = 1.413 GHz) utilizes six pushbroom patch array radiometer receivers with incidence angles of ±7° (antenna 3 and 4), ±21.5° (antenna 2 and 5), and ±38.5° (antenna 1 and 6). Horizontal and vertical polarized TB is measured using a polarization switch (Panciera et al. 2008). Pre-flight and post-flight calibration against a black body target (warm point) and clear sky (cold point) was applied on the data as described (Panciera et al. 2009). Georectification was performed taking into consideration the aircraft's position and inertial navigation information (roll, pitch and yaw) by ARA. The beam centers were projected on a 90 m digital elevation model to calculate the effective footprint size and local incidence angles depending on the specific terrain topography. Therefore, local terrain slope, aircraft attitude and beam geometry were taken into consideration. Using a reduced antenna beam width, reduced flight speed and low altitude a ground spatial resolution of 50 m was achieved.

A microwave polarization difference index was calculated using the vertical (TB_v) and horizontal (TB_h) polarization:

$$MPDI = \frac{(TB_v - TB_h)}{(TB_v + TB_h)} \tag{4.1}$$

The brightness temperature is related to the emissivity ε, the physical temperature of the observed surface and to contributions from atmosphere. Since the atmospheric contribution on L-band data can be neglected because of its atmospheric transmission, emissivity can be calculated by:

$$e_i = \frac{TB_h}{T_i} \tag{4.2}$$

T_i is the physical temperature representing a soil or surface layer and measured in Kelvin. In this analysis two emissivity "levels" using equation 2 were calculated using the horizontal polarization (see figure 4-2). To retrieve the emissivity of the soil e_s the soil temperature data T_s was used. The emissivity of the surface e_c, that represents a mixture of soil and vegetation contributions, was calculated using surface temperature measurements T_{TIR}. The surface temperature data was provided by an InfraTec thermal imager that recorded simultaneously with PLMR data acquisition thermal infrared temperature information (TIR). It may be as-

sumed that the surface temperature information provided by T_{TIR} contains a significant contribution of the vegetation.
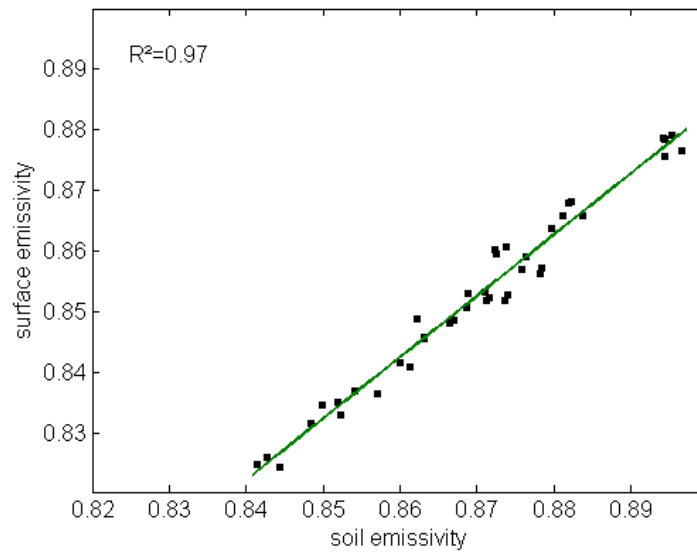
Figure 4-2.   Relationship of soil and surface emissivity at ground truth location in Grossbardau, R²=0.97 for linear regression.

4.2.3   Imaging spectrometer data

To provide further vegetation information for the test sites around Grossbardau, hyperspectral data from an AISA (airborne imaging spectro-radiometer for application) flight campaign on the 10th of June 2008 was used. The time shift of 16 days should be regarded critically in regards to phenological development and its influence on the microwave emission. However, the availability of the AISA data set provides a valuable information source for the spatial vegetation canopy heterogeneity.

There were 252 spectral channels collected in the visible and near infrared range of the solar spectrum from 400-970 nm with a pixel ground resolution of 1.5 m x 1.5 m. Current calibration coefficients from spectral laboratory calibration were applied to "rescale" the raw DN to radiance units using SPECIM CaliGeo 4.9.5 which runs under ENVI software (ITT Visual Information Solution, Boulder, CO). Surface rreflectance was achieved by applying the atmospherically correction algorithm MODTRAN using ENVI FLAASH.

From the AISA reflectance data an initially set of 18 spectral vegetation indices (VI) was calculated and applied in empirical modelling. According to which, the calculated spectral VI represented water, pigment and light use efficiency spectral VI groups. The following three narrow band spectral VI where finally used in this work, where R_{xxx} represents the centre wavelength of a narrow spectral band with 2.3 nm width:

The Gitelson Green Index (GI) was proposed to estimate LAI and green leaf biomass and is regarded in this study as a proxy of these plant and canopy parameters (Gitelson et al. 2003):

$$GI = \frac{R_{800}}{R_{550}} - 1 \qquad (4.3)$$

The Modified Soil Adjusted Vegetation Index (MSAVI2) was found as a good LAI estimator in terms of sensitivity to changes in vegetation canopy cover and the influence of the soil (Qi et al. 1994):

$$MSAVI2 = \frac{1}{2}\left[2(R_{800}+1) - \sqrt{(2R_{800}+1)^2 - 8(R_{800} - R_{670})}\right] \qquad (4.4)$$

The Modified Triangular Vegetation Index (MTVI1) was developed to improve LAI estimations for dense vegetation (Haboudane et al. 2004):

$$MTVI1 = 1.2[1.2(R_{800} - R_{550}) - 2.5(R_{670} - R_{550})] \qquad (4.5)$$

4.3 Methods

4.3.1 Correction of incidence angle effect

Previous studies using similar sensor designs applied normalization procedures for areas of mixed land cover by calculating correction terms over flight lines (Jackson 2001, Jackson et al. 1999, Jackson et al. 1995). Using this method, the main assumption involves the fly-over line, and the differences in the time averaged means (μ_i) of each beam position i (incidence angle) are due solely to the angular effect. The pattern of variation appearing between different beam positions reflects the Fresnel effect and depends on the land cover characteristics. This procedure assumes that the longer the line and the more homogeneous the area is, the more reliable the correction factors are. In the studies mentioned above, daily averages were used to calculate correction terms for individual beam positions. Using daily averages does not seems appropriate for the TERENO study area and for the collected PLMR data since the test sites show high variations in their land surface characteristics (see figure 4-1) which result in different microwave response. As can be seen in figure 4-3, the TB data is more scattered when comparing the outer (beam position 1 and 6) viewing angles within the comparison of the two inner (beam position 3 and 4) viewing angles. This mainly represents the signal detection from different targets because the outer viewing angles have the highest distance from each other and view more likely different surface targets than the two close nadir beam positions. Therefore, for the data used in this study, single flight line sections were used to calculate correction terms for a viewing angle normalization. The flight line

sections were carefully selected over homogeneous agricultural use sites. Information about land use was obtained from land use maps, farmers and personal site inspection during ground truth campaigns. Additionally, a grid map of standard deviation by the original TB values was generated for 500 m cells resolution. Finally, flight lines were selected on homogeneous agricultural used sites of low standard deviation of the TB data itself.
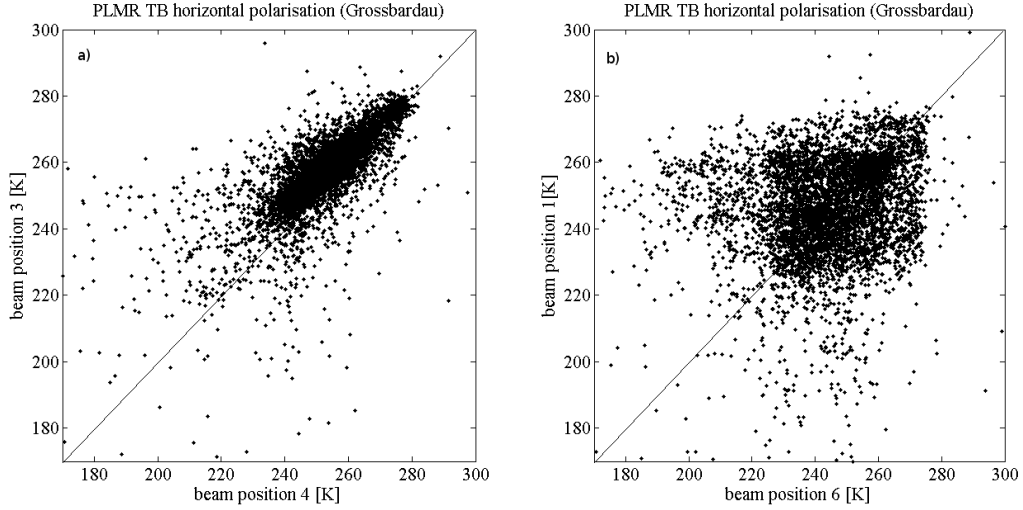
Figure 4-3.   Relationship between observed TB of the innermost (a) and outermost (b) beam positions for the complete Grossbardau data set.

The incidence angle normalization in this study was performed to the two nadir beam positions antenna 3 and 4 ($\pm 7°$). Hence, TB of antenna 1 and 2 are corrected to antenna 3 and TB of antenna 5 and 6 are corrected to antenna 4. Correction terms (CT_i) for the four outer PLMR antennas are calculated by:

$$\mu_i = \frac{\sum_{i=1}^{n=6} TB_i}{m} \qquad (i = 1,2,3,4,5,6)$$ (4.6)

$$CT_1 = \mu_3 - \mu_1$$ (4.7)

$$CT_2 = \mu_3 - \mu_2$$ (4.8)

$$CT_5 = \mu_4 - \mu_5$$ (4.9)

$$CT_6 = \mu_4 - \mu_6$$ (4.10)

The correction terms are finally added to all data (TB_i) for the appropriate beam position.

$$TB_{1N} = TB_1 + CT_1$$ (4.11)

$$TB_{2N} = TB_2 + CT_2 \tag{4.12}$$

$$TB_{3N} = TB_3 \tag{4.13}$$

$$TB_{4N} = TB_4 \tag{4.14}$$

$$TB_{5N} = TB_5 + CT_5 \tag{4.15}$$

$$TB_{6N} = TB_6 + CT_6 \tag{4.16}$$

4.3.2   Empirical analyses of PLMR data vs. ground soil moisture

Multi-variate least square regression models (equation 17) of surface soil moisture measurements as a function of different variable sets were applied.

$$Y = \beta_0 + \sum_{i=1}^{n} \beta_i \cdot X_i + \varepsilon \tag{4.17}$$

Furthermore, a neural network was trained for predicting soil moisture using the same input sets as for regression analyses. Therefore, a feed-forward neural network trained by a back-propagation algorithm (multi-layer preceptor) was applied. The activation function used is the usual sigmoid function. Therefore, the value ranges of the attributes are scaled to -1 and +1. The inputs are fully connected to one hidden layer which is in turn fully connected to one output node. There were 500 training cycles carried out.

All models were run with validation using bootstrapping (Efron et al. 1993) and compared using the coefficient of determination R^2 and root mean square error (RMSE). For Boot-strapping, ten random examples were picked out of each data set.

The number of analysed sampling points using only ground truth information (LAI, canopy height, SPAD), PLMR (TB_h, TB_v, $TB_h + TB_v$, $TB_h - TB_v$, $MPDI$,) and calculated emissivity (e_c, e_s) data is 43 for winter barley and 47 for winter rye. Analyses were spectral VI from AISA data are implemented as vegetation proxy are performed on a lower number of sampling points (23 for winter barley, 17 for winter rye) because of coverage gaps between the AISA and PLMR data swaths.

4.4   Results

Section 4.4.1 presents the characteristics of the flight lines chosen for calibration and the calculated correction terms for all four test sites. In Section 4.4.2, the model results for soil moisture retrieval over the two crop sites from the Grossbardau data set are presented.

4.4.1 Incidence angle corrected data set

The correction terms applied were chosen from calibration sites with the lowest standard deviation inside the single flight lines (see table 4-2). The corresponding number of beam position varies, with 27 for Grossbardau, 17 for Klieken, 26 for Schaefertal and 26 for Bad Lauchstaedt. In the case of the land use heterogeneity and spatial variability of agricultural crops, the flight line sets are not longer.

The correction terms for the horizontal polarization are mostly positive, which means that TB values of the two nadir beam positions are predominantly higher than the TB from the outer antennas of the same beam line. On the contrary, for the vertical polarization the TB values of the two nadir beam positions are mostly lower which results in negative correction terms. As expected from theory the correction terms of the two outer antennas (1 and 6) are frequently higher than for the inner antennas (2 and 5).

Table 4-2.   Applied correction terms of antenna 1,2,5,6 and characteristics of flight lines for incidence angle correction of the four test TERENO test sites, all values are in [K].

Grossbardau, 27 beam positions							
	vertical			*horizontal*			
beam position	*average TB*	*standard deviation*	*correction term*	*average TB*	*standard deviation*	*correction term*
1	281.48	1.41	-4.26	269.44	3.34	5.53
2	279.32	1.68	-2.10	274.07	2.27	0.90
3	277.22	3.32	-	274.97	3.84	-
4	279.87	2.66	-	274.05	3.31	-
5	277.98	1.38	1.89	273.28	1.91	0.78
6	282.66	1.37	-2.79	271.49	3.18	2.56
Klieken, 17 beam positions							
beam position	*average TB*	*standard deviation*	*correction term*	*average TB*	*standard deviation*	*correction term*
1	272.09	1.65	-13.10	241.13	1.73	16.38
2	264.99	2.26	-6.00	251.94	2.17	5.57
3	258.99	3.08	-	257.51	3.31	-
4	255.16	3.89	-	251.26	4.64	-
5	259.84	2.14	-4.67	249.09	3.98	2.17
6	273.65	1.50	-18.49	243.75	3.14	7.51
Schaefertal, 26 beam positions							
beam position	*average TB*	*standard deviation*	*correction term*	*average TB*	*standard deviation*	*correction term*
1	268.89	2.19	-2.52	240.72	2.92	22.55
2	267.91	1.14	-1.54	258.08	1.63	5.18
3	266.37	1.14	-	263.26	1.07	-
4	261.19	1.37	-	259.41	1.74	-
5	265.14	1.30	-3.94	255.75	1.62	3.66
6	270.08	1.43	-8.89	242.30	2.29	17.12
Bad Lauchstaedt, 26 beam positions							
beam position	*average TB*	*standard deviation*	*correction term*	*average TB*	*standard deviation*	*correction term*
1	277.34	1.89	-21.02	240.79	3.51	13.27
2	266.10	3.10	-9.79	251.37	5.08	2.69
3	256.32	4.05	-	254.06	5.55	-
4	244.17	5.79	-	242.92	8.17	-
5	260.11	5.06	-15.94	245.14	8.48	-2.22
6	269.56	4.97	-25.39	236.21	11.94	6.71

By evaluating the correction terms for all flight lines a lack of symmetry about the nadir beam position was found (see figure 4-4). The data range of antenna three is frequently higher than that of antenna 4. That effect might be caused by uncertainties in the warm and cold point calibration or attributed to a receiver specific problem.
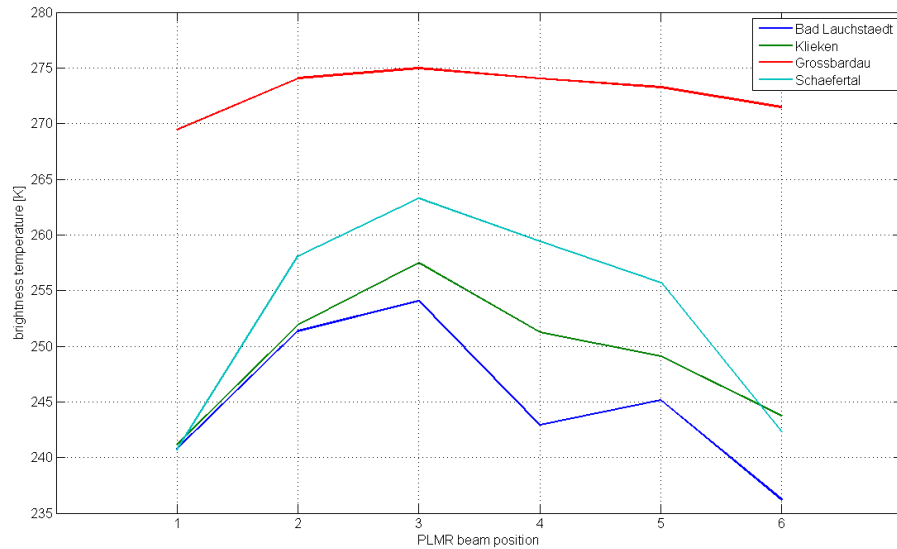
Figure 4-4.   Averaged TB values of the PLMR horizontal polarization for each beam position within a different flight line of each TERENO test site.

4.4.2   Soil moisture prediction

Multi-variate regression models and neural networks were applied to analyse the sensitivity of PLMR data and calculated microwave emissivity (e_c, e_s) to model spatial distributed surface soil moisture below a crop canopy. Therefore, field soil moisture data from a winter rye and winter barley field of the data set Grossbardau were tested together and crop type specific as dependent variable. The given soil moisture on the day of data was generally low and varies only within less Vol. %. Nevertheless, as can be seen in figure 4-5, a bias between TB_h and ground measured soil moisture obviously exists where TB increases with decreasing soil moisture. The noise is assumed to represent mainly the vegetation influence on the PLMR signal. Therefore, various proxies to account for the vegetation influence are tested.
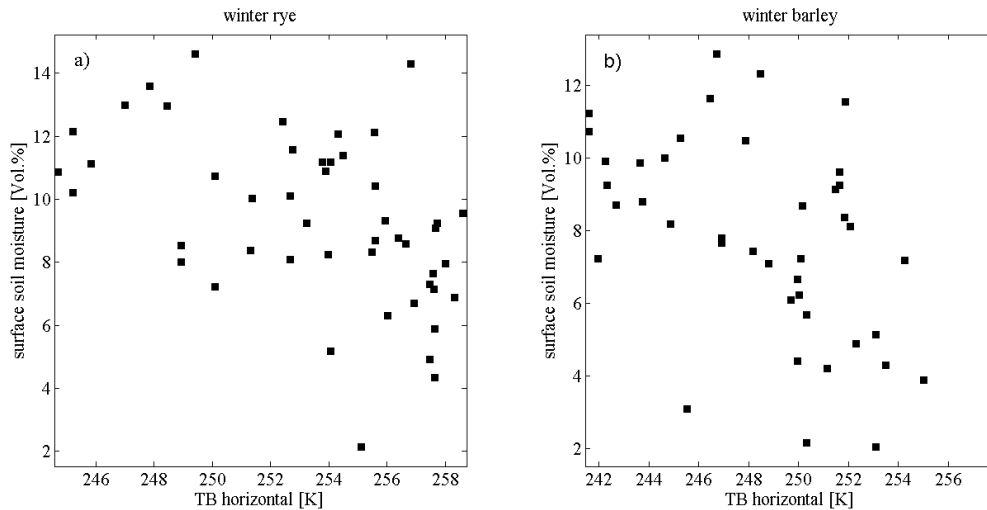
Figure 4-5.   Observed 0-6 cm soil moisture (y-axis) plotted against brightness temperature at horizontal polarization(x-axis), a) 48 ground truth points of the winter rye field, b) 43 ground truth points of the winter barley field.

Frequently, the best results were obtained on the winter barley site by multi-variate regression (see table 4-3). Model 2 achieves the best prediction performance (R²=0.92) using a Gitelson Greeness Index (GI) and LAI as vegetation proxies and e_c as independent variables. Canopy height showed a consequently less influence than LAI on model performance and is not applied in the final models. The best performance without any ground information (R²=0.91) as independent variable was achieved by model 3 using the sum of TB_h and TB_v and GI from AISA data.

Table 4-3.   Coefficient of determination (R^2) and root mean square error (RMSE) of multi- variate regression and neural network for estimating surface soil moisture by different sets of independent variables using ground truth data and hyperspectral vegetation indices from winter barley test site.

multi-variate regression			
model	independent variable set	R²	RMSE
model 1	LAI, GI, e_s	0.91	0.85
model 2	LAI, GI, e_c	0.92	0.82
model 3	$TB_h + TB_v$, GI	0.91	0.88
model 4	LAI, e_s	0.69	1.46
model 5	LAI, e_c	0.71	1.47
neural network			
model 6	TB_h, MSAVI2	0.81	1.29
model 7	SPAD, MTVI1, e_c	0.86	1.07

Generally, a strong improvement exists on all models adding a spectral VI to the independent variable set (figure 4-6). Using e_c than e_s improves the model results as well. However, using only emissivity and LAI (model 4 and 5), quite moderate coefficients of determination

are achieved but the RMSE remains much higher than when using additional spectral VI information (model 1, 2, 3) as vegetation proxy.

The best results by neural network application were achieved by completely different input variables than for regression. The best result are reached using e_c and canopy chlorophyll information represented by SPAD chlorophyll measurements and the chlorophyll related spectral VI MTVI1 (model 7). Predictions without ground information were best using only TB_h and MSAVI2 from AISA data (model 6).
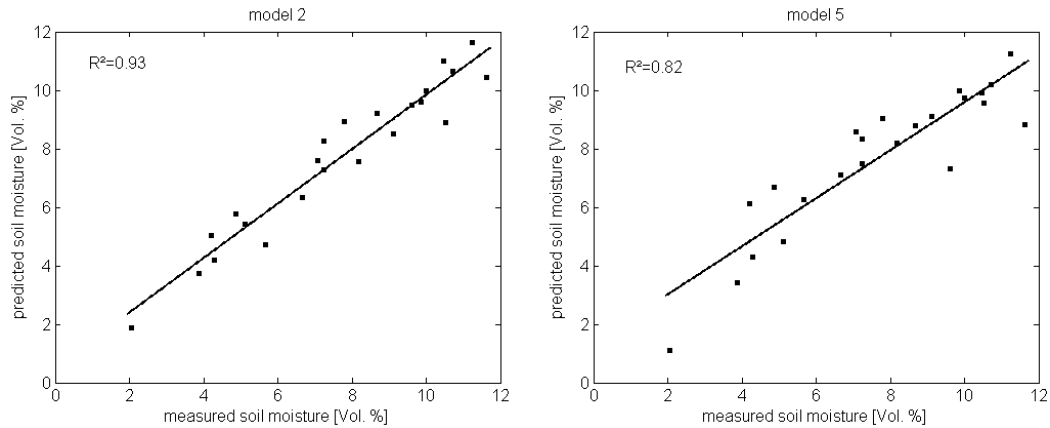
Figure 4-6. Comparison between predicted and measured soil moisture over winter barley for model 2 and model 5.

For winter rye, only very low model performance ($R^2 < 0.5$) was achieved on all sets of tested variables. Hence, the single results are not shown anymore. Through performing the analyses on the combined data set (winter rye and winter barley) the model performance remains weak ($R^2 < 0.5$). The weak soil moisture retrieval results for the winter rye field can very likely be explained by the differences in the vegetation height between the two crop types. The average canopy height of winter rye is 20 cm more than that of winter barley, which clearly results in more biomass per ground unit even when the LAI is lower. Unfortunately, no biomass weight data is available, which is used in other studies to show the limitations of L-band soil moisture retrieval below vegetation canopy (Jackson et al. 1991, Schmugge et al. 2002).

4.5   Discussion

As can be seen in the result section 4.4.1, the correction terms can vary much dependent on the selected calibration field, flight line extent and consequently for the test sites. For high spatial resolution L-band data it is therefore highly recommended to choose calibration sites carefully by up-to-date information about the vegetation canopy.

The empirical analysis has shown a strong field fruit dependent sensitivity of the PLMR data and ancillary independent variables. L-band sampling of soil moisture depends mainly on vegetation characteristics, as this study shows on a field scale level. Vegetation absorbs and scatters microwave radiation from the soil and contributes an own emission to the signal received. This reduces the retrieval opportunity of any soil moisture model (Jackson et al. 1996, Van de Griend et al. 1985). Hence, for application oriented data use it is generally not clear how strong the signals soil moisture sensitivity changes from pixel to pixel regarding spatial variation of vegetation characteristics. However, the general spatial pattern of vegetation influence on the microwave signal seems well reflected by the applied spectral VI regarding the model improvements using vegetation indices as vegetation proxy. Especially the Gitelson Green Index (GI), which is sensitive to chlorophyll represented by LAI, shows very good results and might be applied even without additional information about LAI (model 3). In microwave soil moisture studies GI might also be treated as a proxy for fresh green leaf biomass which in turn is related to fresh biomass weight of crops.

More importantly, the results demonstrate that reasonable estimates of surface soil moisture on field scale are possible using multi-variate regression or neural networks even without in-situ measurements (model 3 and 6).

4.6   Conclusion

Calculation of proper correction terms remains a critical factor for viewing angle normalization of multi-angular radiometers. The TERENO data set reveals that attempts at operational monitoring issue by analysing test site dependent characteristics.

Many field experiments using ground radiometers were performed with the goal of defining the soil moisture signal dominating soil layer at L-band (Newton et al. 1982, Wang 1987). The highest contributing layer is about ¼ the wavelength, which means around 5 cm for the L-band which changes with vegetation attenuation spatially. The results of this study demonstrate that reasonable estimates of surface soil moisture on field scale are possible using FDR soil moisture measurements from the upper 0-6 cm soil layer for training. Furthermore, combined analyses of narrow band vegetation indices from the red and near infrared and L-band TB data or retrieved emissivity provides very good prediction results of soil moisture under a vegetation canopy for field scale monitoring.

Hence, remote detection of surface soil moisture by the PLMR passive microwave sensors in combination with imaging spectrometer data has the advantage of providing spatial integrated information even without in-situ vegetation data as required for monitoring issues. With the launch of the German hyperspectral satellite EnMAP (Environmental Mapping and Analyses Program) in 2013, valuable spatial distributed vegetation information will be

available to support soil moisture retrieval algorithms using airborne and satellite L-band microwave data up to the catchment scale.

5. Soil moisture retrieval using the land surface parameter retrieval model (LPRM) over crops

The aim of this chapter is to retrieve soil moisture over crops from passive L-band microwave data at very dry conditions (< 15 Vol. %) using the land surface parameter retrieval model (LPRM). All analyses are based on experimental airborne L-band brightness temperature observations, remote sensing thermal infrared temperature, and measured field soil temperature and soil moisture. The study is performed over a winter barley and winter rye site in Germany under very dry conditions. As the temperature and the roughness parameterization play a crucial role in soil moisture retrieval from passive microwave observations using a radiative transfer equation a two-step optimization procedure was performed for choosing an optimal parameterization to minimize the uncertainty of final soil moisture estimates. Furthermore, the relationship between the roughness parameter and NDVI (normalized difference vegetation index) data was analysed using imaging spectrometer data. Site specific roughness parameterizations did not show reasonable soil moisture results using LPRM. Nevertheless, very good soil moisture results were achieved by applying a spatial varying roughness parameter achieved from a "pixel"-based optimization. A clear relationship between NDVI data and the spatial varying roughness parameter was found ($R^2 = 0.57$). The results presented in this chapter show that a spatial varying roughness parameter can strongly improve soil moisture results using LPRM even below a vegetation canopy previously have been assumed homogeneous (e.g. winter barley and winter rye).

5.1 Introduction

Soil moisture is a key variable for many hydrological applications and plays a crucial role in agricultural practice at field scale level. Passive L-band microwave observations from airborne sensors may provide soil moisture estimates with a high spatial resolution (< 100 m for that kind of data product) useful for agricultural applications (Jackson et al. 1987a, Wigneron et al. 1998). Theoretical models like radiative transfer models are important to support the understanding of the interaction between the electromagnetic waves and various surface targets (e.g. soil, vegetation) and may be applied to retrieve soil moisture from L-band brightness temperature observations.

The land surface parameter retrieval model (LPRM) was developed by Owe et al. 2001 and uses a radiative transfer model to solve for surface soil moisture and optical depth simultaneously with a nonlinear iterative optimization procedure. It is specially designed and pro-

posed for surface soil moisture retrieval from satellite data because it does not require any field observations of soil moisture or canopy characteristics. LPRM requires dual-polarized brightness temperature data, namely horizontal and vertical polarization and temperature information from the emitting surface. Several studies have demonstrated that LPRM is one of the most promising approaches to retrieve soil moisture from passive microwave radiometer data (de Jeu et al. 2003, de Jeu et al. 2008, Meesters et al. 2005, Owe et al. 2001). In de Jeu et al. (2009) LPRM was successfully applied for the first time on airborne L-band observations using National Airborne Field Experiment 2005 (NAFE'05).

The thermally emitted radiation from the land surface is controlled by two major factors: 1) the surface temperature and 2) the surface emissivity. The emissivity is the efficiency of the surface for transmitting the radiant energy generated in the soil into the atmosphere. The soil's emissivity depends on its physical properties (e.g. soil moisture), surface roughness and varies with the wavelength. In due to a lack of data in most retrieval studies, it is assumed that effective soil temperature is in equilibrium with the vegetation temperature. For early morning or even night observations of L-band brightness temperature and thermal infrared temperature, that assumption can be valid. Applying LPRM on the NAFE'05 data set de Jeu et al. (2009) considered the canopy temperature equal to the effective temperature and satisfactory soil moisture results could be achieved by performing an optimization on the roughness parameter h_r depending on the incidence angle of the brightness temperature observations and soil moisture.

Increasing surface roughness increases the apparent emissivity due to an increase of the emitting surface area (Schmugge 1985). Therefore, the empirical roughness parameter h_r is a key parameter to account for the rough soil emissivity, which is a major part of the soil moisture retrieval using LPRM (Wang et al. 1981). The roughness parameterization is proposed to account for i) a geometric roughness effect that is related to the spatial variation of the soil surface height and, ii) a dielectric roughness effect that can be caused by spatial variability of the combined effect of soil moisture and soil characteristics (Mo et al. 1987, Wigneron et al. 2001). For bare soil the roughness parameter was found to be dependent on the standard deviation and the correlation length of the soil surface height profile and the soil moisture (Wigneron et al. 2001). The dependence of the roughness parameter on soil moisture was explained by the spatial variation of the soil dielectric constant, which is stronger during dry conditions and can be explained by an effect of volume scattering.

Many roughness studies have been performed at the plot scale using ground based radiometers over bare soil or including only a few planted rows. The ratio between radiometer footprint to the roughness height is orders of magnitudes greater at the landscape scale using airborne or satellite data than at the plot scale. It is assumed that the roughness effect is

smaller at the airborne and satellite scale than for tower based radiometer footprints (Owe et al. 2001, Van de Griend et al. 1994). However, the roughness parameter not only changes with the observation characteristics but also with the type of the vegetation covering the soil surface and various empirically determined roughness parameter values were proposed depending on the vegetation (Panciera et al. 2009, Saleh et al. 2007, Wigneron et al. 2007).

The objective of this study is to retrieve soil moisture using the land surface parameter retrieval model (LPRM) for very dry conditions (< 15 Vol. %) at the field scale. Therefore, airborne L-band brightness temperature observations, remote sensing thermal infrared temperature, measured field soil temperature and in-situ measured soil moisture from a winter barley and winter rye site in Germany are applied. A two-step optimization using Monte-Carlo simulation to find one scene-based roughness parameter value using LPRM was performed. Furthermore a pixel-based (ground sampling location specific) optimization was applied to analyse the spatial dynamic of the roughness parameter values regarding spatially changing vegetation conditions. Additionally, all analyses were applied using different temperature input data to analyse the effect of the temperature on the LPRM soil moisture results and a potential temperature uncertainty was considered within the optimization.

5.2   Dataset

5.2.1   L-band brightness temperature data

The used data is part of the TERENO (Terrestial Environmental Observatories) (Bogena et al. 2006) soil moisture experiment within the Harz/Central German Lowland observatory. In May 26, 2008 airborne high spatial resolution (50 m) L-band brightness temperature data (*TB)* was collected with the Polarimetric L-Band Multibeam Radiometer (PLMR) over several sites within the observatory. The analyses presented in this study are performed on a winter barley (~27 ha) and winter rye (~37 ha) site located in south-east Germany (51° 13' N, 12° 40' E). The topography of the site is gentle and the soil properties do not vary much within the analysed sites.

Horizontal (TB_h) and vertical (TB_v) polarized brightness temperature was measured at six PLMR antennas with incidence angles of $\pm 7°$, $\pm 21.5°$ and $\pm 38.5°$. TB_h and TB_v were normalized to the outer beam positions ($\pm 38.5°$) to avoid viewing angle dependent effects on the soil moisture retrieval results.

5.2.2   Field soil moisture data

During the period of PLMR data sampling soil moisture was measured by mobile capacitance sensors (ML2 Theta probes) for the upper 6 cm soil layer. On the winter barley site at

43 and on the winter barley at 47 ground truth locations field soil moisture data were collected. As can be seen in figure 5-1 the adjacent soil moisture conditions were very dry ($<$ 15 Vol. %) during the time of data acquisition. Average soil moisture values of 7.8 Vol. % on the winter barley field and 9.3 Vol. % on the winter rye field were observed at the day of observation.
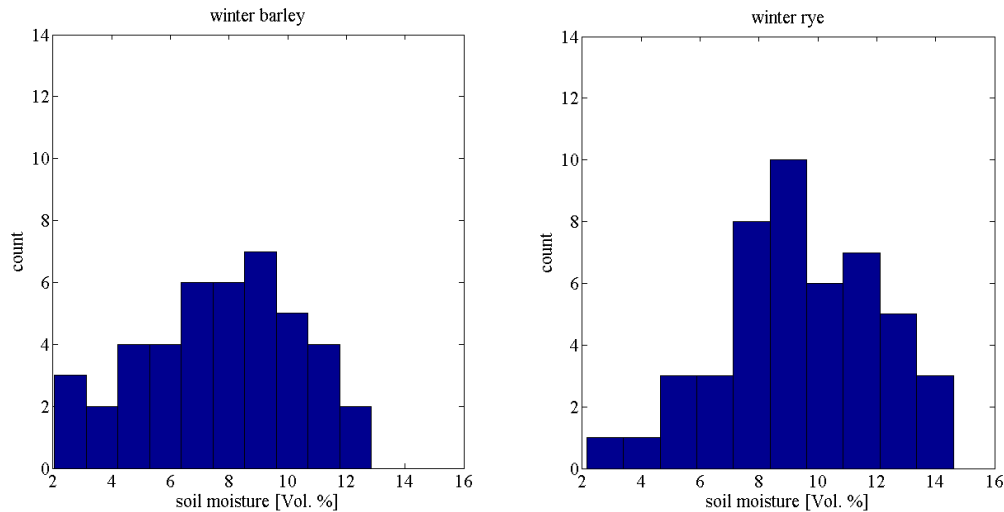
Figure 5-1.   Histogram of the measured soil moisture on the winter barley (left) and winter rye (right) test sites during PLMR data acquisition.

5.2.3   Ancillary vegetation data

For all soil moisture ground sampling points LAI (leaf area index) and canopy height data was collected to provide information about the geometrical vegetation canopy characteristics. LAI was measured using a LI-COR, Inc. (Lincoln, Nebraska, USA) LAI-2000 Plant Canopy Analyzer, which is a handheld technique and a rapid method for field applications. Canopy height was simply measured using a foot rule. The value ranges and standard deviation of LAI and canopy height for the winter barley and winter rye site are given in table 5-1. At the day of field and airborne data acquisition, the main phenological stage for the two crop types was flowering (main shoot). It should be noted that for winter barley the flowering was more pronounced and fruit sets were mostly visible. With respect to the phenological stage and confirmed by random field samples the vegetation water content (vwc) for winter barley and winter rye can assumed to vary between 2 and 3 kg m^{-2}.

Table 5-1.   Characteristics of LAI and canopy height for the winter barley and winter rye data.

vegetation parameter	average	min	max	standard deviation
LAI	4.3	2.7	5.2	0.5
canopy height [cm]	99.7	10.0	120.0	17.9
winter rye				
LAI	3.6	2.3	4.5	0.4
canopy height [cm]	120.0	90.0	135.0	7.7

A normalized difference vegetation index (NDVI) (Rouse et al. 1974) was calculated from an AISA Eagle (Airborne Imaging Spectro-Radiometer for Application, SPECIM – Spectral Imaging Ltd. 2007, Finland) imaging spectrometer data set, by

$$NDVI = \frac{(R_{800} - R_{670})}{(R_{800} + R_{670})} \tag{5.1}$$

where R_{xxx} represents the centre wavelength of a narrow spectral band with 2.3 nm band width. Because of coverage gaps between the AISA and PLMR observation swaths NDVI is available only at 40 ground truth locations (23 for winter barley, 17 for winter rye) for the two crop sites.

5.2.4   Temperature data

Soil temperature was measured next to the soil moisture measurement locations. Simple field thermometers were used to provide integrated temperature information about the upper 6 cm soil layer.

Thermal infrared temperature (T_{TIR}) obtained simultaneously during the PLMR data acquisition yielding a composite of canopy and soil surface temperature. The thermal infrared radiation of a spectral range between 7.5 – 14 µm was collected whereby the emissivity was set to 0.98 during data acquisition.

The effective soil temperature is the temperature contributing to the soil microwave emission and can be determined using measured profiles of soil temperature by (Choudhury et al. 1982). Temperature of the moisture profile is important as the range of the soil effective temperature increase as the soil moisture decreases.

$$T_{eff} = T_{depth} + (T_{surf} - T_{depth})C \tag{5.2}$$

where

T_{depth} deep soil temperature (approximately 50-100cm)

T_{surf} surface temperature (0-5 cm)

C   empirical parameter depending on frequency and soil moisture.

C is given by

$$C = \left(w_s / w_0\right)^{b_{w0}} \tag{5.3}$$

where w_s is the surface soil moisture at the top 0-2cm layer and w_0 and b_{wo} are semi-empirical parameters depending on soil characteristics (e.g. texture, structure, density). As the empirical retrieval of C was impossible within this operational experiment a default value of C for L-band equal to 0.246 was used (Wigneron et al. 2008).

In an operational context it is not possible to provide soil temperature profile measurements. Therefore, in this study equation (5.2) was applied assuming that T_{surf} is equal to the thermal infrared temperature T_{TIR} and T_{depth} represents the soil temperature T_s of the upper 6 cm.

Therefore, three different temperature input data sets are applied in this study:

-      Ground measured soil temperature: T_s
-      Spatially integrated thermal infrared temperature: T_{TIR}
-      Calculated soil effective temperature using the formulation proposed by Choudhury et al (1982): T_{eff}

The temperature dependent average values and standard deviations are given in table 5-2. As can be seen the standard deviation of T_s is higher than of T_{eff} and T_{TIR}. T_{TIR} is generally warmer than T_s and T_{eff}.

Table 5-2.   Number of sampling points, mean value and standard deviation of temperature data for the winter rye and winter barley site.

	winter barley		winter rye		all	
sample size	43		47		90	
statistic	mean	std	mean	std	mean	std
T_s [K]	287.64	1.08	287.49	0.73	287.56	0.91
T_{TIR} [K]	293.37	0.62	293.48	0.35	293.43	0.50
T_{eff} [K]	289.05	0.90	288.96	0.57	289.01	0.74

Figure 5-2 shows the relationship of measured soil moisture and T_{TIR} where a slight decrease of the soil moisture values with increasing T_{TIR} was found. That bias may be explained by the phenomena of an increase of evapotranspiration with increasing biomass that in turn may be found at moisture locations within the field and causes an increase of temperature. As can be seen in figure 5-3 that assumption might be valid for the measured soil moisture, T_{TIR} and LAI regarded as a proxy for biomass (higher LAI values indicating more biomass).
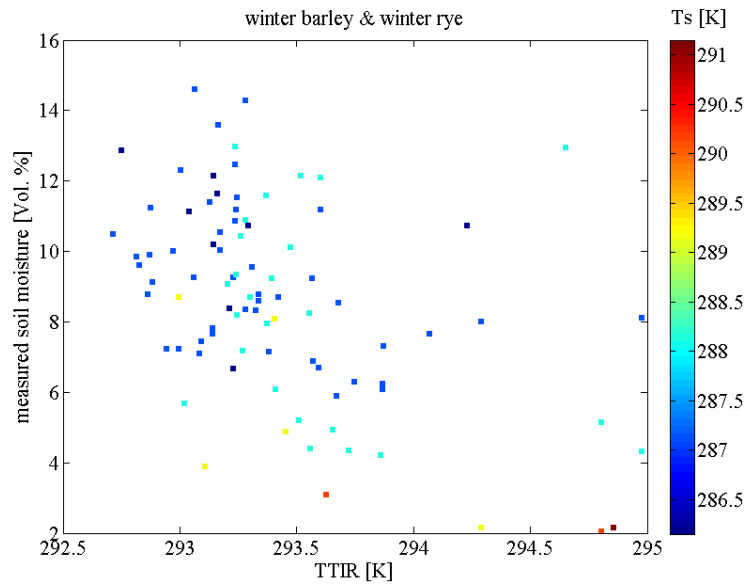
Figure 5-2.   Observed thermal infrared temperature (T_{TIR}) and soil moisture of winter barley and winter rye data.
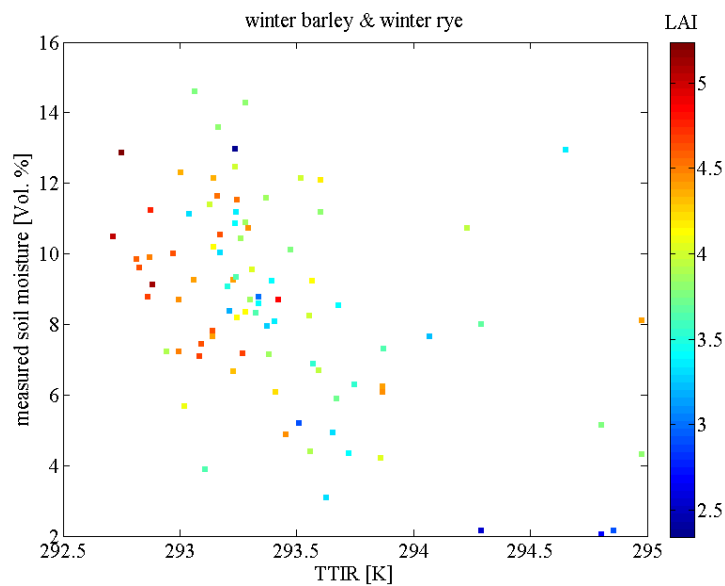
Figure 5-3.   Relationship of observed thermal infrared temperature (T_{TIR}), measured soil moisture and LAI of the winter barley and winter rye data.

5.3   LPRM: Land Surface Parameter Retrieval Model

LPRM was used for this study to retrieve soil moisture on the two crop sites (winter barley and winter rye) by applying the high spatial resolution PLMR data, the different provided temperature data and in-situ soil moisture information as described in the previous chapter. LPRM was originally developed and tested with microwave brightness temperature from the 6.6 GHz (C-band) scanning multichannel radiometer (SMMR). In de Jeu (2008) soil mois-

ture accuracy of 6 Vol. % was obtained using C-band data. In de Jeu et al. (2009) a soil moisture retrieval accuracy of ~ 5.5 Vol. % was achieved using L-band data. The ground observed soil moisture varied between almost zero to 60 Vol. %. A special question that needs to address within this study is how good LPRM estimate the experiment specific very dry soil moisture conditions (< 15 Vol. %). No study in scientific literature was found where experimental data was analysed to distinguish soil moisture of such a small range.

An advantage using LPRM is in the low requirement on the supply of ancillary data that makes it interesting for operational soil moisture retrieval. There is no parameterization for vegetation characteristics necessary. The approach uses a theoretical relationship between brightness temperature *TB*, the microwave polarization difference index (MPDI) and the soil dielectric constant to compute soil moisture (*sm*) and optical depth (τ). LPRM combines different modules that are summarized in table 5-3 together with the required input parameters and the several model outputs. A detailed description including the equations used in LPRM is given in Appendix A. The deviation of the optical depth module is provided with Appendix B. The description of the dielectric mixing model is given in Appendix C. The notation of LPRM model parameters and default parameterization is provided in table 5-4.

Table 5-3. Summary of applied LPRM modules and parameterization

module	input parameter	output parameter	reference
dielectric mixing model	effective temperature, frequency, sand content, clay content, bulk density or wilting point, soil moisture	dielectric constant	Wang et al. 1980
reflectivity model – Fresnel Law	incidence angle, dielectric constant	smooth surface reflectivity	
roughness model	smooth surface reflectivity, roughness parameter, incidence angle	rough surface reflectivity	Choudhury et al. 1979, Wang et al. 1981
vegetation optical depth model	polarization ratio, incidence angle, rough surface emissivity	vegetation optical depth	Meesters et al. 2005
radiative transfer model	effective temperature, canopy temperature, rough surface emissivity of horizontal polarization, optical depth	brightness temperature	Mo et al. 1982

Table 5-4.   LPRM global model parameters and default values.

Observation characteristics:	parameter	value	reference
Incidence angle	u	38.5°	campaign specific
Frequency	f	1.413	campaign specific
Soil parameters:			
roughness parameter	h_r	0.1	Wigneron et al. (2007)
soil porosity	p	0.465	site specific
wilting point	WP	0	site specific
sand content	s	0.52	site specific
clay content	c	0.11	site specific
model parameters:			
polarization mixing fraction	Q	0	de Jeu et al. (2009)
vegetation single scattering albedo	ω	0	de Jeu et al. (2009)
zenith atmospheric opacity	opt_atm	0	de Jeu et al. (2009)

5.4   LPRM optimization procedure

Within the optimization procedure described in the following to aspects are considered, i) the roughness parameter h_r and, ii) a shift of the temperature, which directly influences the microwave thermal emission.

T_{TIR} measured from thermal infrared represents an integrated temperature information containing contributions from the soil and vegetation layers. Assuming the temperature within the vegetation layer in equilibrium with the top soil temperature is a common assumption in soil moisture retrieval studies using passive microwave data due to a lack of appropriate vegetation temperature and soil profile data (Panciera et al. 2009, Van de Griend et al. 2003). Nevertheless, such an assumption represents a main uncertainty since the temperature is a major factor controlling emissivity at L-band and finally the soil moisture retrieval using physically based models. As presented in section 5.2.4, the temperature data may vary significantly (~ 5 K difference between T_s and T_{TIR}) dependent on the source of data. Furthermore, T_{TIR} data yields an operational uncertainty related to the pre-defined emissivity setting at the camera. Even within a given crop canopy, the emissivity at thermal infrared may vary much (0.98 – 0.95) depending on the vegetation water status and changes of the canopy architecture (Olioso et al. 2007). Olioso et al. (2007) found that emissivity at thermal infrared over senescent crops (dry) can be significantly lower than emissivity over well-watered green vegetation. A change of emissivity over crops of ~ 0.03 may lead (regarding the relationship temperature = brightness temperature/emissivity) to differences of ~ 10 K on the collected thermal infrared temperature T_{TIR}.

Several studies in literature have shown that the roughness parameter h_r varies from site to site and that the roughness has a crucial effect on the soil moisture results within physically based models (Escorihuela et al. 2007, Wigneron et al. 2001). In de Jeu et al. (2009), con-

vergence of LPRM retrieved TB_h and observed TB_h could only be achieved applying a dynamic roughness parameter depending on incidence angle and soil moisture. As no measurements of the soil surface roughness are available within this study an optimization of h_r was performed to improve LPRM soil moisture retrieval results.

For applying the optimization described in the following two notifications are here introduced i) "scene-based" denotes the application of the optimization to find one optimal h_r and temperature shift T_{shift} for all ground truth and PLMR data pairs (43 for winter barley, 47 for winter rye) together, and ii) to find "pixel-based" optimal h_r and temperature shift values. For the latter, the 40 ground truth and PLMR data pairs are used where also NDVI data is available. In order to analyse the relationship between the spatially varying h_r values and the NDVI data, here the NDVI is used as a proxy for the presence of green vegetation.

In table 5-4 the value ranges of the temperature shift T_{shift} and h_r applied during the optimization are specified. For all other model parameters the default values as represented in table 5-3 are used.

Table 5-5.   Value range for the roughness parameter h_r and the temperature shift T_{shift} applied within the optimization procedure

Parameter		LPRM
temperature shift	T_{shift}	-5 - 5 K
roughness parameter	h_r	0 – 1.2

5.4.1   Scene-based optimization

The aim of the scene-based optimization was to retrieve soil moisture with LPRM assuming a uniform parameterization crop type wise (winter barley and winter rye separately) and for the two crop types combined. Therefore, the analyses using the scene-based optimization for h_r and T_{shift} were performed using all 90 ground truth locations for soil moisture. Additionally, the winter barley (43 sampling points) and the winter rye (47 sampling points) data were analysed separately within the optimization procedure. Analyzing the performance, differences could possibly be caused by crop type specific conditions (e.g. LAI, canopy height, phenological stage). Three variant data sets (winter barley, winter rye, winter barley and winter rye combined) were applied each using LPRM with T_s, T_{TIR}, T_{eff} to analyse the effect of the different temperature data source on the achieved values for h_r and T_{shift}. Therefore, the optimization procedure was performed on nine input data sets.

The scene based optimization was performed as a two-step optimization with a Monte-Carlo simulation. In the first step, the optimal soil moisture value sm_o is determined where a minimum RMSE between LPRM computed TB_h and the measured TB_h is achieved. To find the optimal soil moisture value sm_o the Monte-Carlo simulation on all soil moisture ground truth

points is applied. The simulation was set up with a uniformly distributed number of samples of 1000 elements across the specified value ranges for T_{shift} and h_r given in table 5-4. The soil moisture values used within LPRM during the forward modeling were constrained by the measured soil moisture. Within the second optimization step, the roughness value h_r and the temperature shift T_{shift} that minimizes the RMSE between measured and LPRM retrieved soil moisture was determined.

5.4.2 Pixel-based optimization

As the dependence of the roughness parameter on soil moisture was found to be related to spatial variations of the soil dielectric constant with an influence stronger during dry conditions the roughness parameter h_r was assumed to be highly spatial variable because of the very dry soil moisture conditions (< 15 Vol. %) during the PLMR data acquisition. Furthermore, h_r was found to change with the type of vegetation cover or litter over the soil. For instance, in Saleh et al. (2007) a $h_r = 0.5$ over grassland and in Wigneron et al. (2007) a h_r varying between 0.1 and 0.7 for different crops were applied. Consequently, it is assumed within this study that h_r is spatially variable depending on the vegetation conditions that have previously been assumed homogeneous within a crop site. Considering a spatially varying h_r may lead to improved LRPM soil moisture retrieval as it also compensates for vegetation influence on the observed brightness temperature. To address the assumptions of a spatially variable h_r a pixel-based optimization for h_r and a temperature shift T_{shift} is performed to investigate its effect on the LPRM soil moisture retrieval results. Toward that purpose, the optimization procedure for h_r described in section 5.4.1 is performed at each single ground truth point and corresponding brightness temperature (TB_h, TB_v) and temperature data (T_s, T_{TIR}, T_{eff}). LPRM is than applied using individual h_r values for each ground truth point to compute soil moisture. To directly investigate the relationship between the achieved h_r and vegetation conditions the results of the local optimization are explicitly analysed at the set of the 40 ground truth points were also VI calculated from the AISA imaging spectrometer data were available.

5.5 Soil moisture results

The next three sections present the soil moisture results using LPRM with the default parameterization and the scene-based and pixel-based optimization. Section 5.5.1 gives retrieval results using LPRM default values. Section 5.5.2 presents LPRM soil moisture results achieved from a scene based optimization of h_r and the temperature shift T_{shift}. Section 5.5.3 presents the results for the pixel based optimization of h_r and the temperature. The perfor-

mance of LPRM was analysed using the RMSE and the coefficient of determination R² using a linear regression between LPRM retrieved and ground measured soil moisture.

5.5.1 Soil moisture retrieval with LPRM default parameters

LPRM was first applied using the default parameterization as given in table 5-3 and without a priori information of soil moisture within the inversion process of LPRM. The soil moisture input was set to a standard range from 5 – 70 Vol. %. Figure 5-4 presents the default LPRM soil moisture results using T_s, T_{TIR} and plotted against the in-situ soil moisture for all 90 ground truth locations (winter barley and winter rye combined). Clearly, the soil moisture results using T_{TIR} are generally higher than if T_s is applied with a mean shift of 5.6 Vol. % compared to T_s. The coefficient of determination of the two achieved soil moisture results (using T_s and T_{TIR}) is R² = 0.91 and the RMSE = 1.19 Vol. %. Using T_{eff} mean soil moisture difference of 4.3 Vol. % were found compared to soil moisture results using T_s.

However, the retrieved soil moisture values are extremely outside of the measured range exhibited at the day of observation. The LPRM soil moisture results over the crops and during the dry conditions are generally overestimated. Hence, it is essential to have any information about the real soil moisture conditions and use them within the forward modeling of TB_h.
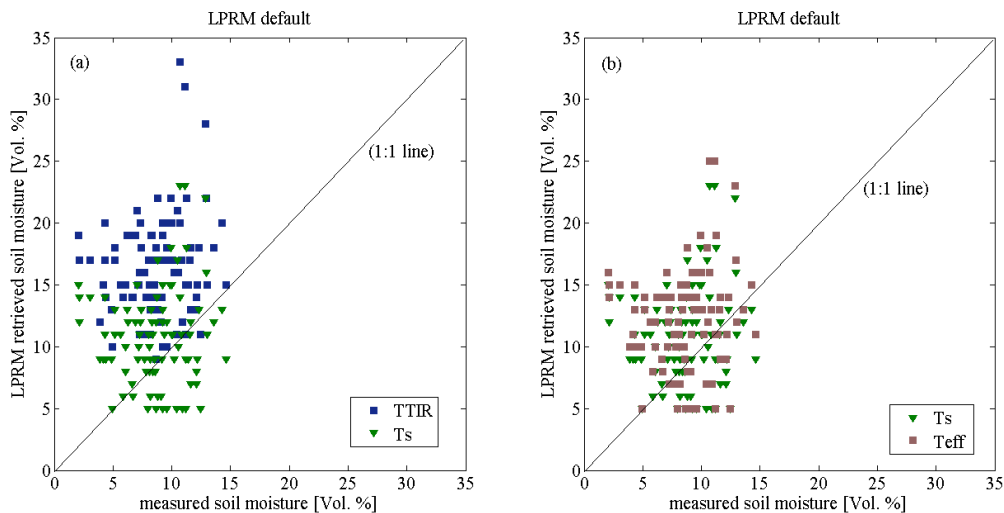
Figure 5-4.   Comparison of LPRM retrieved (default parameterization) soil moisture using T_s, T_{TIR}, T_{eff} and plotted against the measured in-situ soil moisture for all 90 ground truth locations for winter barley and winter rye.

5.5.2 LPRM soil moisture results for scene-based optimization

Within the scene-based optimization procedure, the soil moisture range for the forward modeling of TB_h was constrained by the soil porosity.

The motivation for the application of the scene-based optimization procedure was to find one optimal h_r parameter that minimizes the RMSE between observed and LPRM retrieved soil moisture. Furthermore, the variation of h_r depending on the applied temperature data (T_s, T_{TIR}, T_{eff}) is discussed. In table 5-5 the performed LPRM runs for the different temperature input data and ground truth data used are specified. As can be seen, the found optimal values for h_r vary much (0.16 – 1.05) dependent on the used ground truth data set and the applied temperature source. The RMSE values achieved by comparing the LPRM retrieved soil moisture and measured soil moisture are quite similar for all nine applied input data sets.

Table 5-6.   Determined h_r and temperature shift T_{shift} achieved within the scene-based optimization procedure using MC simulated data. Default settings of Q = 0.2, ω = 0, P = 0.465, S = 0.52 and C = 0.11 are applied.

runs	winter rye	winter barley	source of temperature	h_r	T_{shift}	R^2	RMSE [Vol. %]
set1		x	T_{TIR}	0.61	-3.99	0.32	1.15
set2		x	T_s	0.79	-0.03	0.23	1.23
set3		x	T_{eff}	1.05	-2.10	0.25	1.23
set4	x		T_{TIR}	0.16	2.12	0.02	1.69
set5	x		T_s	0.27	3.21	0.03	1.22
set6	x		T_{eff}	0.50	4.89	0.04	1.48
set7	x	x	T_{TIR}	0.87	3.17	0.04	1.51
set8	x	x	T_s	0.56	1.96	0.02	1.37
set9	x	x	T_{eff}	0.96	3.15	0.03	1.50

Figure 5-5 presents the relationship between the found optimal h_r and the appropriate scene-based temperature shift T_{shift} on the input temperature. It was found that h_r slightly decreases with a positive temperature shift or in other words if the exhibiting temperature is warm.
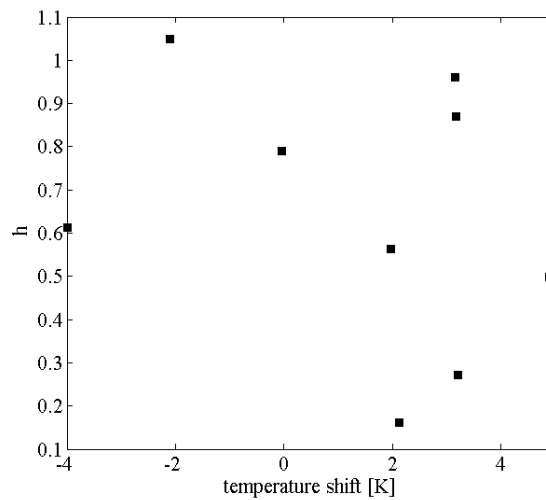
Figure 5-5.   Scatter plot of optimized scene-based h_r and temperature shift T_{shift} from all nine LPRM runs.

The RMSE between LPRM retrieved and measured soil moisture are generally low but the results are not well distributed around the 1:1 line if regarding the combined results for winter barley and winter rye (see figure 5-6). That may be caused by an inappropriate global parameterization of h_r by regarding the natural occurring differences of the two crop types. A main hampering factor for the retrieval of better soil moisture results may be caused by the canopy height of the winter rye, which was approximately 20 cm higher than the winter barley canopy. Therefore, the scattering processes and attenuation of the soils microwave emission at L-band is more affected within the winter rye canopy. Vertical structure of the stems has a dominating effect on the scattering within the crop canopy (Ulaby 1995, Wigneron et al. 2004). Even small differences in vegetation parameter characteristics (e.g. vegetation water content, LAI, canopy height) within a crop site may result in significant limitations of soil moisture sensitivity on observed brightness temperature.

set 7 - winter barley & winter rye
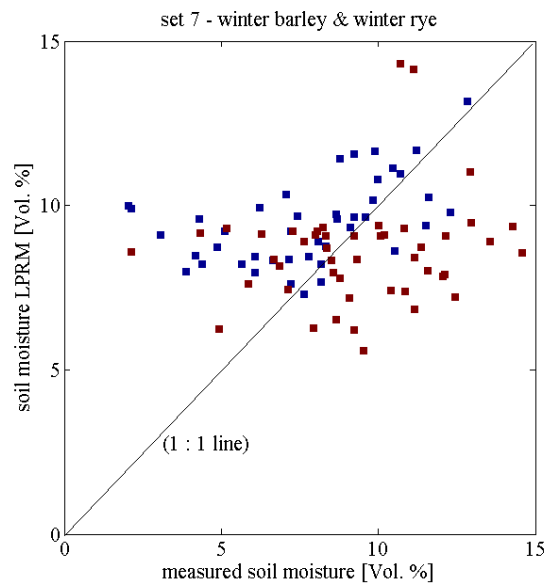
Figure 5-6.   Comparison of predicted and measured soil moisture achieved from the scene-based parameter optimization using T_{TIR} for winter barley and winter rye data (set 7, blue squares – winter barley, red squares – winter rye).

As no convergence between LPRM retrieved soil moisture and measured soil moisture could be achieved using the ground truth data from the two crop sites together a scene-based optimization was performed individually for each site (winter barley and winter rye separately). As can be seen in figure 5-7 (a) for the winter barley data the LPRM retrieved soil moisture results scatter reasonably well around the 1:1 line to the measured soil moisture. Regarding the narrow range of soil moisture the sensitivity of LPRM is still good enough to link small changes of observed brightness temperature (TB_h, TB_v, $MPDI$) and T_{TIR} information to soil moisture changes. Although, the soil moisture variation below the winter rye canopy could not be approximated satisfactorily using the scene-based parameterization of h_r.
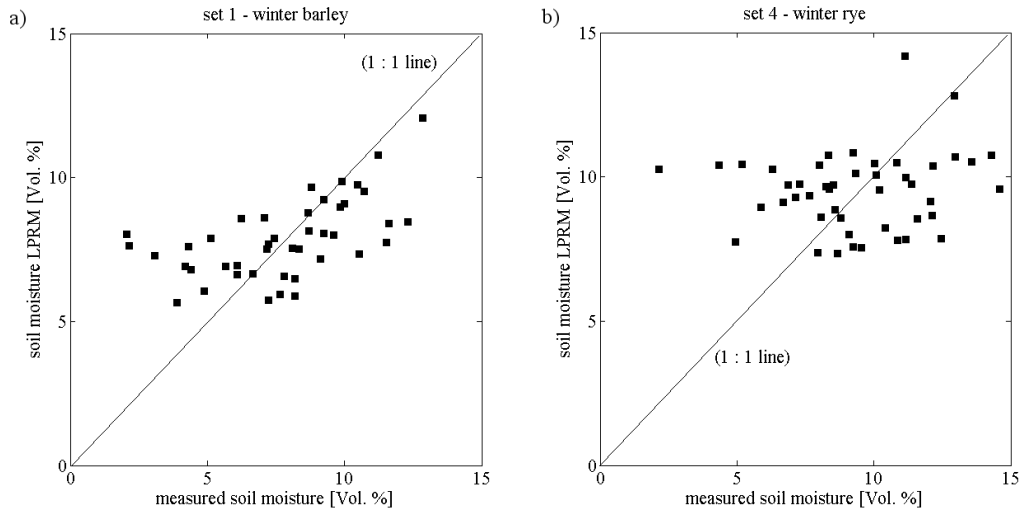
Figure 5-7.   Comparison of LPRM retrieved and measured soil moisture achieved from the scene-based parameter optimization using T_{TIR} for winter barley (a) and winter rye (b).

The LPRM retrieved soil moisture values are still overestimated compared to the measured soil moisture. As a result, a scene-based optimization of h_r is not sufficient to determine reliable soil moisture estimates below a crop canopy either using the data of the two crop sites together or separately.

Within figure 5-8, the relationship between the roughness parameter values h_r achieved from the Monte-Carlo simulated data and the RMSE from LPRM retrieved and measured soil moisture is shown. It can be seen that there is a strong equifinality regarding the roughness parameter h_r and resulting in similar RMSE. The parameter response surface, as represented by the data points with a small RMSE, is complex and without any clear peaks, which implies that the model is ambiguous in terms of its parameterization for h_r. As a result, no optimal roughness value h_r can clearly be determined.
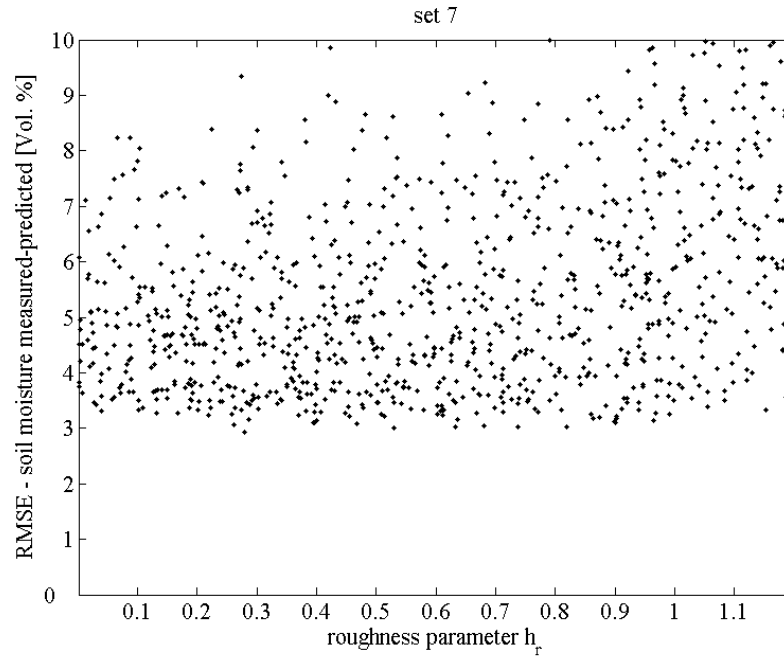
Figure 5-8.   Scatter plot of the RMSE between measured and LPRM retrieved soil moisture using LPRM and tested roughness parameters. Results achieved on the winter barley and winter rye ground truth points and for a MC set of 1000/100.

Furthermore, the problem of equifinality is demonstrated in figure 5-9 on the relationship of the simulated data for h_r and the temperature shift T_{shift}. There is clearly no relationship between h_r and the temperature shift T_{shift}, but as can be seen by the colour schema equifinality appears for the RMSE between measured and LPRM retrieved soil moisture. The same "goodness of fit" represented by the RMSE can be achieved from completely different combinations of h_r and a temperature shift T_{shift}. It was found that the RMSE slightly increases for h_r values close to 0 and 1.2 and corresponding temperature shifts T_{shift} with absolute values close to the defined maximum of 5 K.
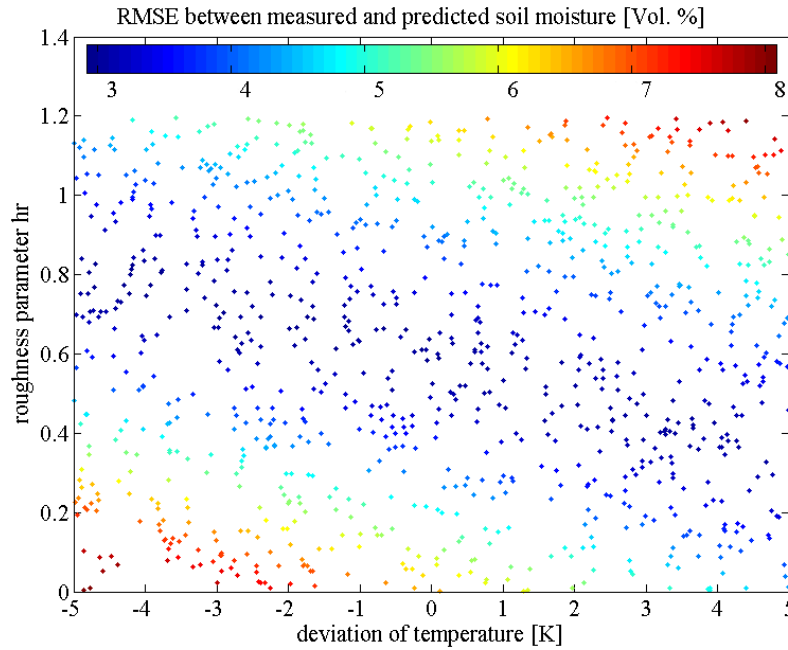
Figure 5-9.   Scatter plot of roughness parameter h_r and temperature shifts T_{shift} for set 7. The colour schema represents the RMSE between measured and LPRM retrieved soil moisture.

5.5.3   LPRM soil moisture results for pixel-based optimization

With the application of a pixel-based optimization for h_r and the temperature shift T_{shift} the coefficient of determination R² and the RMSE between measured and LPRM retrieved soil moisture were strongly improved as can be seen in table 5-6. The results are comparable with results achieved in de Jeu (2009) were coefficients of determination were found up to R² = 0.98 (using linear regression) between LPRM retrieved and ground measured soil moisture. They applied a dynamic roughness parameterization h_r (roughness values varying between 0.2 and 0.45) but in contrary to this study it was optimized for soil moisture and the incidence angle.

Table 5-7.   Coefficient of determination R² and RMSE between measured and LPRM retrieved soil moisture using pixel-based optimization. Default settings of Q = 0.2, ω = 0, P = 0.465, S = 0.52 and C = 0.11 are applied.

	number of sampling points	source of temperature	standard deviation of h_r	R²	RMSE [Vol. %]
set1-l	40	T_{TIR}	0.34	0.99	0.11
set2-l	40	T_s	0.30	0.98	0.38
set3-l	40	T_{eff}	0.31	0.99	0.28
set4-l	90	T_{TIR}	0.31	0.99	0.09

The effect of the temperature data (T_s, T_{TIR}, T_{eff}) applied seems to be negligible in terms of the RMSE by applying the pixel-based optimization for h_r. Figure 5-10 represents the model performance at the 40 ground sampling points using T_{TIR} were a coefficients of determination was found with R² = 0.99 (using linear regression). The differences between LPRM retrieved and measured soil moisture does not exceed an absolute value of 2.5 Vol. % (using T_s within LPRM). An average deviation between the soil moisture results of 0.24 Vol. % was found using T_{TIR}.and for T_{eff} with 1.65 Vol. %. The found optimal values for h_r vary much, with a standard deviation of ~ 0.30 (see table 5-6) at the different ground truth locations.
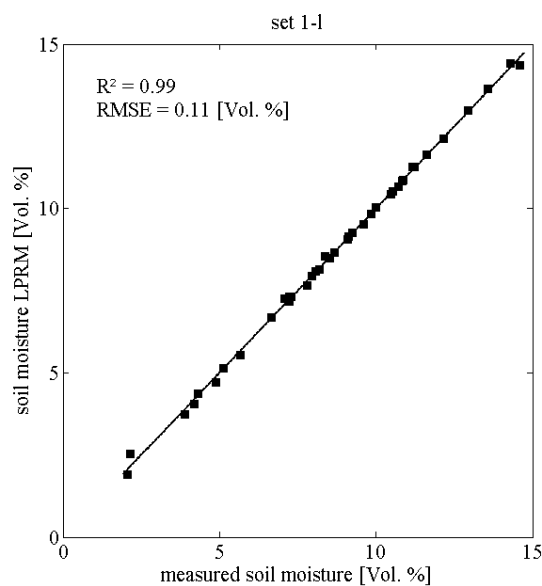
Figure 5-10.   Comparison of LPRM retrieved and measured soil moisture achieved using T_{TIR} within the pixel-based optimization of h_r for winter barley and winter rye data at the AISA ground truth locations.

As can be seen in figure 5-11 there is an obvious correlation between the roughness parameter h_r and the measured soil moisture where h_r increases with increasing soil moisture. The dependence of h_r on soil moisture can be explained by the so-called dielectric roughness, which is assumed to be related to dielectric variations within the soil (Saleh et al. 2007, Wigneron et al. 2001). Furthermore, a rough clustering of NDVI values depending on h_r and soil moisture is found. Higher NDVI values appear at locations with higher h_r values and higher soil moisture. The results indicate that the roughness parameter h_r also compensates effect of the vegetation on the observed brightness temperature data.
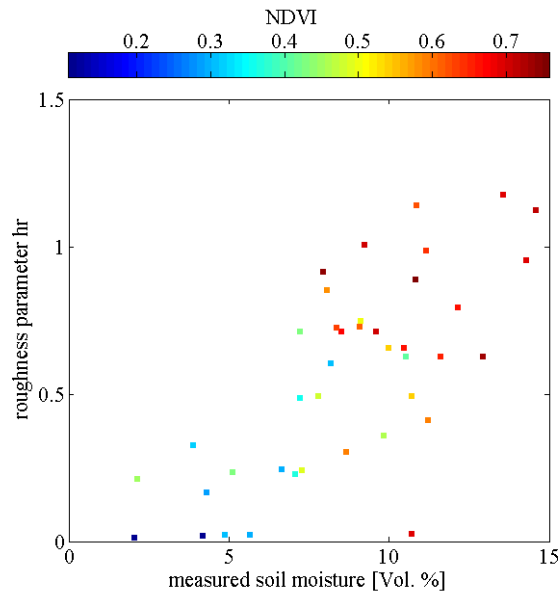
Figure 5-11.   Relationship between roughness parameter h_r (set 1-l), measured soil mois-
ture and NDVI for all AISA ground truth locations.

The dependency of h_r on the presence of developed green vegetation is more clearly pre-
sented in figure 5-12. At the winter barley and winter rye ground truth locations spatially-
explicit comparisons between calculated spectral narrow band NDVI and h_r show clearly an
increasing h_r with increasing NDVI. Based on theory, h_r actually regarded to account for soil
roughness, though it is below a crop canopy also affected by the vegetation. Obviously, the
roughness parameter also includes a roughness effect controlled by the vegetation and as
vegetation characteristics are spatially variable also h_r is spatially variable. Therefore,
roughness parameterizations derived from bare soil studies can not simply be transfered to
vegetated soils and roughness parameter values from vegetated areas are temporally dy-
namic depending on plant phenology. Note, that the findings within this study are valid for
very specific soil moisture and phenological conditions. However, the appearing phenome-
non represents the problem of de-coupling single effects influencing the microwave emis-
sion and hampering the clear identification of natural characteristics controlling model pa-
rameters such as h_r. Microwave scattering effects of the soil surface are not clearly to de-
couple from overlaying scattering effects within the vegetation canopy.
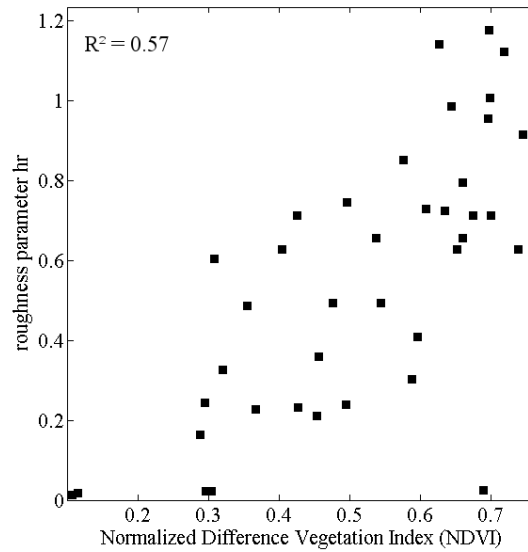
Figure 5-12.   Scatter plot of roughness parameter h_r and NDVI. The coefficient of determination R² was derived from a linear regression.

5.6   Discussion and Conclusion

This study demonstrated the use of LPRM for soil moisture retrieval from spatial high resolution passive L-band microwave observations below two crop type canopies (winter barley and winter rye) and measured very dry soil moisture conditions (< 15 Vol. %) at the time of observation. The following aspects were considered within this study:

-   Using LPRM with the default parameterization but different temperature data (T_s, T_{TIR}, T_{eff}) to quantify the differences in the LPRM retrieved soil moisture caused by the temperature input.

-   A scene-based optimization using Monte-Carlo simulation was performed to find one crop type dependent uniform roughness parameter value h_r by considering a temperature shift T_{shift} on the applied input temperature data and improve LPRM soil moisture results.

-   A pixel-based optimization using Monte-Carlo simulation to find input data pair (measured soil moisture, brightness temperature, temperature) specific optimal roughness parameter values h_r to improve LPRM soil moisture results.

-   To investigate the relationship between the roughness parameter h_r and spatially varying vegetation conditions represented by NDVI data.

As the temperature is a main controlling factor on the microwave emission at L-band, the analyses are applied using different temperature input data, namely the soil temperature T_s,

thermal infrared temperature T_{TIR} and the calculated soil effective temperature T_{eff}. Regarding the aspects outlined above the results are summarized as follows:

- Using LPRM with the default parameterization of h_r the results were generally overestimated and not within the measured soil moisture range during the PLMR observation. Therefore, to optimize the retrieval of TB_h using LPRM it is essential to have pre-information about the real exhibiting soil moisture conditions. Furthermore, using T_{TIR} the soil moisture results are generally higher than if T_s or T_{eff} is applied. This phenomenon can probably be related to the fact that T_{TIR} contains a major contribution of the vegetation and of the vegetation water, which causes higher soil moisture retrieval results using LPRM. The application of T_{eff} did not show any significant difference to the LPRM soil moisture results using T_{TIR} or T_s. Note, that T_{eff} is evaluated over bare soil or using simulated data (Wigneron et al. 2008). Furthermore, the calculation differs between studies in terms of the used soil moisture profile (sampling depth) data. Differences in the observation time of PLMR data and ground soil moisture can be neglected in this study since the observations took place within a two hour time window in the late morning.

- No uniform parameterization of h_r performing the scene-based optimization was found for the two crop sites to reasonably estimate the soil moisture conditions using LPRM by considering the measured soil moisture range. It was found that the roughness parameter h_r change with the type of temperature data (T_s, T_{TIR}, T_{eff}) used and with the crop input data type (winter barley or winter rye). Applying the scene-based optimization for winter barley and winter rye separately the performance between measured soil moisture and LPRM retrieved soil moisture increases for winter barley. The best soil moisture estimates (but still not satisfactory with $R^2 = 0.32$) for the winter barley were achieved using T_{TIR} and $h_r = 0.61$. LPRM retrieved soil moisture for winter rye still did not match satisfactorily the measured values. The reason for the bad performance may lay in the differences of the two crop type vegetation canopies. In the same phenological stage (flowering, main shoot) both actually have an average difference of the canopy height with 20 cm. That difference seems a likely reason why no uniform h_r value can provide reasonable soil moisture results using LPRM.

- Performing the pixel-based optimization it is demonstrated that considering h_r as spatially variable the soil moisture retrieval using LPRM can be improved significantly. It was demonstrated that the roughness parameter value h_r can change much even within a vegetation canopy previously have been regarded homogeneous. As the soil surface characteristics can be assumed homogeneous over the field because the day of the experi-

ment during the vegetation period was late and the soil surface is stable below the canopy.

- Furthermore, it was shown that the roughness parameter values h_r are clearly related to the vegetation conditions represented using the NDVI. Therefore, the roughness parameter physically necessary to account for the rough soil surface emissivity is over vegetated soils influenced by the vegetation conditions.

- The study demonstrated the problem of equifinality in terms of the definition of the roughness parameter h_r. Equifinality in the sense that equal good results (e.g. a specific RMSE) may be achieved by a great number of parameter value combinations (e.g. h_r and T_{shift}). As a result, there is no clear single optimum parameter set. An optimum is defined depending on observed experimental conditions and available data. Therefore, for physically based models also an empirically effort exists to optimize the parameter value for the experiment specific conditions.

The results of this study show that good soil moisture results can be achieved using LPRM by applying spatially dynamic roughness parameter values. Since the roughness parameter h_r changes from pixel to pixel, a scene-based roughness parameterization yields a deficit of accuracy of LPRM soil moisture retrieval results.

Therefore, a number of tests still have to be made analyzing high spatial resolution experimental data to retrieve soil moisture and consider spatially changing roughness conditions. Especially for agricultural applications where it is a major issue to monitor the spatial distribution of soil moisture on a small scale (field, only several hectares) it is important to consider the spatial variation of model parameters like h_r. and its relation to the soil covered vegetation.

6.   General Conclusions

In this thesis airborne passive L-band microwave observations (PLMR) were applied to re-trieve soil moisture underneath a crop canopy. Additionally, high spatial resolution (1.5 m) airborne imaging spectrometer (AISA) data was used to analyse the vegetation influence on the high spatial resolution (50 m) brightness temperature data. Field measurements of soil moisture and vegetation canopy parameters (e.g. LAI) were used as ground truth. A crop vegetation canopy which is in many studies been assumed homogeneous was considered heterogeneous within this study. All analyses are performed on data gathered on a winter barley and winter rye site during one day of observation.

This study is unique in that the soil moisture conditions, which had to be estimated, exhib-ited in a very small and dry soil moisture range (< 15 Vol. %) at the day of the L-band pas-sive microwave observations. Two methods, namely empirical multi-variate regression and the land surface parameter retrieval model (LPRM) were applied to retrieve soil moisture from the L-band brightness temperature data. A special feature and basis for the analyses of the vegetation effect on the microwave data was the availability of spectral narrow band vegetation indices calculated from airborne imaging spectrometer data collected over the crop sites. That data allowed unique analyses of the relationship between passive microwave data, spatially varying vegetation canopy conditions (LAI, NDVI) and the roughness pa-rameter used within LPRM at field scale.

The preceding chapters have shown:

-     An obvious relationship of the microwave signal dependent on i) the PLMR pixel average LAI, ii) sub-pixel variability of LAI, and iii) the viewing angle of the bright-ness temperature observations were found within a vegetation canopy that are usually assumed being homogeneous (see chapter 3). The findings are important for support-ing the understanding of the effect of vegetation on high spatial resolution L-band data, which has to be considered for soil moisture estimations below crop canopies. Furthermore, the findings are also very useful for the application of passive L-band microwave data to retrieve vegetation biomass data.

-     The combined empirical analyses of spectral narrow band vegetation indices and brightness temperature data at L-band provides a simple and fast approach to estimate soil moisture below crops as it is interesting for operational agricultural applications (see chapter 4). Soil moisture estimates with an accuracy equal to 0.82 Vol. % (RMSE) were obtained. The availability of imaging spectrometer data provides a very valuable source of information about vegetation conditions. Compared to ground point

- measurements (e.g. of LAI) it is already a spatially integrated data product and can directly be included within the data analyses.
- In chapter 5 it was found that using a default parameterization for the roughness (h_r = 0.1) no reasonable soil moisture results could be achieved using LPRM. Furthermore, results based on a scene-based parameterization for the roughness parameter did not provide satisfactory results on the two crop types.
- Very good results for soil moisture were achieved by applying a pixel-based optimization using Monte-Carlo simulation for the roughness parameter at the ground truth locations on a winter barley and winter rye site. Linear regression between LPRM retrieved and measured soil moisture showed convergence up to $R^2 = 0.99$ (see chapter 5). The good results are in cause of an optimization of the roughness parameter for each single ground truth location, which resulted in spatially varying roughness parameter values.
- A clear relationship between NDVI data and local optimized roughness parameter values ($R^2 = 0.57$) were found. This indicates an obvious dependency of the roughness from the vegetation conditions covering the soil surface. This can be interpreted as the roughness parameter has to consider a vegetation "roughness" influence if vegetation is present on the soil surface (see chapter 5).

Beside the critical vegetation canopy characteristics (flowering, main shoot) only a small range of soil moisture conditions was measured during the day of the experiment. No study was found in the literature where a radiative transfer model was applied to similar site conditions and experimental passive L-band microwave data. From the point of view of agricultural irrigation management such dry conditions are of special interest to ensure and improve agricultural yield. Therefore, a strong motivation exists to provide applicability of LPRM for different soil moisture conditions and at field scale like it was performed within this study for a very dry soil.

However, by comparing soil moisture results from 50 m PLMR pixels with ground measured point soil moisture differences obviously have to occur. The footprint integrated and to square pixels resampled PLMR observation represent a completely different measurement compared to the point ground measurement taken as reference. Nevertheless, the field soil moisture data measured by mobile capacitance sensors (ML2 Theta probes) seem an appropriate ground truth to account for the spatially varying soil moisture for operational applications.

No study in literature was found where the roughness parameter, which is a controlling parameter to account for the surface emissivity of a rough soil, was discussed in terms of its correlation to NDVI data for vegetated soils. The soil surface and crop canopy conditions of

the two test sites (winter barley and winter rye) did not correspond to extreme conditions in terms of within field heterogeneities (e.g. of soil type, LAI). Therefore, the roughness parameter values are highly spatial variable even for a vegetation canopy which is generally assumed to be homogeneous. This indicates that over vegetated soils and under similar experiment conditions (e.g. spatial resolution of data sampling) the roughness parameter may also be related to vegetation conditions (e.g. represented by NDVI data) to improve soil moisture retrievals using radiative transfer models.

The previous section demonstrated that physical explanations to account for a model parameter within a physically based mathematical function (e.g. rough soil emissivity) are uncertain in their expression and unclear in their way of parameterization. The dependence of single model parameters (e.g. roughness) on surface characteristics is not clear and experiment specific assumptions are applied. The soil roughness parameter as it controls mainly the rough surface emissivity is not achievable in an operational manner and is in many studies simply transferred between test sites. Because the results, as demonstrated in chapter 5, show the roughness parameterization strongly influences the performance of LPRM and not only vegetation canopy type but especially also the specific phenological stage should be considered by evaluating roughness parameterizations for application purposes. Comprehensive value tables are missing for the roughness parameterization at a variety of vegetation species and a wide range of phenological conditions that highly change during the growing cycle.

Key criterions for the decision of an appropriate model type either empirically or physically are the availability and the effort in providing input data for calibration. Empirical approaches require a large amount of data to account for the variability of the dependent variable. Physically based models mostly require a selection of physical parameters that can not easily be measured during any ground truth campaign. However the main limiting factor of both approaches is the site dependency (soil type, vegetation type) of the model parameters. Using physically based models such as radiative transfer equations truly quantitative estimates of soil moisture can be retrieved. Empirical models are of interest where no correct parameterization of a physically based model can be provided or where the inversion of such models failed. This thesis shows the high potential and simple application of the combined analyses using high spatial resolution L-band radiometer observations together with imaging spectrometer data for soil moisture estimation. Note, the analyses were performed using very specific remote sensing data (e.g. spatial resolution, viewing angle) and over specific site conditions represented by the phenological stage of the crops and the very dry soil moisture (< 15 Vol. %) conditions.

As the top canopy is a geometrically complex structure that is strongly influenced by rain and wind and phenological and physiological differences occur spatially variable especially the upcoming EnMAP (Environmental Mapping and Analyses Program) satellite mission (scheduled launch 2013) promises detailed information about vegetation conditions, which can be applied for soil moisture retrieval using L-band brightness temperature. Furthermore, recent and new terrestrial monitoring networks (e.g. TERENO in Germany) provide useful reference data to establish operational soil moisture retrieval using new and upcoming remote sensing data product e.g. SMOS or SMAP. High spatial resolution airborne data is an appropriate method to analyse sub-pixel heterogeneities for disaggregation purpose of coarse scale soil moisture data. Beside the requirement on global soil moisture maps provided from satellite missions local airborne campaigns have a great potential to support hydrological catchment management and support agricultural management. However, to improve exsisting model approachs or develop new methods it is important for future work to provide validatation for a wide range of land cover conditions and a wide range of phenological stages.

7.   Summary

Soil moisture is a key variable at the global water cycle. The water content of the soil's few upper centimeters controls the partitioning of water and energy fluxes on the land surface including the splitting of rainfall into surface runoff, infiltration and evapo-transpiration, as well as the redirection of incoming solar radiation into albedo, thermal radiation, sensible and latent heat fluxes. Information about spatial surface soil moisture is therefore an important boundary condition for process based hydrological, climate or ecological models ranging from the field scale up to the global scale and its knowledge is essential in order to improve operational hydrological, climate and weather predictions including flood forecasting, drought monitoring or eco-climatological projections via calibration or data assimilation techniques. The aim of this thesis is to retrieve soil moisture over agriculturally used sites using high spatial resolution airborne L-band radiometer data (50 m).

Low-frequency passive microwave remote sensing at L-band (~ 1.4 GHz) has been found to be the most promising remote sensing method for soil moisture monitoring due to the direct link between microwave radiation and dielectric properties, its deeper penetration into vegetation, its all-weather capabilities and its negligible atmospheric attenuation. The large amount of research on estimating soil moisture from L-band radiometers resulted in a consensus regarding the major factors that should be incorporate in data analyses. The soil moisture sensitivity of L-band brightness temperature changes spatially with soil, vegetation and terrain characteristics. The contribution of soil moisture on observed brightness temperature at L-band is highly spatial variable as it is strongly influenced from the vegetation cover of the soil. Attenuation and scattering processes within a vegetation canopy are strongly influenced by specific geometrical (e.g. leaf area index - LAI, canopy height) and biophysical (e.g. vegetation water content) vegetation canopy characteristics. In order to estimate soil moisture below a vegetation canopy it is essential to provide spatial distributed information about vegetation characteristics.

To account for the spatial distribution of vegetation characteristics within this study, high spatial resolution airborne imaging spectrometer data (1.5 m) are analysed together with L-band brightness temperature data. Spectral vegetation indices computed from spectrometer data provide a high potential to account for spatially varying vegetation canopy characteristics. The analyses from this thesis are performed over crops (winter barley, winter rye) by using in-situ field measurements as ground truth for vegetation condition and soil moisture. This study is unique in that the soil moisture conditions, which had to be estimated, exhibited in a very small and dry soil moisture range (< 15 Vol. %) at the day of the L-band passive microwave observations.

The key questions of the study are summerized as follow:

1. Is there a unique relationship between LAI and high spatial resolution L-band brightness temperature at sub-pixel level?

2. Does the combined use of L-band data and hyperspectral vegetation indices provide reasonable estimates of surface soil moisture using empirical models?

3. How strongly does the temperature information affect the soil moisture estimates using the land surface parameter retrieval model (LPRM)?

4. Is there a relationship between within field variations of the vegetation canopy and the roughness parameter used with the land surface parameter retrieval model (LPRM)?

The results show an obvious ($0.23 < R^2 > 0.90$) relationship between the microwave brightness temperature data and LAI variations within a vegetation canopy that is usually assumed being homogeneous (e.g. crops). Furthermore, the combined empirical analyses of spectral narrow band vegetation indices and brightness temperature data at L-band provides a simple and fast approach to estimate soil moisture below crops (RMSE = 0.82 Vol. %). The applied imaging spectrometer data and calculated spectral vegetation indices represented the spatially changing vegetation canopy characteristics (e.g. LAI or vegetation greenness) very well. Using LPRM with a default parameterization for the roughness ($h_r = 0.1$), no reasonable soil moisture results could be achieved. Soil moisture results using LPRM and different temperature input data showed average differences of 5.6 Vol. %. Very good results ($R^2 = 0.99$) for soil moisture were achieved by applying spatially varying values for the roughness parameter, which were achieved from an optimization of LPRM using Monte-Carlo simulation at the ground truth locations on the winter barley and winter rye site. An obvious relationship between NDVI data and the spatial varying roughness parameter values ($R^2 = 0.57$) were found. This indicates a dependency of the roughness from the vegetation conditions covering the soil surface.

Using the airborne remote sensing and field data collected in the course of this research, in this study it is demonstrated that either the empirical models and the LPRM model provides good estimates for the occuring very dry soil moisture conditions (< 15 Vol. %) at the day of the L-band data acqusition. Considering the relationship of the roughness parameter and NDVI, a spatial varying parameterization of the roughness within radiative transfer models may be realized to finally improve soil moisture estimates below a vegetation canopy. The analyses within this were performed using very specific L-band brightness temperature data (e.g. spatial resolution, viewing angle) achieved at experiment specific site conditions represented by the phenological stage of the crops and the very dry soil moisture conditions.

Therefore, it is generally important for future work to provide validatation for a wide range of land cover conditions and a wide range of phenological stages. Recent and new terrestrial monitoring networks (e.g. TERENO in Germany) provide useful reference data to establish operational soil moisture retrieval using new and upcoming remote sensing data product e.g. SMOS or SMAP.

References

Alvarez-Mozos, J., Casali, J., Gonzalez-Audicana, M. and Verhoest, N. E. C., 2005, Correlation between ground measured soil moisture and RADARSAT-1 derived backscattering coefficient over an agricultural catchment of Navarre (North of Spain). Biosystems Engineering, 92, 119-133.

Bastiaanssen, W. G. M., Molden, D. J. and Makin, I. W., 2000, Remote sensing for irrigated agriculture: examples from research and possible applications. Agricultural Water Management, 46, 137-155.

Belcher, D.J., Cuykendall, T.R., Sack, H.S., 1950, The measurement of soil moisture and density by neutron and gamma-ray scattering. Technical Development and Evaluation Center, 1-20.

Beven, K.J. and Kirkby, M.J., 1979, A physically based, variable contributing area model of basin hydrology Bulletin of the International Association of Scientific Hydrology, 24, 43 - 69.

Bindlish, R. and Barros, A. P., 2000, Multifrequency soil moisture inversion from SAR measurements with the use of IEM. Remote Sensing of Environment, 71, 67.

Bindlish, R. and Barros, A. P., 2002, Subpixel variability of remotely sensed soil moisture: An inter-comparison study of SAR and ESTAR. IEEE Transactions on Geoscience and Remote Sensing, 40, 326-337.

Bindlish, R., Crow, W. T. and Jackson, T. J., 2009, Role of passive microwave remote sensing in improving flood forecasts. IEEE Geoscience and Remote Sensing Letters, 6, 112-116.

Blyth, K., 1993, The use of microwave remote-sensing to improve spatial parameterization of hydrological models. Journal of Hydrology, 152, 103-129.

Bogena, H., Schulz, K. and Vereecken, H., 2006, Towards a network of observatories in terrestrial environmental research. Advances in Geoscience, 9, 109-114.

Bouma, J., Stoorvogel, J., Van Alphen, B. J. and Booltink, H. W. G., 1999, Pedology, precision agriculture, and the changing paradigm of agricultural research. Soil Science Society of America Journal, 63, 1763-1768.

Brunfeldt, D. R. and Ulaby, F. T., 1984, Measured micrwoave emission and scattering in vegetation canopies. IEEE Transactions on Geoscience and Remote Sensing, 22, 520-524.

Brunfeldt, D. R. and Ulaby, F. T., 1986, Mircowave emission from row crops. IEEE Transactions on Geoscience and Remote Sensing, 24, 353-359.

Burke, E. J., Shuttleworth, W. J. and Houser, P. R., 2004, Impact of horizontal and vertical heterogeneities on retrievals using multiangle microwave brightness temperature data. IEEE Transactions on Geoscience and Remote Sensing, 42, 1495-1501.

Burke, E. J. and Simmonds, L. P., 2003, Effects of sub-pixel heterogeneity on the retrieval of soil moisture from passive microwave radiometry. International Journal of Remote Sensing, 24, 2085-2104.

Capehart, W. J. and Carlson, T. N., 1997, Decoupling of surface and near-surface soil water content: A remote sensing perspective. Water Resources Research, 33, 1383-1395.

Castillo, V. M., Gomez-Plaza, A. and Martinez-Mena, M., 2003, The role of antecedent soil water content in the runoff response of semiarid catchments: a simulation approach. Journal of Hydrology, 284, 114-130.

References

Choudhury, B. J., Schmugge, T. J., Chang, A. and Newton, R. W., 1979, Effect of surface-roughness on the microwave emission from soils. Journal of Geophysical Research-Oceans and Atmospheres, 84, 5699-5706.

Choudhury, B. J., Schmugge, T. J. and Mo, T., 1982, A parameterization of effective soil-temperature for microwave emission. Journal of Geophysical Research-Oceans and Atmospheres, 87, 1301-1304.

Cognard, A. L., Loumagne, C., Normand, M., Olivier, P., Ottle, C., Vidalmadjar, D., Loua-hala, S. and Vidal, A., 1995, Evaluation of the ERS-1 synthetic aperture radar capac-ity to estimate surface soil-moisture - 2-years results over the Naizin watershed. Wa-ter Resources Research, 31, 975-982.

Crow, W. T., Bindlish, R. and Jackson, T. J., 2005, The added value of spaceborne passive microwave soil moisture retrievals for forecasting rainfall-runoff partitioning. Geo-physical Research Letters, 32.

Davenport, I. J., Sandells, M. J. and Gurney, R. J., 2008, The effects of scene heterogeneity on soil moisture retrieval from passive microwave data. Advances in Water Re-sources, 31, 1494-1502.

De Jeu, R. A. M., Holmes, T. R. H., Panciera, R. and Walker, J. P., 2009, Parameterization of the Land Parameter Retrieval Model for L-Band Observations Using the NAFE'05 Data Set. IEEE Geoscience and Remote Sensing Letters, 6, 630-634.

De Jeu, R. A. M. and Owe, M., 2003, Further validation of a new methodology for surface moisture and vegetation optical depth retrieval. International Journal of Remote Sensing, 24, 4559-4578.

De Jeu, R. A. M., Wagner, W., Holmes, T. R. H., Dolman, A. J., Van De Giesen, N. C. and Friesen, J., 2008, Global soil moisture patterns observed by space borne microwave radiometers and scatterometers. Surveys in Geophysics, 29, 399-420.

Delwart, S., Bouzinac, C., Wursteisen, P., Berger, M., Drinkwater, M., Martin-Neira, M. and Kerr, Y. H., 2008, SMOS validation and the COSMOS campaigns. IEEE Transac-tions on Geoscience and Remote Sensing, 46, 695-704.

Doan Minh, C., Bui Doan, T. and Vo Thi Lan, A., 2003, Passive microwave remote sensing for estimation of rice water content in Vietnam. Paper read at Geoscience and Re-mote Sensing Symposium, 2003. IGARSS '03. Proceedings. 2003 IEEE Internation-al, 21-25 July 2003.

Dobson, M. C., Ulaby, F. T., Hallikainen, M. T. and Elrayes, M. A., 1985, Microwave di-electric behavior of wet soil - Part II: Dielectric mixing models. IEEE Transactions on Geoscience and Remote Sensing, 23, 35-46.

Du, Y., Ulaby, F. T. and Dobson, M. C., 2000, Sensitivity to soil moisture by active and passive microwave sensors. IEEE Transactions on Geoscience and Remote Sensing, 38, 105-114.

Efron, B. and Tibshirani, R., 1993, An introduction to the bootstrap. London: Chapman & Hall.

Engman, E. T., 1991, Applications of microwave remote-sensing of soil-moisture for water-resources and agriculture. Remote Sensing of Environment, 35, 213-226.

Entekhabi, D., Njoku, E. G., O'neill, P. E., Kellogg, K. H., Crow, W. T., Edelstein, W. N., Entin, J. K., Goodman, S. D., Jackson, T. J., Johnson, J., Kimball, J., Piepmeier, J. R., Koster, R. D., Martin, N., Mcdonald, K. C., Moghaddam, M., Moran, S., Reichle, R., Shi, J. C., Spencer, M. W., Thurman, S. W., Tsang, L. and Van Zyl, J., 2010, The soil moisture active passive (SMAP) mission. Proceedings of the IEEE, 98, 704-716.

References

Escorihuela, M. J., Kerr, Y. H., De Rosnay, P., Wigneron, J. P., Calvet, J. C. and Lemaitre, F., 2007, Simple model of the bare soil microwave emission at L-band. IEEE Transactions on Geoscience and Remote Sensing, 45, 1978-1987.

Ferrazzoli, P., Wigneron, J. P., Guerriero, L. and Chanzy, A., 2000, Multifrequency emission of wheat: Modeling and applications. IEEE Transactions on Geoscience and Remote Sensing, 38, 2598-2607.

Galantowicz, J. F., Entekhabi, D. and Njoku, E. G., 2000, Estimation of soil-type heterogeneity effects in the retrieval of soil moisture from radiobrightness. IEEE Transactions on Geoscience and Remote Sensing, 38, 312-316.

Gitelson, A. A., Vina, A., Arkebauer, T. J., Rundquist, D. C., Keydan, G. and Leavitt, B., 2003, Remote estimation of leaf area index and green leaf biomass in maize canopies. Geophysical Research Letters, 30.

Grayson, R. B. and Western, A. W., 1998, Towards areal estimation of soil water content from point measurements: time and space stability of mean response. Journal of Hydrology, 207, 68-82.

Haboudane, D., Miller, J. R., Pattey, E., Zarco-Tejada, P. J. and Strachan, I. B., 2004, Hyperspectral vegetation indices and novel algorithms for predicting green LAI of crop canopies: Modeling and validation in the context of precision agriculture. Remote Sensing of Environment, 90, 337.

Haubrock, S. N., Chabrillat, S., Lemmnitz, C. and Kaufmann, H., 2008a, Surface soil moisture quantification models from reflectance data under field conditions. International Journal of Remote Sensing, 29, 3-29.

Haubrock, S. N., Chabrillat, Sabine, Kuhnert, Matthias, Hostert, Patrick and Kaufmann, Hermann, 2008b, Surface soil moisture quantification and validation based on hyperspectral data and field measurements. Journal of Applied Remote Sensing, 2, 023552.

Houser, P. R., Shuttleworth, W. J., Famiglietti, J. S., Gupta, H. V., Syed, K. H. and Goodrich, D. C., 1998, Integration of soil moisture remote sensing and hydrologic modeling using data assimilation. Water Resources Research, 34, 3405-3420.

Hupet, F. and Vanclooster, M., 2002, Intraseasonal dynamics of soil moisture variability within a small agricultural maize cropped field. Journal of Hydrology, 261, 86-101.

Huszar, T., Mika, J., Loczy, D., Molnar, K. and Kertesz, A., 1999, Climate change and soil moisture: a case study. Physics and Chemistry of the Earth Part a-Solid Earth and Geodesy, 24, 905-912.

Idso, S. B., Jackson, R. D., Reginato, R. J., Kimball, B. A. and Nakayama, F. S., 1975, Dependence of bare soil albedo on soil-water content. Journal of Applied Meteorology, 14, 109-113.

Ivanov, V. Y., Vivoni, E. R., Bras, R. L. and Entekhabi, D., 2004, Catchment hydrologic response with a fully distributed triangulated irregular network model. Water Resources Research, 40.

Jackson, R. D. and Huete, A. R., 1991, Interpreting vegetation indexes. Preventive Veterinary Medicine, 11, 185-200.

Jackson, R. D., Idso, S. B. and Reginato, R. J., 1976, Calculation of evaporation rates during transition from energy-limiting to soil-limiting phases using albedo data Water Resources Research, 12, 23-26.

Jackson, T. J., 1993, Measuring surface soil-moisture using passive microwave remote sensing. Hydrological Processes, 7, 139-152.

References

Jackson, T. J., 2001, Multiple resolution analysis of L-band brightness temperature for soil moisture. IEEE Transactions on Geoscience and Remote Sensing 39, 151-164.

Jackson, T. J., 2001, Multiple resolution analysis of L-band brightness temperature for soil moisture. IEEE Transactions on Geoscience And Remote Sensing, 39, 151-164.

Jackson, T. J., Bindlish, R., Cosh, M., Gasiewski, A., Stankov, B., Klein, M., Weber, B. and Zavorotny, V., 2005, Soil moisture experiments 2004 (SMEX04) polarimetric scanning radiometer, AMSR-E and heterogeneous landscapes. Paper read at Geoscience and Remote Sensing Symposium, 2005. IGARSS '05. Proceedings. 2005 IEEE International, 25-29 July 2005.

Jackson, T. J., Chen, D., Cosh, M., Li, F., Anderson, M., Walthall, C., Doriaswamy, P. and Hunt, E. R., 2004, Vegetation water content mapping using Landsat data derived normalized difference water index for corn and soybeans. Remote Sensing of Environment, 92, 475.

Jackson, T. J., Hawley, M. E. and O'neill, P. E., 1987a, Preplanting soil-moisture using passive microwave sensors. Water Resources Bulletin, 23, 11-19.

Jackson, T. J., Hawley, M. E. and Oneill, P. E., 1987, Preplanting soil-moisture using passive microwave sensors. Water Resources Bulletin, 23, 11-19.

Jackson, T. J. and Le Vine, D. E., 1996, Mapping surface soil moisture using an aircraft-based passive microwave instrument: Algorithm and example. Journal of Hydrology, 184, 85-99.

Jackson, T. J., Le Vine, D. M., Hsu, A. Y., Oldak, A., Starks, P. J., Swift, C. T., Isham, J. D. and Haken, M., 1999, Soil moisture mapping at regional scales using microwave radiometry: The Southern Great Plains Hydrology Experiment. IEEE Transactions on Geoscience and Remote Sensing, 37, 2136-2151.

Jackson, T. J., Le Vine, D. M., Swift, C. T., Schmugge, T. J. and Schiebe, F. R., 1995, Large area mapping of soil moisture using the ESTAR passive microwave radiometer in Washita'92. Remote Sensing of Environment, 54, 27-37.

Jackson, T. J. and O'Neill, P. E., 1987b, Salinity effects on the microwave emission of soils. IEEE Transactions on Geoscience and Remote Sensing GE-25, 214-220.

Jackson, T. J. and Schmugge, T. J., 1991, Vegetation effects on the microwave emission of soils. Remote Sensing of Environment, 36, 203-212.

Jackson, T. J., Schmugge, T. J. and O'Neill, P., 1984, Passive microwave remote sensing of soil moisture from an aircraft platform. Remote Sensing of Environment, 14, 135-150.

Jackson, T. J., Schmugge, T. J. and Wang, J. R., 1982, Passive microwave sensing of soil-moisture under vegetation canopies. Water Resources Research, 18, 1137-1142.

Kerr, Y. H., 2007, Soil moisture from space: Where are we? Hydrogeology Journal, 15, 117-120.

Kerr, Y. H., Waldteufel, P., Wigneron, J. P., Martinuzzi, J. M., Font, J. and Berger, M., 2001, Soil moisture retrieval from space: The soil moisture and ocean salinity (SMOS) mission. IEEE Transactions on Geoscience and Remote Sensing, 39, 1729-1735.

Kirdyashev, K. P., Chukhlantsev, A. A. and Shutko, A. M., 1979, Microwave radiation of grounds with vegetative cover. Radiotekhhnika i Elektronika, 24, 256-264.

Li, H. B., Robock, A. and Wild, M., 2007, Evaluation of Intergovernmental Panel on Climate Change Fourth Assessment soil moisture simulations for the second half of the twentieth century. Journal of Geophysical Research-Atmospheres, 112.

References

Lillesand, T.M. and Kiefer, R.W., 1994, Remote sensing and image interpretation 3rd ed. John Wiley and Sons, New York, 750pp.

Loew, A. and Mauser, W., 2008, On the disaggregation of passive microwave soil moisture data using a priori knowledge of temporally persistent soil moisture fields. IEEE Transactions on Geoscience and Remote Sensing, 46, 819-834.

Majurec, N., Park, J., Niamsuwan, N., Frankford, M. and Johnson, J. T., 2009, Airborne L-band RFI observations in the smapvex08 campaign with the L-band interference suppressing radiometer. Paper read at Geoscience and Remote Sensing Symposium,2009 IEEE International, IGARSS 2009, 12-17 July 2009.

Markwell, J., Osterman, J. C. and Mitchell, J. L., 1995, Calibration of the Minolta SPAD-502 leaf chlorophyll meter. Photosynthesis Research, 46, 467-472.

Mattia, F., Le Toan, T., Picard, G., Posa, F. I., D'alessio, A., Notarnicola, C., Gatti, A. M., Rinaldi, M., Satalino, G. and Pasquariello, G., 2003, Multitemporal C-band radar measurements on wheat fields. IEEE Transactions on Geoscience and Remote Sensing, 41, 1551-1560.

Meesters, Agca, De Jeu, R. A. M. and Owe, M., 2005, Analytical derivation of the vegetation optical depth from the microwave polarization difference index. IEEE Geoscience and Remote Sensing Letters, 2, 121-123.

Merlin, O., Walker, J. P., Kalma, J. D., Kim, E. J., Hacker, J., Panciera, R., Young, R., Summerell, G., Hornbuckle, J., Hafeez, M. and Jackson, T., 2008, The NAFE'06 data set: Towards soil moisture retrieval at intermediate resolution. Advances in Water Resources, 31, 1444-1455.

Merz, R. and Bloschl, G., 2004, Regionalisation of catchment model parameters. Journal of Hydrology, 287, 95-123.

Merzlyak, M. N., Gitelson, A. A., Chivkunova, O. B. and Rakitin, V. Y., 1999, Non-destructive optical detection of pigment changes during leaf senescence and fruit ripening. Physiologia Plantarum, 106, 135-141.

Mo, T., Choudhury, B. J., Schmugge, T. J., Wang, J. R. and Jackson, T. J., 1982, A model for microwave emission from vegetation-covered fields. Journal of Geophysical Research-Oceans and Atmospheres, 87, 1229-1237.

Mo, T. and Schmugge, T. J., 1987, A parameterization of the effect of surface-roughness on microwave emission. IEEE Transactions on Geoscience and Remote Sensing, 25, 481-486.

Narayan, U., Lakshmi, V. and Jackson, T. J., 2006, High-resolution change estimation of soil moisture using L-band radiometer and radar observations made during the SMEX02 experiments. IEEE Transactions on Geoscience and Remote Sensing, 44, 1545-1554.

Newton, R. W., Black, Q. R., Makanvand, S., Blanchard, A. J. and Jean, B. R., 1982, Soil-moisture information and thermal microwave emission IEEE Transactions on Geoscience and Remote Sensing, 20, 275-281.

Newton, R. W. and Rouse, J. W., 1980, Microwave radiometer measurements of soil-moisture content. IEEE Transactions on Antennas and Propagation, 28, 680-686.

Njoku, E. G., Hook, S. J. And Chehbouni, 1996, Effects of surface heterogeneity on thermal remote sensing of land parameters. A., E. T. E. J. B. Stewart, R. A. Feddes, and Y. Kerr (Eds). Scaling Up in Hydrology Using Remote Sensing. Wiley, New York, 19-39.

References

Njoku, E. G., Wilson, W. J., Yueh, S. H., Dinardo, S. J., Li, F. K., Jackson, T. J., Lakshmi, V. and Bolten, J., 2002, Observations of soil moisture using a passive and active low-frequency microwave airborne sensor during SGP99. IEEE Transactions on Geoscience and Remote Sensing, 40, 2659-2673.

Olioso, A., Soria, G., Sobrino, J. and Duchemin, B., 2007, Evidence of Low Land Surface Thermal Infrared Emissivity in the Presence of Dry Vegetation. IEEE Geoscience and Remote Sensing Letters, 4, 112-116.

Owe, M., De Jeu, R. and Walker, J., 2001, A methodology for surface soil moisture and vegetation optical depth retrieval using the microwave polarization difference index. IEEE Transactions on Geoscience and Remote Sensing, 39, 1643-1654.

Panciera, R., 2009, Effect of Land Surface Heterogeneity on Satellite Near-Surface Soil Moisture Observations. PhD theses. University of Melbourne, Australia.

Panciera, R., Walker, J. P., Kalma, J. D., Kim, E. J., Hacker, J. M., Merlin, O., Berger, M. and Skou, N., 2008, The NAFE'05/CoSMOS data set: Toward SMOS soil moisture retrieval, downscaling, and assimilation. IEEE Transactions on Geoscience and Remote Sensing, 46, 736-745.

Panciera, R., Walker, J. P., Kalma, J. D., Kim, E. J., Saleh, K. and Wigneron, J.-P., 2009, Evaluation of the SMOS L-MEB passive microwave soil moisture retrieval algorithm. Remote Sensing of Environment, 113, 435-444.

Piles, M., Entekhabi, D. and Camps, A., 2009, A change detection algorithm for retrieving high-resolution soil moisture from SMAP radar and radiometer observations. IEEE Transactions on Geoscience and Remote Sensing, 47, 4125-4131.

Prigent, C., Aires, F., Rossow, W. B. and Robock, A., 2005, Sensitivity of satellite microwave and infrared observations to soil moisture at a global scale: Relationship of satellite observations to in situ soil moisture measurements. Journal of Geophysical Research-Atmospheres, 110.

Qi, J., Chehbouni, A., Huete, A. R., Kerr, Y. H. and Sorooshian, S., 1994, A modified soil adjusted vegetation index. Remote Sensing of Environment, 48, 119-126.

Ranatunga, K., Nation, E. R. and Barratt, D. G., 2008, Review of soil water models and their applications in Australia. Environmental Modelling & Software, 23, 1182-1206.

Robinson, D. A., Campbell, C. S., Hopmans, J. W., Hornbuckle, B. K., Jones, S. B., Knight, R., Ogden, F., Selker, J. and Wendroth, O., 2008, Soil moisture measurement for ecological and hydrological watershed-scale observatories: A review. Vadose Zone Journal, 7, 358-389.

Rouse, J. W., Haas, R. H., Schell, J. A., Deering, D. W. and Harlan, J. C., 1974, Monitoring the vernal advancements and retrogradation of natural vegetation. NASA/GSFC, Final Report, Greenbelt, MD, USA, 1-137.

Ryu, D., Jackson, T. J., Bindlish, R. and Le Vine, D. M., 2007, L-band microwave observations over land surface using a two-dimensional synthetic aperture radiometer. Geophysical Research Letters, 34.

Saleh, K., Wigneron, J.-P., De Rosnay, P., Calvet, J.-C. and Kerr, Y., 2006, Semi-empirical regressions at L-band applied to surface soil moisture retrievals over grass. Remote Sensing of Environment, 101, 415.

Saleh, K., Wigneron, J. P., Calvet, J. C., Lopez-Baeza, E., Ferrazzoli, P., Berger, M., Wursteisen, P., Simmonds, L. and Miller, J., 2004, The EuroSTARRS airborne campaign in support of the SMOS mission: first results over land surfaces. International Journal of Remote Sensing, 25, 177-194.

References

Saleh, K., Wigneron, J. P., De Rosnay, P., Calvet, J. C., Escorihuela, M. J., Kerr, Y. and Waldteufel, P., 2006, Impact of rain interception by vegetation and mulch on the L-band emission of natural grass. Remote Sensing of Environment, 101, 127-139.

Saleh, K., Wigneron, J. P., Waldteufel, P., De Rosnay, P., Schwank, M., Calvet, J. C. and Kerr, Y. H., 2007, Estimates of surface soil moisture under grass covers using L-band radiometry. Remote Sensing of Environment, 109, 42.

Schmugge, T. J., 1978, Remote-sensing of surface soil-moisture. Journal of Applied Meteorology, 17, 1549-1557.

Schmugge, T. J., 1983, Remote sensing of soil-moisture with microwave radiometers. Transactions of the Asae, 26, 748-753.

Schmugge, T. J., 1985, Chapter 5: Remote sensing of soil moisture. M. G. Anderson and T. P. Burt (Eds), Hydrological Forecasting, John Wiley and Sons, New York, 101-124.

Schmugge, T. J., Gloersen, P., Wilheit, T. and Geiger, F., 1974, Remote -sensing of soil-moisture with microwave radiometers. Journal of Geophysical Research, 79, 317-323.

Schmugge, T. J., 1983, Remote sensing of soil-moisture - recent advances. IEEE Transactions on Geoscience and Remote Sensing, 21, 336-344.

Schmugge, T. J., Jackson, T. J. and Mckim, H. L., 1980, Survey of methods for soil-moisture determination. Water Resources Research, 16, 961-979.

Schmugge, T. J., Jackson, T. J., Kustas, W. P. And Wang, J. R., 1992, Passive microwave remote sensing of soil moisture: results from HAPEX, FIFE, and MONSOON'90. ISPRS Journal of Photogrammetry and Remote Sensing, 47, 127-143.

Schmugge, T. J., Kustas, W. P., Ritchie, J. C., Jackson, T. J. and Rango, A., 2002, Remote sensing in hydrology. Advances in Water Resources, 25, 1367-1385.

Sridhar, V., Hubbard, K. G., You, J. S. and Hunt, E. D., 2008, Development of the soil moisture index to quantify agricultural drought and its "User Friendliness" in severity-area-duration assessment. Journal of Hydrometeorology, 9, 660-676.

Srivastava, H. S., Patel, P., Sharma, Y. and Navalgund, R. R., 2009, Large-area soil moisture estimation using multi-incidence-angle RADARSAT-1 SAR data. IEEE Transactions on Geoscience and Remote Sensing, 47, 2528-2535.

Troch, P. A., Detroch, F. P. and Brutsaert, W., 1993, Effective water-table depth to describe initial conditions prior to storm rainfall in humid regions. Water Resources Research, 29, 427-434.

Uitdewilligen, D. C. A., Kustas, W. P. and Van Oevelen, P. J., 2003, Estimating surface soil moisture with the scanning low frequency microwave radiometer (SLFMR) during the Southern Great Plains 1997 (SGP97) hydrology experiment. Physics and Chemistry of the Earth, 28, 41-51.

Ulaby, F. T., Aslam, A. and Dobson, M. C., 1982, Effects of vegetation cover on the radar sensitivity tp soil-moisture. IEEE Transactions on Geoscience and Remote Sensing, 20, 476-481.

Ulaby, F. T., Dubois,P., Zyl,V. J., 1995, Radar mapping of surface soil moisture. Journal of Hydrology.

Ulaby, F. T., Moore, R. K., Fung, A. K., 1986, Microwave remote sensing: Active and passive. From theory to application, vol III. Artech House, Dedham, MA.

Van de Griend, A. A. and Engman, E. T., 1985, Partial area hydrology and remote sensing. Journal of Hydrology, 81, 211-251.

References

Van de Griend, A. A. and Owe, M., 1994, Microwave vegetation optical depth and inverse modeling of soil emissivity using NIMBUS SMMR satellite-observations. Meteorology and Atmospheric Physics, 54, 225-239.

Van de Griend, A. A., Owe, M., Deruiter, J. and Gouweleeuw, B. T., 1996, Measurement and behavior of dual-polarization vegetation optical depth and single scattering albedo at 1.4- and 5-GHz microwave frequencies. IEEE Transactions on Geoscience and Remote Sensing, 34, 957-965.

Van de Griend, A. A., Wigneron, J. P. and Waldteufel, P., 2003, Consequences of surface heterogeneity for parameter retrieval from 1.4-GHz multiangle SMOS observations. IEEE Transactions on Geoscience and Remote Sensing, 41, 803-811.

Van de Griend, A. A. and Wigneron, J. P., 2004, The b-factor as a function of frequency and canopy type at h-polarization. IEEE Transactions on Geoscience and Remote Sensing, 42, 786-794.

Vivoni, E. R., Entekhabi, D., Bras, R. L. and Ivanov, V. Y., 2007, Controls on runoff generation and scale-dependence in a distributed hydrologic model. Hydrology and Earth System Sciences, 11, 1683-1701.

Wagner, W., Bloschl, G., Pampaloni, P., Calvet, J. C., Bizzarri, B., Wigneron, J. P. and Kerr, Y., 2007, Operational readiness of microwave remote sensing of soil moisture for hydrologic applications. Nordic Hydrology, 38, 1-20.

Walker, J. P., Willgoose, G. R. and Kalma, J. D., 2001, One-dimensional soil moisture profile retrieval by assimilation of near-surface measurements: A simplified soil moisture model and field application. Journal of Hydrometeorology, 2, 356-373.

Wang, J. R., 1983, Passive microwave sensing of soil-moisture content - the effects of soil bulk-density and surface-roughness. Remote Sensing of Environment, 13, 329-344.

Wang, J. R., 1987, Microwave emission from smooth bare fields and soil-moisture sampling depth. IEEE Transactions on Geoscience and Remote Sensing, 25, 616-622.

Wang, J. R. and Choudhury, B. J., 1981, Remote-sensing of soil-moisture content over bare field at 1.4 GHz frequency. Journal of Geophysical Research-Oceans and Atmospheres, 86, 5277-5282.

Wang, J. R. and Schmugge, T. J., 1980, An empirical-model for the complex dielectric permittivity of soils as a function of water-content IEEE Transactions on Geoscience and Remote Sensing, 18, 288-295.

Wang, J. R., Shiue, J. C., Schmugge, T. J. and Engman, E. T., 1990, The L-band PBMR measurements of surface soil-moisture in FIFE. IEEE Transactions on Geoscience and Remote Sensing, 28, 906-914.

Welles, J. M. and Norman, J. M., 1991, Instrument for indirect measurements of canopy architecture. Agronomy Journal, 83, 818-825.

Western, A. W., Zhou, S. L., Grayson, R. B., Mcmahon, T. A., Bloschl, G. and Wilson, D. J., 2004, Spatial correlation of soil moisture in small catchments and its relationship to dominant spatial hydrological processes. Journal of Hydrology, 286, 113-134.

Wigneron, J.-P., Chanzy, A., Calvet, J.-C. and Bruguier, N., 1995, A simple algorithm to retrieve soil moisture and vegetation biomass using passive microwave measurements over crop fields. Remote Sensing of Environment, 51, 331-341.

Wigneron, J. P., Calvet, J. C., Pellarin, T., Van De Griend, A. A., Berger, M. and Ferrazzoli, P., 2003, Retrieving near-surface soil moisture from microwave radiometric observations: current status and future plans. Remote Sensing of Environment, 85, 489.

Wigneron, J. P., Chanzy, A., De Rosnay, P., Rudiger, C. and Calvet, J. C., 2008, Estimating the effective soil temperature at L-band as a function of soil properties. IEEE Transactions on Geoscience and Remote Sensing, 46, 797-807.

Wigneron, J. P., Ferrazzoli, P., Olioso, A., Bertuzzi, P. and Chanzy, A., 1999, A simple approach to monitor crop biomass from C-band radar data. Remote Sensing of Environment, 69, 179-188.

Wigneron, J. P., Kerr, Y., Chanzy, A. and Jin, Y. Q., 1993, Inversion of surface parameters from passive microwave measurements over a soybean field. Remote Sensing of Environment, 46, 61-72.

Wigneron, J. P., Kerr, Y., Waldteufel, P., Saleh, K., Escorihuela, M. J., Richaume, P., Ferrazzoli, P., De Rosnay, P., Gurney, R., Calvet, J. C., Grant, J. P., Guglielmetti, M., Hornbuckle, B., Mätzler, C., Pellarin, T. and Schwank, M., 2007, L-band Microwave Emission of the Biosphere (L-MEB) Model: Description and calibration against experimental data sets over crop fields. Remote Sensing of Environment, 107, 639.

Wigneron, J. P., Laguerre, L. and Kerr, Y. H., 2001, A simple parameterization of the L-band microwave emission from rough agricultural soils. IEEE Transactions on Geoscience and Remote Sensing, 39, 1697-1707.

Wigneron, J. P., Parde, M., Waldteufel, P., Chanzy, A., Kerr, Y., Schmidl, S. and Skou, N., 2004, Characterizing the dependence of vegetation model parameters on crop structure, incidence angle, and polarization at L-band. IEEE Transactions on Geoscience and Remote Sensing, 42, 416-425.

Wigneron, J. P., Schmugge, T. J., Chanzy, A., Calvet, J. C. and Kerr, Y., 1998, Use of passive microwave remote sensing to monitor soil moisture. Agronomie, 18, 27-43.

Appendix A

LPRM - Land Surface Parameter Retrieval Model

The radiative brightness temperature is expressed as a radiative transfer equation and based on two main parameters, the optical depth τ and the single scattering albedo ω (Kirdyashev et al. 1979, Mo et al. 1982)

$$TB_p = T_s e_{r,p} \Gamma_p + (1 - \omega_p) T_c (1 - \Gamma_p) + (1 - e_{r,p})(1 - \omega_p) T_c (1 - \Gamma_p) \Gamma_p \qquad (A.1)$$

where T_s and T_c are the soil and vegetation temperatures, e_r and Γ are respectively the rough surface emissivity and the transmissivity of the vegetation layer. The index $_p$ refers to the polarization state. The single scattering albedo ω accounts for the scattering of the soil microwave emission within the vegetation.

The first term of equation (A.1) describes the emission from the soil as attenuated by the overlaying vegetation. The second term describes the emission from the vegetation. The third term accounts for the downward radiation from the vegetation, reflected upward by the soil and is again attenuated by the vegetation canopy. For illustration see figure A-1.
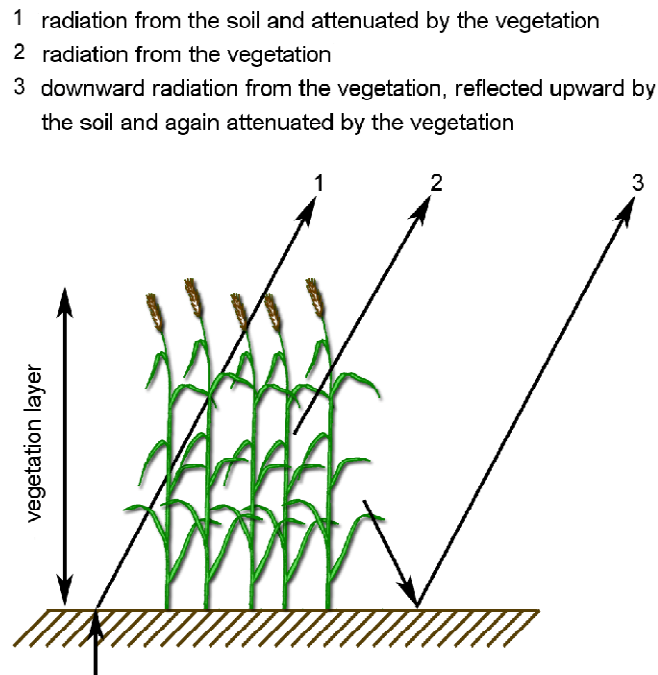

Figure A-1.   Contribution of soil and vegetation to observed passive microwave signal.

In LPRM, the vegetation attenuation factor or transmissivity Γ is assumed to be equal for vertical and horizontal polarization. Γ is defined in terms of the optical depth τ and is given by

$$\Gamma = \exp(\frac{-\tau}{\cos u}) \tag{A.2}$$

where u is the incidence angle.

Within this study LPRM is applied with the vegetation optical depth module proposed by Meesters et al. (2005). The final equation to compute τ is given by

$$\tau = \cos u \ln(ad + \sqrt{(ad)^2 + a + 1}) . \tag{A.3}$$

For detailed description of the derivation of equation (A.3) see Appendix B.

In general the soil brightness temperature TB is a function of soil emissivity e and the soil temperature T_s and is simplified given by

$$TB_p = e_p \cdot T_s . \tag{A.4}$$

The emissivity e_p is generally calculated as one minus soil reflectivity r_p ($e_p = 1 - r_p$). Within LPRM the reflectivity r_p is related to the surface soil moisture content through the dielectric mixing model proposed by Wang and Schmugge (1980). The dielectric model is an essential part of the forward modeling procedure as it realizes the connection to the soil water content. A detailed derivation and description of the Wang-Schmugge Model is provided in Appendix C.

The reflectivity r_p is calculated from the Fresnel equations that defines the behavior of electromagnetic waves at a smooth dielectric boundary by

$$r_h = \left| \frac{\cos u - \sqrt{\varepsilon - \sin^2 u}}{\cos u + \sqrt{\varepsilon - \sin^2 u}} \right|^2 \tag{A.5}$$

$$r_v = \left| \frac{\varepsilon \cos u - \sqrt{\varepsilon - \sin^2 u}}{\varepsilon \cos u + \sqrt{\varepsilon - \sin^2 u}} \right|^2 \tag{A.6}$$

where ε is the absolute value of the complex dielectric constant of the soil.

The rough surface emissivity $e_{r,p}$ is described by a semi-empirical approach to account for soil roughness effects on the microwave emission (Wang et al. 1981). Rough surfaces are characterized by higher emissivity and the differences between horizontal and vertical polarizations are reduced. The rough surface emissivity $e_{r,p}$ is developed as a function of the smooth surface reflectivity $r_{s,p}$ and the parameters Q, h_r and u

$$e_{r,p1} = 1 - ((Q \cdot r_{s,p1} + (1 - Q) \cdot r_{s,p2}) \cdot \exp(-h_r \cos^2 u)) \tag{A.7}$$

for $Q = 0$

$$e_{r,p1} = 1 - (\cdot r_{s,p2} \cdot \exp(-h_r \cos^2 u) \tag{A.8}$$

where Q is the polarization mixing fraction that can be assumed to be zero at L-band (Wigneron et al. 2001). h_r is a dimensionless empirical roughness parameter. The index $p1$ and $p2$ refer to the polarization states (horizontal or vertical).

$$e_{r,p1} = 1 - (\cdot r_{s,p2} \cdot \exp(-h_r \cos^2 u)$$

Appendix B

Vegetation optical depth model

The analytical derivation of the vegetation optical depth from the microwave polarization difference index (MPDI) was proposed by Meesters et al. (2005).

Within the radiative transfer equations, given by

$$TB_h = T_s e_{r,h} \Gamma_h + (1 - \omega_h) T_c (1 - \Gamma_h) + (1 - e_{r,h})(1 - \omega_h) T_c (1 - \Gamma_h) \Gamma_h \qquad \text{(B.1)}$$

$$TB_v = T_s e_{r,v} \Gamma_v + (1 - \omega_v) T_c (1 - \Gamma_v) + (1 - e_{r,v})(1 - \omega_v) T_c (1 - \Gamma_v) \Gamma_v \qquad \text{(B.2)}$$

with the assumption Ts = Tc = T the vegetation canopy transmissivity is defined as

$$\Gamma = \exp(\frac{-\tau}{\cos u}). \qquad \text{(B.3)}$$

The microwave polarization difference index (MPDI) is defined as

$$MPDI = \frac{TB_v - TB_h}{TB_v + TB_h}. \qquad \text{(B.4)}$$

A new expression for B.3 is derived by substituting B.1 and B.2 in B.4 and can be rewritten as follows

$$\frac{1}{MPDI} = \frac{e_v + e_h}{e_v - e_h} + \frac{2(1 + \Gamma)(1 - \Gamma)(1 - \omega)}{\omega\Gamma + (1 - \omega)\Gamma^2} \frac{1}{e_v - e_h}. \qquad \text{(B.5)}$$

Equation B.5 can be formulated as

$$2a = \frac{2(1 - \Gamma^2)}{2d\Gamma + \Gamma^2} \qquad \text{(B.6)}$$

with

$$a(k,u) = \frac{1}{2}\left[\frac{e_v(k,u) - e_h(k,u)}{MPDI} - e_v(k,u) - e_h(k,u)\right] \qquad \text{(B.7)}$$

and

$$d = \frac{1}{2}\frac{\omega}{(1 - \omega)}. \qquad \text{(B.8)}$$

Substituting B.7 and B.8 in B.6 yields a quadratic equation in Γ, where

$$(1 + a)\Gamma^2 + 2ad\Gamma - 1 = 0. \qquad \text{(B.9)}$$

Dividing B.9 by Γ^2 and then solving for $1/\Gamma$ a general solution is given by

$$\frac{1}{\Gamma} = ad \pm \sqrt{(ad)^2 + a + 1} \qquad \text{(B.10)}$$

where by definition that $0 \le \Gamma \le 1$ only the form

$$\frac{1}{\Gamma} = ad + \sqrt{(ad)^2 + a + 1} \tag{B.11}$$

of equation B.10 yields positive result.

Combining equation B.11 with equation B.3 a formulation for the optical depth is given by

$$\tau = \cos u \ln(ad + \sqrt{(ad)^2 + a + 1}) \tag{B.12}$$

Equation B.12 can now be used in a forward modeling approach using equation B.1.

$$\frac{1}{\Gamma} = ad + \sqrt{(ad)^2 + a + 1}$$

Appendix C

Wang-Schmugge Model: semi-empirical dielectric mixing model

The dielectric constant ε of a soil-water mixture is described as

$$\varepsilon = \theta \cdot \varepsilon_x + (P - \theta) \cdot \varepsilon_a + (1 - P) \cdot \varepsilon_r \qquad \theta \leq \theta_t \qquad (C.1)$$

where

θ volumetric water content of the soil [m^3 m^{-3}]

P   porosity of the dry soil

ε_x dielectric constant of the initially absorbed water

ε_a dielectric constant of the air

ε_r dielectric constant of the rock.

Furthermore ε_x is defined as

$$\varepsilon_x = \varepsilon_i + (\varepsilon_w - \varepsilon_i) \cdot \frac{\theta}{\theta_t} \cdot \gamma \qquad (C.2)$$

and

$$\varepsilon = \theta_t \cdot \varepsilon_x + (\theta - \theta_t) \cdot \varepsilon_w + (P - \theta) \cdot \varepsilon_a + (1 - P) \cdot \varepsilon_r \qquad (C.3)$$

$$\theta \geq \theta_t$$

with

$$\varepsilon_x = \varepsilon_i + (\varepsilon_w - \varepsilon_i) \cdot \gamma \qquad (C.4)$$

where

ε_i dielectric constant of ice

ε_w dielectric constant of water

γ empirical parameter

θ_t the transition moisture [m^3 m^{-3}].

θ_t is defined as the moisture content at which the free water phase begins to dominate the soil system and can be described as

$$\theta_t = 0.49 \cdot WP + 0.165 \qquad (C.5)$$

WP is the wilting point of the soil which can be calculated by

$$WP = 0.06774 - 0.00064 \cdot S + 0.00478 \cdot C \qquad (C.6)$$

where S and C are respectively the sand and clay contents in percent of dry weight of a soil.

γ can be determined by

$$\gamma = -0.57 \cdot WP + 0.481 \tag{C.7}$$

The complex dielectric constants for ice, solid rock and air are

$$\varepsilon_i = 3.2 + 0.1i$$

$$\varepsilon_r = 5.5 + 0.2i$$

$$\varepsilon_a = 1 + 0i.$$

The dielectric constant for water ε_w is given by the Debye Equation

$$\varepsilon_w = \varepsilon_{w\infty} + \frac{\varepsilon_{w0} - \varepsilon_{w\infty}}{1 + (2 \cdot \pi \cdot t_w \cdot f)i} \tag{C.8}$$

where

$\varepsilon_{w\infty}$ is the high frequency limit of the dielectric constant of pure water (~ 4.9), ε_{w0} is the static dielectric constant of pure water, t_w is the relaxation time of pure water in seconds and f is the electromagnetic frequency in Hz. Equation (C.8) can be rewritten in a real and imaginary part. The real part is defined by Ulaby et al. (1986), as

$$\varepsilon_w' = \varepsilon_{w\infty} + \frac{\varepsilon_{w0} - \varepsilon_{w\infty}}{1 + (2 \cdot \pi \cdot t_w \cdot f)^2} \tag{C.9}$$

and the imaginary part as

$$\varepsilon_w'' = \frac{2 \cdot \pi \cdot t_w \cdot f \cdot (\varepsilon_{wo} - \varepsilon_{w\infty})}{1 + (2 \cdot \pi \cdot t_w \cdot f)^2} \tag{C.10}$$

The static dielectric constant of pure water is given as

$$\varepsilon_{w0} = 88.045 - 0.4147 \cdot (T - 273.15) + 6.295 \cdot 10^{-4} \cdot (T - 273.15)^2 + 1.075 \cdot 10^{-5} \cdot (T - 273.15)^3 \tag{C.11}$$

where T is the effective temperature of the emitting layer in Kelvin.

The relaxation time of pure water is

$$2\pi t_w = 1.1109 \cdot 10^{-10} - 3.824 \cdot 10^{-12} \cdot (T - 273.15) + 6.938 \cdot 10^{-14} \cdot (T - 273.15)^2 - 5.096 \cdot 10^{-16} \cdot (T - 273.15)^3 \tag{C.12}$$

Acknowledgement

Curriculum Vitae

Personal

Name:	Marion Pause
Date of Birth:	September 10, 1979
Place of Birth:	Grimma (Saxony), Germany
Nationality:	German

School and Education

07.2007 - 09.2010	PhD - Student at the Helmholtz Centre for Environmental Research - UFZ, Department Computational Landscape Ecology, Scholarship of the German Federal Environmental Foundation DBU
10.2001 – 11.2006	Study of Geodesy at the Technical University of Dresden (subject areas: Remote Sensing, Photogrammetry, GIS), Diploma Thesis at the Helmholtz Centre for Environmental Research - UFZ, Department Computational Landscape Ecology "Musterdynamik von ENVISAT ASAR Rückstreukoeffizienten auf landwirtschaftlich genutzten Flächen" (Pattern dynamics of ENVISAT ASAR backscatter coefficients over agricultural used sites)
04.2001 –09.2001	Study of Mine-Surveying and Geodesy at the Technical University of Clausthal-Zellerfeld, Germany
10.1998 -03.2001	Study of Mine-Surveying and Geodesy at the Technical University of Freiberg, Germany
1991 - 1998	Gymnasium St. Augustin zu Grimma, Germany
1989 – 1991	Grammar school, Trebsen, Germany
1986 - 1989	Primary school, Altenhain, Germany

Scientific career

Since 01.2011	Research Scientist for Environmental Sensing at WESS (Water and Earth System Science Competence Center) in Tübingen, Germany
10.2010 – 12.2010	Research Assistant at the Helmholtz Centre for Environmental Research - UFZ, Department Monitoring & Exploration Technologies
11.2009 - 04.2010	Research stay at Airborne Research Australia and Flinders University in Adelaide, Australia
12.2006 – 06.2007	Research Assistant at the Helmholtz Centre for Environmental Research - UFZ, Department Computational Landscape Ecology